Aus der Klinik für Neurologie

Geschäftsführender Direktor: Prof. Dr. med. Lars Timmermann

Des Fachbereichs Medizin der Philipps-Universität Marburg

Selective cellular vulnerability and pathology progression patterns in two mouse models of Parkinson's disease

Inaugural-Dissertation zur Erlangung des Doktorgrades
der Naturwissenschaften (Dr. rer. nat.)
dem Fachbereich Medizin der Philipps-Universität Marburg

vorgelegt von

Fanni F. Geibl
aus Budapest, Ungarn

Marburg, 2019

Angenommen vom Fachbereich Medizin der Philipps-Universität Marburg
am: 09.10.2019

Gedruckt mit Genehmigung des Fachbereichs Medizin

Dekan: Prof. Dr. med. Helmut Schäfer

Referent: Prof. Dr. Dr. h.c. Wolfgang H. Oertel

1. Korreferent: Prof. Dr. Carsten Culmsee

"If I have seen further it is by standing on the shoulders of Giants."

Isaac Newton

Mainre Krosmotr

Szeretett nagymamámnak

Meiner Großmutter

Table of contents

1 Introduction

1.1 Parkinson's disease

1.1.1 Epidemiology

Parkinson's disease (PD) is the most common movement disorder and the second most common neurodegenerative disease after Alzheimer's disease with a prevalence of approximately 0.3% of the general population in industrialized countries [165, 238, 247, 260]. The mean age of onset is estimated to be in the mid-to-late 60s [130, 162]. Whereas the disease is rare in young adults (prevalence ~0.25% in the population under 50), its prevalence increases to approximately 4% in people over 85 years clearly indicating that PD is an age-dependent disease [21]. According to several studies, prevalence rates in men are higher than in women [20, 50, 73, 174, 192], however, reports of similar prevalence rates in men and women also exist [247, 248, 306].

1.1.2 Symptomatology

Symptoms of PD are traditionally divided into two major categories: (1) motor symptoms, and (2) non-motor symptoms.

1.1.2.1 Motor symptoms

The major clinical picture of PD is the so called parkinsonism. Parkinsonism is an umbrella term for a clinical syndrome featuring Parkinson's-type motor symptoms: slowness of movement (bradykinesia), muscle rigidity (rigor), and rest tremor (4-6 Hz) [231]. The German Society of Neurology (Deutsche Gesellschaft für Neurologie, DGN) lists a fourth feature of parkinsonism: postural instability, which was omitted from the international guidelines due to its late appearance during the disease process [63, 231]. PD accounts for approximately 75% of parkinsonism thereby representing the most common cause.

Motor symptoms usually appear unilaterally, most commonly in one of the upper extremities, and slowly progress to the contralateral and lower limbs, but the initial asymmetry of symptoms remains over the whole course of the disease [218, 251, 335]. The parkinsonian motor deficits are due to the degeneration of the dopaminergic substantia nigra pars compacta (SNc) and evolve when approximately 30% of nigral neurons are degenerated and 50-60% of striatal dopamine is lost [45, 75, 101, 151]. Disease progression is characterized

by increasing severity of motor symptoms, evolvement of additional motor deficits such as postural instability, or gait problems, and appearance of treatment-related complications, such as L-DOPA-induced dyskinesias [136].

1.1.2.2 Non-motor symptoms

Although PD is still considered a movement disorder and the diagnosis is based upon the appearance of parkinsonian motor deficits (see chapter 1.1.5), PD is accompanied by a broad spectrum of non-motor symptoms (NMS) as well. These NMS fall into four major categories: (1) autonomic dysfunctions; (2) disorders of the sleep-wake cycle; (3) neuropsychiatric dysfunctions; and (4) sensory dysfunctions [43]. A thorough list of the NMS associated with PD is found in Figure 1.1.

NMS diversity and severity correlates with advancing disease stages. Remarkably, some NMS, such as constipation, hyposmia, pain, REM sleep behavior disorder (RBD), and mood disorders appear early in the disease process antedating the onset of motor symptoms, and are presenting complaints in up to 20% of patients [214]. This often leads to delayed diagnosis of PD, referrals to specialists other than neurologists, and inappropriate treatments [214, 273, 274]. The time-period, in which certain NMS and subtle motor changes not yet qualifying as parkinsonism are present, is the so called prodromal phase of the disease.

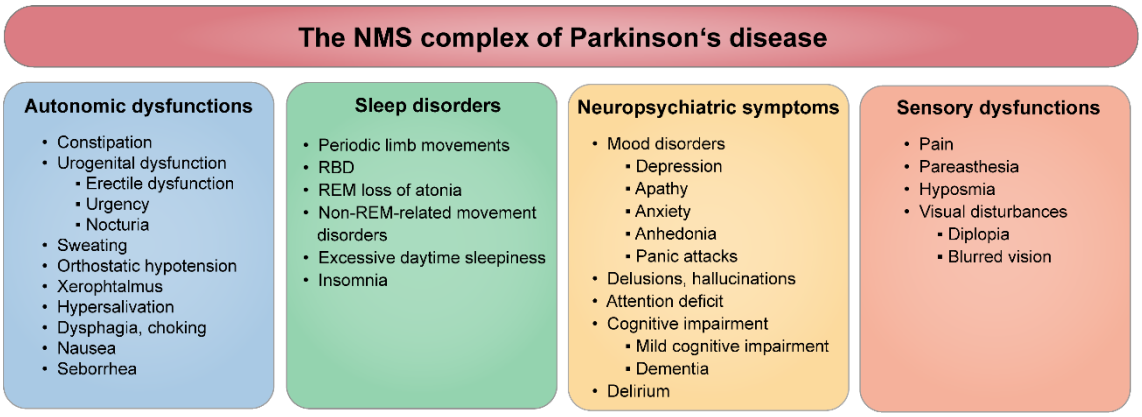

Figure 1.1 | The non-motor symptom complex of Parkinson's disease.

1.1.3 Neuropathology

The major histopathological hallmarks of PD are: (1) progressive accumulation of intraneuronal proteinaceous inclusion bodies called Lewy-bodies (LB) and Lewy-neurites (LN) in predetermined brain regions; and (2) dopaminergic neuronal cell death in specific subregions of the SNc [30, 75].

Two types of LBs can be distinguished: brainstem (classical) type and cortical type [65, 172]. In hematoxylin and eosin-stained sections, brainstem LBs appear as intracytoplasmic, eosinophilic, and spherical bodies of 8-30 μm diameter (Fig. 1.2) [325]. They possess a dense, protein-packed core which is surrounded by a clearer peripheral halo. In contrast to this, cortical type LBs are irregular in shape and lack a peripheral halo [324]. LBs contain a mixture of over 90 different proteins, out of which abnormally misfolded α-synuclein (aSYN) is the most prevalent [85, 290, 325]. Hence, PD belongs to a subgroup of neurodegenerative proteinopathies called α-synucleinopathies. In stark contrast to the previous assumption that LBs are *mainly* composed of proteins, recent research with highly advanced electron tomography technique demonstrated that the major components seem to be fragmented membraneous structures resembling vesicles and dysmorphic organelles including mitochondria, lysosomes, and autophagosomes [281]. Granular forms of proteins were observed to be intermingled in the core of lipid bilayers and fragmented organelles. Pathological forms of aSYN have been found in different layers of the LBs and LNs: truncated aSYN was found in the core of the aggregates, mixed with the lipids, whereas phosphorylated aSYN was typically found in the periphery [200]. The pathophysiological implications and biological relevance of these novel findings are still unclear.

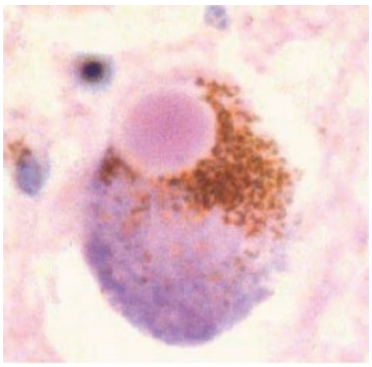

Figure 1.2 | Human Lewy body in a nigral neuron.
Lewy bodies are intraneuronal spheroid eosinophilic structures upon hematoxylin and eosin staining. Nigral neurons contain neuromelanin, an auto-oxidation product of dopamine. Extracted from [112] (Andreas Hartmann, licence: CC BY-NC-ND 3.0).

Based on histopathological examinations of the topographical distribution of Lewy pathology in the brains of unrelated individuals who died of various causes at different ages, Braak and colleagues have elaborated a staging system to describe the putative spatio-temporal pattern of the progression of Lewy pathology in PD [30].

The Braak staging system distinguishes six consecutive stages (Fig. 1.3) [30, 31]. In stage 1, Lewy pathology is evident in the olfactory bulb (OB) and the medullary dorsal motor nucleus of the vagal nerve. From here, the pathology progresses to more rostral regions of the brainstem, to the locus coeruleus (LC), gigantocellular nucleus (GRN), and the nucleus magnus obscurus pallidus (stage 2).

In stage 3, the SNc displays the first LBs, next to the affection of other midbrain and basal forebrain structures, such as the pedunculopontine nucleus (PPN), the magnocellular nuclei of the basal forebrain, the central subnucleus of the amygdala, and the histaminergic tuberomamillary nucleus. No overt neurodegeneration of the SNc is observed in this stage. These three initial stages are considered to correlate with the prodromal phase of PD, and the involvement of the above structures are hypothesized to account for the NMS antedating the motor symptomatology (see chapter 1.1.2.2).

In stage 4, the SNc is markedly demelanized. Additionally, limbic structures including the basolateral and accessory cortical nuclei of the amygdala, parts of the bed nuclei of the stria terminalis, and the first cortical structure (anteromedial temporal mesocortex) display Lewy pathology. The transition from prodromal PD (NMS and subtle motor changes not yet qualifying as parkinsonism) to manifest PD (clear signs of parkinsonism) is hypothesized to occur between stage 3 (LB pathology in SNc, but no overt neurodegeneration) and stage 4 (overt neurodegeneration of the SNc) of the Braak staging. In stages 5 and 6, cortical pathology gradually spreads over the entire neocortex.

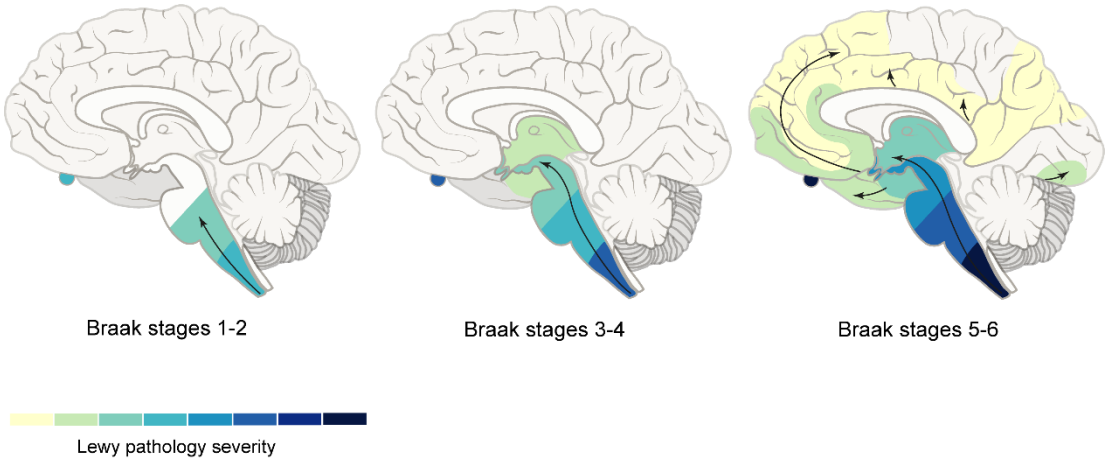

Figure 1.3 | Schematic representation of the Braak staging system of Lewy pathology in Parkinson's disease. Figure adapted from [107].

1.1.4 Hypotheses of disease progression

Currently, two major theories exist which aim to explain the progression pattern of pathology and symptomatology in idiopathic PD: (1) the prion hypothesis; and (2) the hypothesis of selective vulnerability [34, 71, 296, 297].

1.1.4.1 The prion hypothesis of Parkinson's disease

The word prion is derived from 'proteinaceous infectious particle' and refers to the (to our knowledge) smallest infectious particle devoid of any nucleic acid component [234]. Prion variants of the cellular prion protein (PrP^{Sc}) are hypothesized to cause a group of diseases called transmissible spongiform encephalopathies by triggering the misfolding of the naturally occurring, native forms of the prion protein (PrP^{C}) in the neuronal tissue of the infected host resulting in the accumulation and deposition of misfolded proteinaceous aggregates [52]. The putative pathway for disease progression within the neuronal tissue of the infected host is the cell-to-cell transmission of the misfolded prion protein [319].

A similar deposition of aggregated aSYN due to conversion of natively unfolded protein to misfolded protein takes place in PD, thus defining the disease – similarly to other neurodegenerative diseases – as 'neurodegenerative proteinopathy' or 'protein misfolding disorder' [270]. The hypothesis that pathological aSYN is transmissible from a diseased neuron ('donor') to a primarily healthy neuron ('recipient') similar to PrP^{Sc} stems from two major observations [235]: (1) in 2003, Braak and colleagues published their staging system based on the neuropathological assessment of postmortem brains from unrelated humans, in which they describe a sequential progression of Lewy pathology in a deterministic caudo-rostral pattern (see chapter 1.1.3) [30, 31]; (2) in 2008, Kordower and colleagues described the development of aSYN aggregates reminiscent of LBs in striatal engrafted embryonic mesencephalic dopaminergic cells in postmortem brains of PD patients [6, 149].

Taken together, the so-called prion concept of PD hypothesizes that toxic forms of aSYN are formed within a small cell population, are then transported in the retrograde and/or anterograde direction to anatomically interconnected brain regions where they act as seeds and trigger the formation of insoluble, aggregated aSYN [99]. Thus, the reason for progression of the α-synucleinopathy is believed to rely mostly, if not completely on the neuronal connectivity of the affected brain regions. This theory is mainly evidenced by animal models induced by the injection of aSYN pre-formed fibrils (PFF's), in which the inoculated PFF's trigger the aggregation of the endogenous, natively unfolded aSYN into LB- and LN-like aggregates at the inoculation site and interconnected brain regions (see chapter 1.3.3.2).

However, there are also important arguments against the prion hypothesis: (1) retrospective histopathological studies showed that between 6.3 and 43% of PD cases did not follow the ascending progression pattern proposed by Braak and colleagues [9, 15, 30, 106, 134, 219]; (2) development of Lewy-like aggregates in transplanted embryonic cells is seen only in up to 5-10% of engrafted neurons [1, 6, 149]; (3) hereditary forms of PD may show substantial neuropathological heterogeneity, even in siblings carrying the same genetic mutation. Moreover, in some genetic forms of PD, LB development is lacking, implicating that LB-formation is not required for neuronal dysfunction and degeneration [74, 232, 316]. And (4) the hypothesis does not provide an explanation of how aSYN aggregation is initiated in a certain subset of neurons.

1.1.4.2 The hypothesis of selective vulnerability

On the contrary, the hypothesis of selective vulnerability proposes that not neuronal interconnectivity, but rather certain cell-autonomous factors rendering neurons particularly susceptible to the disease process are the major determinants of pathology progression. This hypothesis is based on the following observations: (1) neuropathologically affected brain regions in PD have a set of shared traits, which distinguishes them from non-affected structures; (2) neurons adjacent to LB-displaying brain structures do not automatically develop Lewy pathology during the disease process, e.g. whereas cholinergic neurons of the PPN display Lewy pathology, GABAergic and glutamatergic neurons are devoid of aggregates [108]; (3) the progression pattern of Lewy pathology in humans does not exactly follow the connectomes of the affected structures; (4) in *SNCA*-multiplication and -point mutation-linked PD, although all neurons are exposed to higher levels or mutated aSYN, not all develop aSYN aggregates implicating the presence of certain factors that increase the susceptibility of distinct neurons to the disease process [297].

According to the theory of selective vulnerability, certain neurons are inherently more vulnerable to pathophysiological processes underlying disease initiation and progression, whereas other neurons possess intrinsic properties which make them resilient to the pathogenic process [326]. Common traits hypothesized to account for the selective susceptibility of certain neurons (vulnerability profile) are: (1) long and thinly or unmyelinated axons; (2) axonal hyperbranching leading to high energetic demand; (3) autonomous pacemaking relying on L-type Ca^{2+}-channels; (4) higher basal rate of oxidative phosphorylation in combination with a small reserve capacity; and (5) low Ca^{2+} buffering capacity [217, 297, 333].

1.1.5 Diagnosis

The clinical diagnosis of PD as defined by the International Movement Disorder Society (MDS) consists of two major steps: (1) clinical diagnosis of the typical motor parkinsonism; and (2) identification of Parkinson's disease as the cause of clinical parkinsonism (Fig. 1.4) [231]. The diagnostic criteria were constructed to allow both a high sensitivity and specificity with two levels of diagnostic certainty:

1. *Clinically established PD*: maximal specificity with the goal that at least 90% of patients receiving a clinical diagnosis of PD truly have PD (specificity: ≥90%);
2. *Clinically probable PD*: balancing specificity and sensitivity values with the goal that at least 80% of patients receiving a clinical diagnosis of PD truly have PD (specificity ≥80%), and at least 80% of patients having PD will receive the clinical diagnosis of PD (sensitivity ≥80%).

In the first step, the diagnosis of parkinsonism is made based upon the presence of the cardinal motor features: bradykinesia in combination with rest tremor, muscle rigidity (rigor), or both. As parkinsonism is not a specific syndrome of PD and may be associated with several other diseases, such as atypical Parkinsonian disorders, or secondary Parkinson syndromes [63], in the second step, PD has to be identified as the cause of parkinsonism. Three criteria systems are included (Fig. 1.4).

1. *Absolute exclusion criteria must be absent*. These refer to clinical features and imaging results which suggest an alternate cause of the parkinsonism. For example, the presence of clear cerebellar abnormalities suggests the diagnosis of multiple system atrophy; the presence of vertical supranuclear gaze palsy is indicative of progressive supranuclear palsy; or treatment with a dopamine antagonist, dopamine-depleting agent, or exposure to neurotoxins known to induce parkinsonism suggest the diagnosis of drug- or toxin-induced parkinsonism instead of idiopathic PD.
2. *Red flags should be absent*. These refer to clinical symptoms which are rarely associated with PD, but do not exclude the possibility of PD being present in the patient. For example, severe autonomic failure in the first five years of the disease is suggestive of multiple system atrophy, however, does not exclude the possibility of idiopathic PD.
3. *At least two out of four supportive criteria should be present*. These include: a clear and dramatic response to dopaminergic treatment; classic rest tremor (4-6 Hz); presence of L-DOPA-induced dyskinesia; and hyposmia and/or cardiac denervation evidenced by metaiodobenzylguanidine (MIBG) scintigraphy.

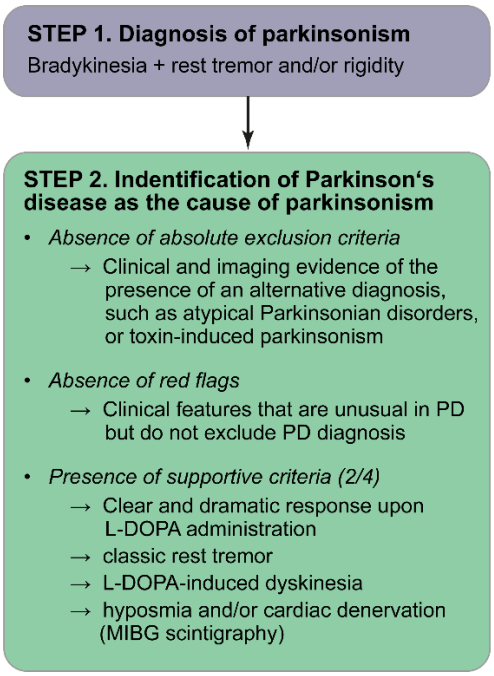

Figure 1.4 | MDS clinical diagnostic criteria of Parkinson's disease. [231]

1.1.6 Therapy

PD is a slowly progressive, highly debilitating disease. Until today, no effective disease-modifying (neuroprotective) therapy has been developed to slow or even halt disease progression [208]. However, pharmacological and non-pharmacological therapies are available which can alleviate (mainly) motor symptomatology and thus significantly increase the quality of life of patients for many years [207, 341].

1.1.6.1 Alleviation of motor symptoms

Since the discovery that dopamine depletion in the striatum of patients is the underlying cause of parkinsonism in PD [36, 37], several pharmacological treatments have been developed which target nigrostriatal dopaminergic neurotransmission at the presynaptic or postsynaptic level.

L-DOPA or levodopa is a blood-brain barrier crossing precursor of dopamine, which is taken up by dopaminergic neurons and subsequently converted into dopamine thereby restoring presynaptic dopamine levels in the nigrostriatal system [208]. Still today, L-DOPA is the most effective drug to alleviate motor symptoms and therefore represents the gold standard for PD therapy [198, 286, 341]. Due to the short plasma half-life of L-DOPA, repeated intake is necessary resulting in a pulsatile plasma profile of the drug [292]. In early disease stages, when

the L-DOPA and dopamine storage capacity of nigrostriatal nerve terminals is only partially decreased, the CNS is hypothesized to effectively buffer the fluctuations of L-DOPA concentration. However, in intermediate and advanced disease stages, with severe nigrostriatal damage, the pulsatile plasma levels result in pulsatile stimulation of postsynaptic striatal dopaminergic receptors, leading to fluctuations in motor symptoms from muscle rigidity and akinesia corresponding to low L-DOPA levels to the emergence of dyskinetic movements, so called L-DOPA-induced dyskinesias with high L-DOPA levels [211]. To increase bioavailability and ameliorate pharmacokinetics of L-DOPA in the CNS, it can be combined with the following drugs: (1) peripheral dopamine decarboxylase inhibitors to decrease its peripheral conversion to dopamine (standard combination); (2) catechol-O-methyltransferase (COMT) inhibitors to block its peripheral degradation; or (3) centrally acting monoamine oxidase B (MAO-B) inhibitors to decrease its central degradation [208].

Another highly effective approach are dopamine receptor agonists which can be applied as a monotherapy or in combination with L-DOPA. They exert their antiparkinsonian effect via direct activation of D_2-, and in part of the D_1 receptors abundantly found in the dorsal striatum [104, 334]. Their plasma half-life is longer than that of L-DOPA, thus, their postsynaptic dopamine receptor activation is more stable over time limiting their potential to induce motor fluctuations [206]. Major limiting factors for their usage in monotherapy are: (1) dopamine receptor agonists only exert a moderate effect on the parkinsonian motor symptomatology; and (2) they induce impulse control disorders, such as compulsive gambling, dopamine dysregulation syndrome, or hypersexuality in up to 17% of patients, possibly owing to their action on the D_3 receptors mainly found in limbic areas of the brain [104, 288, 336, 341].

The use of anticholinergic drugs is limited to PD patients whose greatest source of disability is tremor (tremor-dominant PD), as it shows beneficial effects to alleviate tremor, however, has only minor effect on bradykinesia or rigor [341]. Amantadine, a glutamatergic N-methyl-D-aspartate (NMDA)-receptor blocker, due to its limited efficacy in alleviating parkinsonism, is no longer recommended as first-line therapy [341]. However, it has shown good efficacy in reducing motor fluctuations and L-DOPA-induced dyskinesia [208].

In advanced PD, when pharmacological treatment fails to facilitate adequate relief of motor symptoms, or induces severe motor fluctuations, deep brain stimulation (DBS), most commonly of the subthalamic nucleus (STN) or the internal division of the globus pallidus (GPi) can be taken into consideration as a non-pharmacological treatment [224]. The exact mechanism of action of DBS is still poorly understood, however, it is hypothesized to

modulate abnormal neuronal activity in the basal ganglio-thalamo-cortical and brainstem motor loops [48, 92, 103]. DBS was repeatedly shown to significantly alleviate motor symptoms, enable reduction of pharmacological dopaminergic treatment by up to 62%, and thus substantially decrease the occurrence of disabling dyskinesias [143].

Other non-pharmacological treatment options include physiotherapy, active exercise therapy, or speech therapy, which were repeatedly shown to be effective in amelioration of motor and certain non-motor symptomatology, such as cognitive impairment [63, 66, 294, 339].

1.1.6.2 Alleviation of non-motor symptomatology

In stark contrast to motor symptoms, NMS are often under-recognized and under-diagnosed, although their impact on the quality of life of patients may surpass that of motor symptoms [13]. A prospective study conducted in the US showed that depression and anxiety diagnoses are missed in around 60%, for fatigue in around 75%, and for sleep disturbance in around 40% of consultations by neurologists [284]. Additionally, given the sparse number of randomized, double blind, placebo-controlled clinical trials, evidence-based recommendations for the treatment of specific NMS are limited. Table 1.1 gives a brief summary of available treatments of specific NMS.

Table 1.1 | Treatment options for specific non-motor symptoms according to [63, 269]

Non-motor symptom	Treatment options

Depression and other mood disorders	• Sufficient substitution of dopamine
	• Antidepressants
	  ▪ Tricyclic antidepressants (TCA)
	  ▪ Selective serotonin reuptake inhibitors (SSRI)
	  ▪ Serotonin-noradrenaline reuptake inhibitors (SSNRI)
	• Dopaminergic agents, such as pramipexole
	• Psychotherapy, cognitive behavioral therapy

Mild cognitive impairment	• Neuropsychological cognitive training
Dementia	• Cholinesterase inhibitors ▪ Only: rivastigmine and donepezil
Psychosis	• Treat potential causative factors (e.g. dehydration) • Atypical antipsychotics ▪ Only options: clozapine or quetiapine • If psychosis occurs in combination with dementia, cholinesterase inhibitors are an alternative
Insomnia	• General sleep hygiene recommendations • Reduce night-time motor fluctuations and restless legs syndrome by continuous drug delivery or controlled-release formulations • Zopiclone

Orthostatic hypotension	• Patient education
	• Non-pharmacological therapies
	  ▪ Increased salt intake
	  ▪ Increased water intake
	  ▪ Compression stockings
	• Pharmacological therapies
	  ▪ Noradrenaline precursor (droxidopa)

Urinary dysfunction	• Identify and treat other causative factors (e.g. prostate hyperplasia) • Sufficient substitution of dopamine • Anticholinergics

Constipation	• Non-pharmacological treatment
	  ▪ Increased fiber- and water intake
	  ▪ Physical activity
	• Laxative therapy
	  ▪ Bulk-forming laxatives
	  ▪ Hyperosmotic laxatives

1.3 Animal models of Parkinson's disease

Currently, biomedical research relies heavily on animal models to study pathophysiological mechanisms, and to develop and test therapeutic strategies for human diseases. An animal model was defined by the Institute of Laboratory Animal Resources as [337]:

> *"[…] a living organism with an inherited, naturally acquired, or induced pathological process that in one or more respects closely resembles the same phenomenon occurring in man. Animal models, in this sense, never provide final answers but offer only approximations, for no single animal model can ever duplicate a disease in man. Thus, animal models should not be expected to be ideal, nor to be universally suited to all foreseeable uses. On the other hand, for a model to be a good one, it must provide a new insight, have relevance to a particular problem and respond predictably."*

Animal models, as also stated in the above definition, are not ideal nor universally applicable, as no animal model fully recapitulates human disease. However, they provide a crucial opportunity to expand our knowledge and understanding of the pathophysiology of certain human diseases, and to test therapeutic approaches. To appraise animal models, common validation criteria are used: (1) face validity; (2) construct or etiologic validity; (3) predictive or pharmacological validity (Fig. 1.5) [338].

Face validity indicates whether the animal model recapitulates important symptomatology and neuropathology of the disease it models. Animal models of PD with a high face validity should therefore mimic the slowly progressive nature of symptomatology, develop parkinsonism, and a wide range of non-motor symptoms. Neuropathologically, they should display aSYN-aggregates resembling LBs and LNs, nigrostriatal dopaminergic cell loss, and degeneration in some non-dopaminergic brain regions.

Construct or etiologic validity indicates whether the methods used for the construction (induction) of the animal model are relevant to the etiology of the human disease, i.e. whether the disease in the animal model was triggered by an established cause of the human disease. As PD in humans is idiopathic, which means that the underlying etiology of the disease is to our current knowledge unknown, no PD animal model has a high level of construct validity. However, genetic forms of parkinsonism with mendelian inheritance (e.g. *SNCA* point mutations or duplications/triplication), or toxin-induced parkinsonism can be modelled with high construct validity.

Predictive or pharmacological validity refers to good response to clinically effective pharmacotherapy, which means that a response to treatment in the animal model predicts its effectiveness in humans. In PD animal models, high predictive validity indicates good responsiveness to symptomatic treatment, and, once available, good responsiveness to neuroprotective substances.

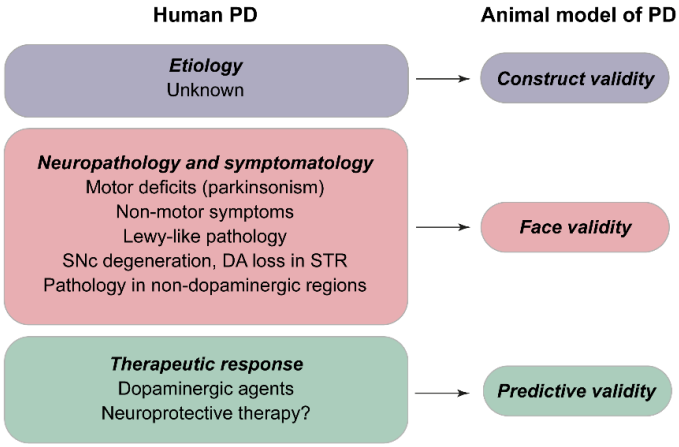

Figure 1.5 | Validation criteria of animal models of Parkinson's disease. Figure adapted from [46].

Currently, PD animal models can be divided into three major groups: (1) traditional, neurotoxin-induced models; (2) genetic models; (3) aSYN-based models.

1.3.1 Neurotoxin-induced animal models of Parkinson's disease

The first attempts to model PD in animals were based on the systemic or local application of distinct neurotoxins inducing nigrostriatal dopaminergic neurodegeneration. These models replicate the degeneration of nigrostriatal dopaminergic neurons and as a consequence, reproduce the motor symptomatology of PD. However, they lack other substantial characteristics: the slowly progressive nature of neuropathology, pathology of non-dopaminergic neural networks, extensive non-motor symptomatology, and aSYN aggregation.

6-hydroxydopamine (6-OHDA), a hydroxylated analogue of dopamine, was the firstly discovered neurotoxin to selectively damage catecholaminergic neurons [256, 314]. Given its hydrophilic nature, systematically administered 6-OHDA cannot cross the blood-brain barrier and thus needs to be stereotactically injected into the SNc, the medial forebrain bundle (mfb), or the striatum (STR) [118, 135, 225, 268, 291]. It enters the neurons via their respective catecholaminergic transporters [dopamine transporter (DAT), noradrenaline transporter (NET)] resulting in the relative selectivity of the neurotoxin to catecholaminergic neurons. Once inside the cells, three distinct mechanisms are proposed to lead to the

observed neurotoxicity: (1) auto-oxidation of 6-OHDA producing highly reactive radicals [256]; (2) MAO-catalyzed metabolism resulting in reactive oxygen species (ROS) production; (3) inhibition of mitochondrial respiratory chain complexes I (NADH:ubiquinone oxidoreductase) and IV (cytochrome x oxidase) resulting in decreased mitochondrial membrane potential, diminished ATP production, and generation of ROS [98]. The major characteristics of the 6-OHDA model are summarized in Table 1.2.

In 1983, Langston and colleagues described four cases of severe and permanent chemically induced parkinsonism in drug abusers due to 1-methyl-4-phenyl-1,2,3,6-tetrahydropyridine (MPTP), a byproduct in the synthesis of the opioid drug 1-methyl-4-phenyl-4-propionoxypiperidine (MPPP) [164]. This discovery has prompted the development of new experimental animal models of PD based on the application of MPTP. As MPTP is highly lipophilic, it readily crosses the blood-brain barrier and thus can be applied systematically (usually intraperitoneally or subcutaneously). Once inside the brain, MPTP is converted to the intermediate 1-methyl-4-phenyl-2,3-dihydropyridinium ($MPDP^+$) in astroglial cells by MAO-B, which then spontaneously oxidizes to the highly neurotoxic 1-methyl-4-phenylpyridinium (MPP^+) [47, 58, 133]. MPP^+ is then taken up via catecholaminergic transporters (DAT, and NET) into catecholaminergic, among others dopaminergic neurons. Once intracellular, it rapidly accumulates in synaptic vesicles and the mitochondrial matrix and exerts its neurotoxic effects by the reversible blockade of the mitochondrial respiratory transport chain complex I resulting in depolarization of the mitochondrial inner membrane, diminished ATP production, and generation of ROS [113, 204, 244]. The major characteristics of the MPTP model are summarized in Table 1.2.

Numerous epidemiological studies have shown that pesticide exposure was associated with a significantly elevated risk to develop PD [12, 64, 86, 119, 302]. This discovery has led to the development of additional neurotoxin-based animal models of PD, such as the chronic rotenone application-model. Rotenone is a naturally occurring compound, which was commonly used as an organic broad spectrum insecticide [26]. It is highly lipophilic and thus, upon systemic administration, it readily crosses the blood-brain barrier and plasma membrane. Once intracellular, similarly to MPP^+, rotenone inhibits the mitochondrial respiratory chain complex I thereby decreasing the inner membrane potential, diminishing ATP production, and generating ROS [26, 283]. Major characteristics of the rotenone-model are summarized in Table 1.2.

Table 1.2 | Common characteristics of neurotoxin-induced animal models of PD. Table adapted from [27]

PD model	Face validity	Construct validity	Predictive validity	Uses	Limitations
6-OHDA	Lesion and temporal manner depends on the injection site (SNc, mfb, STR) • Rapid, massive, and irreversible dopaminergic neurodegeneration • Cell loss SNc > VTA • Robust asymmetric motor deficits • Degeneration of noradrenergic LC neurons *But:* • no aSYN-aggregates	Low level	• Dopaminergic treatment causes rotation due to hemiparkinsonism • Neuroprotection?	• Common and cheap preclinical model • Hemiparkinsonism	• Mortality high with bilateral injections • Intracranial injections needed
MPTP	*Acute dose:* • Dose-dependent degeneration of dopaminergic cells • Cell loss SNc > VTA • Strong motor symptoms • Degeneration of noradrenergic LC neurons *But:* • no aSYN-aggregates *Subacute/chronic dose:* • Progressive model • Moderate to severe degeneration of dopaminergic cells • Cell loss SNc > VTA • Degeneration of noradrenergic LC neurons • aSYN aggregates	High level for MPTP-induced parkinsonism Low level for PD	• Good response to dopaminergic therapy *But* • Several substances which showed neuroprotective efficacy in MPTP models showed no disease-modifying effect in PD	• Common and cheap preclinical model • Commonly used in mice and NHPs	• Rats are resistant • Functional recovery in mice and NHPs
Rotenone	Intragastral application: • Moderate dopaminergic degeneration • Some motor symptoms • aSYN aggregates • Progressive neuropathology Systemic application leads to tauopathy model	High level for pesticide-induced parkinsonism	• Good response to dopaminergic treatment • Good response to Anle138b [323] • Other neuroprotective therapies?	• Environmental risk modeling • Study aSYN aggregation and propagation	• High mortality in rats • Low reproducibility

1.3.2 Genetic models of Parkinson's disease

In 1997, Polymeropoulos and colleagues identified the first mutation leading to an autosomal dominantly inherited familial form of PD: it was a missense mutation of the gene encoding aSYN (*SNCA*) resulting in a change of the amino acid alanine to threonine at position 53 (A53T) in the protein [229]. Soon after this, Spillantini and colleagues discovered that the major component of Lewy bodies, the key neuropathological hallmarks of PD, is the protein aSYN [290]. Furthermore, duplications and triplications of the *SNCA* gene have been identified as an additional cause of early onset hereditary PD. In these cases, a clear relationship between the level of aSYN expression (copy number of the gene) and the age of onset, distribution of neuropathology, severity of disease, and pace of progression could be observed, implicating a dose-dependent effect of aSYN [42, 128]. These major findings have underlined the significance of aSYN in the pathogenesis of PD and prompted the development of genetic mouse models of PD based on the overexpression of aSYN.

The major variables, which have to be considered when evaluating transgenic mouse models overexpressing aSYN: (1) the transgene – which aSYN form is overexpressed [wild-type (WT), mutated, or truncated]; (2) the promotor which drives the transgene expression (pan-cellular, pan-neuronal, or selective for certain neuronal subtypes); (3) the genetic background of the mouse strain, and whether endogenous murine aSYN is expressed; (4) the level of aSYN overexpression (usually ranging between 0.5- to 30-fold of the level of the endogenous aSYN) [77].

Although the developed mouse models recapitulate several key features of human PD, such as aSYN aggregation, mild to severe motor symptoms, striatal DA loss, most of the models fail to exhibit dopaminergic SNc neuronal death despite the fact that they were constructed with a causative mutation of human PD (Table 1.3). Reasons for this might be, among others: (1) differential vulnerability to triggers of neurodegeneration in humans compared to rodents, similar to that observed in toxin-models of PD [236]; (2) for a fully developed disease phenotype, the complex interplay of genetics, cellular and environmental factors are needed, such as microbiome dysbiosis [261]; (3) the transgene affects embryonal stages of development possibly resulting in compensatory mechanisms impacting the expression of the phenotype [153]. Nevertheless, transgenic mouse models are valuable tools to study aSYN-induced cellular dysfunction, differential cellular susceptibility to dysregulated aSYN homeostasis, and to test anti-aggregative drugs as potential disease-modifying therapeutics.

Table 1.3 | Common characteristics of exemplary aSYN-based genetic models of PD

PD model	Face validity	Construct validity	Predictive validity	Uses	Limitations
Thy1-WT-aSYN [79, 80, 155, 163, 343]	• aSYN aggregation in SNc • Severe motor symptoms • Moderate striatal DA loss • Non-motor symptoms (hyposmia, GI dysfunction, autonomic deficits) *But:* • No degeneration of dopaminergic neurons	High level for genetic forms of parkinsonism (SNCA duplication/ triplication) Low level for PD	• Moderate response to dopaminergic therapy • Neuroprotection?	• Modelling familial mutation of *SNCA* • Study aSYN aggregation and propagation • Study non-motor symptoms • Test anti-aggregation drugs	• Limited face validity • Potential compensatory mechanisms during development • Expensive and time-consuming
PrP-A53T-aSYN [96, 185]	• aSYN-aggregates in dopaminergic neurons • Moderate to severe motor symptoms • Mild cognitive dysfunction *But:* • No degeneration of dopaminergic neurons	High level for genetic forms of parkinsonism (A53T-aSYN) Low level for PD	*No data*	• Modelling familial mutation of *SNCA* • Study aSYN aggregation and propagation • Test anti-aggregation drugs	• Limited face validity • Potential compensatory mechanisms during development • Expensive and time-consuming
PrP-A30P-aSYN [173, 323]	• Mild motor symptoms *But:* • No aSYN aggregation • No dopaminergic degeneration	High level for genetic forms of parkinsonism (A30P-aSYN) Low level for PD	• Good response to Anle138b • aSYN immunization?	• Modelling familial mutation of *SNCA* • Study aSYN aggregation and propagation • Test anti-aggregation drugs	• Limited face validity • Potential compensatory mechanisms during development • Expensive and time-consuming
TH-truncated aSYN [282, 307, 331]	• Progressive aSYN aggregation in dopaminergic neurons • Striatal DA loss • Dopaminergic degeneration • Motor and gait impairments	Low level	• Good response to dopaminergic treatment • Good response to Anle138b • aSYN immunization?	• Study aSYN aggregation and propagation • Test anti-aggregation drugs	• Limited face validity • Potential compensatory mechanisms during development • Expensive and time-consuming
PDGFβ-WT-aSYN [11, 186, 187]	• aSYN aggregation in dopaminergic neurons • Striatal DA loss • Motor impairment • Mild cognitive impairment *But:* • No degeneration of dopaminergic cells	High level for genetic forms of parkinsonism (SNCA duplication/ triplication) Low level for PD	• Good response to passive and active immunization against aSYN • Other neuroprotective therapies?	• Modelling familial mutation of *SNCA* • Study aSYN aggregation and propagation • Test anti-aggregation drugs	• Limited face validity • Potential compensatory mechanisms during development • Expensive and time-consuming

1.3.3 α-synuclein-based models of Parkinson's disease

1.3.3.1 Targeted viral vector mediated overexpression of α-synuclein

Viral vectors can be used to transfer genetic material and thus induce protein expression in cells of non-transgenic animals. Loco-regional aSYN overexpression in the central nervous system of model animals with viral vector-mediated approaches represents a valuable alternative to transgenic animal models with numerous distinct advantages: (1) spatial control of transgene expression achieved by loco-regional injection of the vectors; (2) temporal control of the protein expression as the vectors can be injected in adult animals thus limiting the possibility of developmental compensatory mechanisms; (3) the expression level of the protein can be titrated allowing the study of dose-dependent effects; (4) it allows the usage of multiple species ranging from rodents to non-human primates (NHPs) [317]. Nevertheless, as all model systems, viral vector-mediated overexpression models also have some potential caveats: (1) intracerebral delivery requires stereotactic injections, which might disrupt the blood-brain barrier and injure the brain parenchyma resulting in potential confounding effects; (2) the genetic material of some vector systems integrate into the host genome potentially leading to insertional mutagenesis; (3) potential toxicity of viral vectors; (4) lack of absolute specificity to cell types, or –subtypes; (5) due to the overexpression, intracellular aSYN levels are several fold higher than in idiopathic or even *SNCA* multiplication-linked PD are achieved, questioning the relevance of the pathophysiological mechanisms leading to the disease phenotype in the experimental model [53, 67].

Until now, two viral vector systems have been explored to model PD in animals: recombinant adeno-associated viral (rAAV) vectors, and lentiviral vectors (LV). The major characteristics of the two viral vector systems are summarized in Table 1.4. As the animal model used in this dissertation is based on rAAV vector-mediated overexpression of aSYN, and the rAAV vectors are far more commonly used than LVs, we will focus on the rAAV vector system.

Table 1.4 | Major characteristics of the rAAV and LV vector systems

	rAAV	LV
Genome	ssDNA	ssRNA
Packaging capacity	4.5-5 kilobase	7-7.5 kilobase
Integration into host genome	Rarely	No
Long-lasting gene expression	Yes	Yes
Pathogenic	No	Yes
Transduction of dividing cells	Yes	Yes
Transduction of non-dividing cells	Yes	Yes
Host immune response	Low	Low
Limitations	Low packaging capacity	Insertional mutagenesis

Recombinant AAV vectors are small, single-stranded DNA (ssDNA) viruses, which *per se* are non-pathogenic and non-replicative and are therefore considered to be safe [317]. Once injected *in vivo*, viral particles are taken up by host cells via receptor-mediated internalization, and transported to the nucleus where the viral genome (the transgene) is released and the second strand of DNA is replicated. Thereafter, the gene of interest is transcribed leading to stable and long-lasting expression of the required protein [175].

Thus far, eleven serotypes of rAAV vectors are known (rAAV1-11), which differ in their antigenic profile and their tissue and cell tropism, i.e. in their ability to transduce different tissue- and cell types [40, 342]. To optimize transduction efficiency and tropism of the viral vectors, rAAVs can be pseudotyped, that is, the genome of a certain serotype (most commonly AAV2) is packed into the capsid derived from a different rAAV serotype [35, 161, 342]. In these cases, rAAV vectors are named as rAAV2/5, rAAV2/6, etc., where the first number refers to the genome serotype, whereas the second number implicates the capsid serotype [317]. Specificity of the viral vector can additionally be ameliorated with the choice of the promotor driving transgene expression. Whereas cytomegalovirus (CMV) or chicken β-actin (CBA) promotors allow robust protein expression, but possess no cell type specificity, cell type specific promotors, such as Olig1 (for oligodendroglial cells), synapsin-1 (for neuronal cells), or tyrosine hydroxylase (TH) promotor (for dopaminergic and noradrenergic neurons) allow the highly specific targeting of determined cell types or –subtypes [60, 182].

A major advantage of viral vector mediated overexpression is the spatial control of expression, that is, they allow the transduction of definite brain regions of interest when injected stereotactically [53]. In experimental animals modeling PD, the dopaminergic SNc is most commonly targeted with rAAV vectors containing the transgene of human WT or mutated aSYN. In contrast to transgenic animal models, viral vector mediated overexpression of aSYN driven leads to the accumulation of aggregated aSYN reminiscent of human LBs and LNs in dopaminergic neurons, progressive dopaminergic deafferentation of the STR and nigrostriatal dopaminergic cell death as well as L-DOPA responsive motor deficits mimicking parkinsonism (Table 1.5) [60, 72, 131, 142, 147]. Anterograde transport of the expressed human aSYN is observed over long distances to known SNc and ventral tegmental area[1] output regions, such as the STR, olfactory tubercle, nucleus accumbens, lateral septum, and the anterior cingulate cortex [142]. Characteristics of common rAAV- and LV-models of PD are summarized in Table 1.5.

[1] Dopaminergic cell group adjacent to the SNc. Targeted delivery of viral vectors to the SNc transduce VTA neurons as well due to the unspecificity of the viral vectors.

Table 1.5 | Common characteristics of exemplary viral vector-based animal models

PD model	Face validity	Construct validity	Predictive validity	Uses	Limitations
rAAV2/2-CBA-A53T- or WT-aSYN in SNc **Rat** [142]	• aSYN aggregation in SNc • Moderate to severe dopaminergic degeneration • Moderate striatal DA loss • Mild to moderate motor symptoms	Low level	• Good response to dopaminergic treatment • Beneficial response to STN-DBS therapy	• Study aSYN aggregation and propagation • Study aSYN-induced dopaminergic cellular dysfunction	• Expensive and time-consuming • Potential vector toxicity • Requires intracranial injections
rAAV1/2-CMV-A53T-aSYN in SNc **Mouse** [131, 147, 202]	• aSYN aggregation in SNc • Moderate degeneration of dopaminergic neurons • Moderate striatal DA loss • Moderate motor deficits	Low level	• Beneficial response to STN-DBS therapy • Neuroprotection?	• Study aSYN aggregation and propagation • Study aSYN-induced dopaminergic cellular dysfunction	• Expensive and time-consuming • Potential vector toxicity • Requires intracranial injections
rAAV2/5-CBA-A53T-aSYN in SNc **NHP** [72]	• aSYN aggregation • Moderate degeneration of dopaminergic neurons • Moderate motor deficits	Low level	*No data*	• Study aSYN aggregation and propagation • Study aSYN-induced dopaminergic cellular dysfunction	• Expensive and time-consuming • Potential vector toxicity • Requires intracranial injections
rAAV2/6-Syn1-WT-aSYN in SNc **Rat** [60]	• aSYN aggregation in SNc • Severe degeneration of dopaminergic neurons • Moderate motor deficits	Low level	• Good response to dopaminergic treatment	• Study aSYN aggregation and propagation • Study aSYN-induced dopaminergic cellular dysfunction	• Expensive and time-consuming • Potential vector toxicity • Requires intracranial injections
rAAV2/6-WT-aSYN in vagal nerve **Mouse** [255, 311]	• aSYN aggregation in DMV and AMB • Neurodegeneration in LC, distant from the injection site *But* • No degeneration of DMX (injection site) • No degeneration of SNc	Low level	*No data*	• Study aSYN aggregation and propagation • Study aSYN-induced cellular dysfunction	• Expensive and time-consuming • Requires injections • Potential vector toxicity • Biosafety issues
LV-CMV-A30P in SNc **Rat** [166, 176]	• aSYN aggregation in SNc • Mild to moderate degeneration of dopaminergic neurons • Mild motor phenotype	Low level	• Good response to dopaminergic treatment • No beneficial effect of GDNF therapy • Neuroprotection?	• Study aSYN aggregation and propagation • Study aSYN-induced cellular dysfunction	• Expensive and time-consuming • Requires intracranial injections • Potential vector toxicity • Biosafety issues

1.3.3.2 α-synuclein pre-formed fibril models

In vitro, recombinant monomeric aSYN readily self-aggregates and assembles into highly ordered amyloid fibrils reminiscent of aSYN fibrils extracted from LBs of postmortem PD brains (Fig. 1.6) [54, 56, 95, 280, 315]. This self-aggregative process can be catalyzed by the addition of aSYN PFF's in which scenario the lag phase (nucleation process) is omitted and the exogenously added PFF's serve as templates for the aggregation facilitating the polymerization process (Fig. 1.6) [340]. It is proposed that a similar reaction takes place when PFF's are introduced to *in vitro* cellular models. It was shown that PFF's, when added to primary neuronal cell cultures are readily taken up by neurons into their intracellular space where they seed the recruitment of endogenous aSYN thereby leading to neuronal dysfunction and cell death [62, 83, 320, 321]. These observations led to the development of *in vivo* PFF animal models, in which aSYN PFF's are introduced stereotactically into distinct brain regions of WT- or transgenic experimental animals.

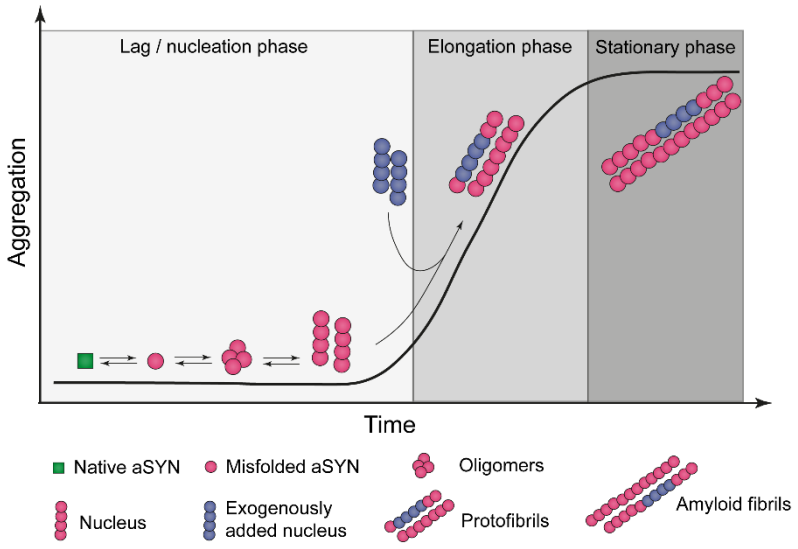

Figure 1.6 | Schematic representation of the aggregation process of aSYN *in vitro*.
The polymerization of aSYN *in vitro* can be divided into three phases. In the lag phase or nucleation phase, native aSYN monomers become misfolded, assemble into oligomers and build prefibrillar forms of aSYN (nucleus). This is followed by the elongation phase, in which the previously developed prefibrillar forms of aSYN serve as templates for the aggregation of the aSYN in the solution. In the stationary phase, maximum fibril growth has occurred. This process can be catalyzed by the addition of exogenous seeds (PFF's, dark blue circles), with the help of which the nucleation phase is omitted.

PFF models possess numerous advantages: (1) they allow the targeted induction of pathology via stereotactic injection into predetermined brain regions (spatial control); (2) PFF's can be introduced into elder animals omitting the possibility of developmental compensatory mechanisms as seen in transgenic animal models (temporal control); (3) aSYN aggregation is triggered in the presence of physiological aSYN concentrations, which likely resembles the pathophysiological state of idiopathic PD more, (4) it allows the usage of multiple species ranging from rodents to NHPs [67]. Nevertheless, certain caveats also need to be considered: (1) administration of PFF's need intracerebral injections leading to disruption of the blood-brain barrier and injury of the brain parenchyma potentially resulting in confounding factors; (2) the production and sonication parameters of PFF's likely influence their seeding capacity leading to potentially significant inter-laboratory differences.

Thus far, PFF's have been injected into various brain regions, gastric and intestinal wall, and even muscle of mice, rats, and NHPs [125, 179, 189, 190, 222, 257]. Regardless of the targeted region, PFF inoculation led to formation of hyperphosphorylated, p62-, and Ubi-1-positive aSYN aggregates highly reminiscent of human LBs and LNs at the inoculation site. Moreover, aggregate formation was not restricted to the vicinity of the injection but also involved neuronal structures far away from the site of inoculation. Pathology was found in axons as well as somata of neurons in distant brain regions.

The most often targeted regions to model PD are the STR and SNc. Injection of these two brain regions led to aSYN aggregate formation in the SNc, reactive microgliosis at the injection site, progressive dopaminergic deafferentation of the STR and nigrostriatal dopaminergic cell death manifesting as mild to severe motor symptomatology resembling human parkinsonism (Table 1.6). Over time, PFF induced pathology progressed in the brain in a stereotypical temporo-spatial manner to regions such as the amygdala, septal nucleus, entorhinal, motor, and somatosensory cortices [189].

Characteristics of available PFF-induced animal models of PD are summarized in Table 1.6.

Table 1.6 | Common characteristics of PFF-induced animal models

PD model	Face validity	Construct validity	Predictive validity	Uses	Limitations
PFF's or LB extracts in STR or SNc [179, 189, 190, 222, 239, 308, 332]	• aSYN aggregates in SNc and in brain regions distant from the injection site • Moderate to severe degeneration of SNc dopaminergic neurons • Moderate to severe motor deficits	Low level	• Good response to passive immunotherapy	• Study aSYN aggregation and propagation • Study aSYN-induced cellular dysfunction	• Requires special equipment to produce PFF's • Requires intracranial injections • Biosafety issues
PFF's in OB [242, 243]	• aSYN aggregates in OB and in brain regions distant from the injection site • Progressive olfactory deficit • Moderate cell loss in the AON	Low level	*No data*	• Study aSYN aggregation and propagation • Study aSYN-induced cellular dysfunction	• Requires special equipment to produce PFF's • Requires intracranial injections • Biosafety issues
PFF's or LB extracts in stomach or intestines [125, 140]	• aSYN aggregates in the gut and the central nervous system distant from the injection site • Moderate degeneration of dopaminergic SNc neurons • Moderate to severe DA loss in the STR • Significant reduction of DAT SPECT signal in the STR • Motor symptoms, olfactory deficits, anxiety, depressive-like symptomatology	Low level	*No data*	• Study aSYN aggregation and propagation • Study aSYN-induced cellular dysfunction	• Requires special equipment to produce PFF's • Requires intragastric injections • Biosafety issues
PFF's in hind limb muscle **M83 and M20 transgenic mice** [257]	• aSYN aggregates in the spinal cord and central nervous system distant from the injection site • Mild to severe motor impairment *But* • No data on SNc dopaminergic degeneration	Low level	*No data*	• Study aSYN aggregation and propagation from the periphery • Study aSYN-induced cellular dysfunction	• Requires special equipment to produce PFF's • Biosafety issues
rAAV-Syn1-WT-aSYN and PFF's in SNc [223, 304]	• Extensive aSYN aggregation at the injection site and STR • Moderate to severe degeneration of SNc dopaminergic neurons *But* • No data on motor phenotype	Low level	*No data*	• Study aSYN aggregation and propagation • Study aSYN-induced cellular dysfunction	• Requires special equipment to produce PFF's • Requires two intracranial injections • Biosafety issues

1.4 The pedunculopontine nucleus

1.4.1 Functional neuroanatomy of the pedunculopontine nucleus

The pedunculopontine nucleus (PPN) is a small nucleus located in the dorsal tegmentum of the mesencephalon and upper pons. The PPN is neurochemically heterogeneous and encompasses three distinct neuronal subtypes: (1) large, darkly staining cholinergic neurons; (2) small to medium sized γ-aminobutyric acid-synthetizing (GABAergic) neurons; and (3) small glutamatergic neurons [327]. A recent stereological study estimating the ratio of the three cell types in the rat PPN revealed that cholinergics make up for approximately 25%, glutamatergics for 43%, and GABAergics for around 32% of neurons [181], largely confirming older studies reporting similar proportions [327]. The distribution of the different neuronal subtypes is not homogeneous over the rostro-caudal extent: small to medium sized GABAergic neurons are more abundant in the rostral part of the PPN, whereas large cholinergic and glutamatergic neurons are rather found in caudal subregions (Fig. 1.7A) [227]. Indeed, the uneven caudo-rostral distribution of cholinergic neurons led to the subdivision of the PPN into two major parts: (1) pars dissipatus, mainly comprising small GABAergic neurons and a few scattered large, cholinergic neurons in the rostral part; and (2) pars compacta, comprising densely clustered large cholinergic neurons intermingled with glutamatergic neurons located caudally [212].

The projection targets of the three neuronal subtypes are largely different. Single-cell tracing studies of cholinergic PPN neurons revealed thin, highly arborizing axons innervating large areas of the CNS. Two pathways could be distinguished: (1) an ascending pathway innervating brain regions rostral from the PPN; and (2) a descending pathway innervating caudal regions such as the pontine reticular formation, and the spinal cord [196]. The ascending pathway could be further subdivided into a ventral stream innervating midbrain dopaminergic cells, hypothalamic structures, amygdala, and the STN; and a dorsal stream innervating vast parts of the thalamus, and the inferior and superior colliculi [196]. Viral vector mediated cell-type specific anterograde tracing studies have largely confirmed these results and identified additional target regions of cholinergic neurons: medial and lateral septal nuclei, basal forebrain structures, midbrain periaqueductal gray, and sublaterodorsal tegmental nucleus (Fig. 1.7B) [154].

The projectomes of glutamatergic and GABAergic PPN neurons are much more sparsely investigated. A recent study utilizing cell-type specific anterograde tracing technique investigated target regions of the different PPN neuronal subtypes. They revealed that

glutamatergic PPN neurons densely innervated the caudal basal forebrain, limbic areas such as the bed nuclei of the stria terminalis, STN, ventral tegmental area, and both parts of the substantia nigra. Weak innervation was observed of distinct hypothalamic and thalamic regions, and caudal portions of the globus pallidus (Fig. 1.7C) [154]. In contrast to previous reports, the majority of axons of GABAergic PPN neurons remained within the boundaries of the PPN implicating that these neurons are local inhibitory interneurons rather than projection neurons (Fig. 1.7D) [154].

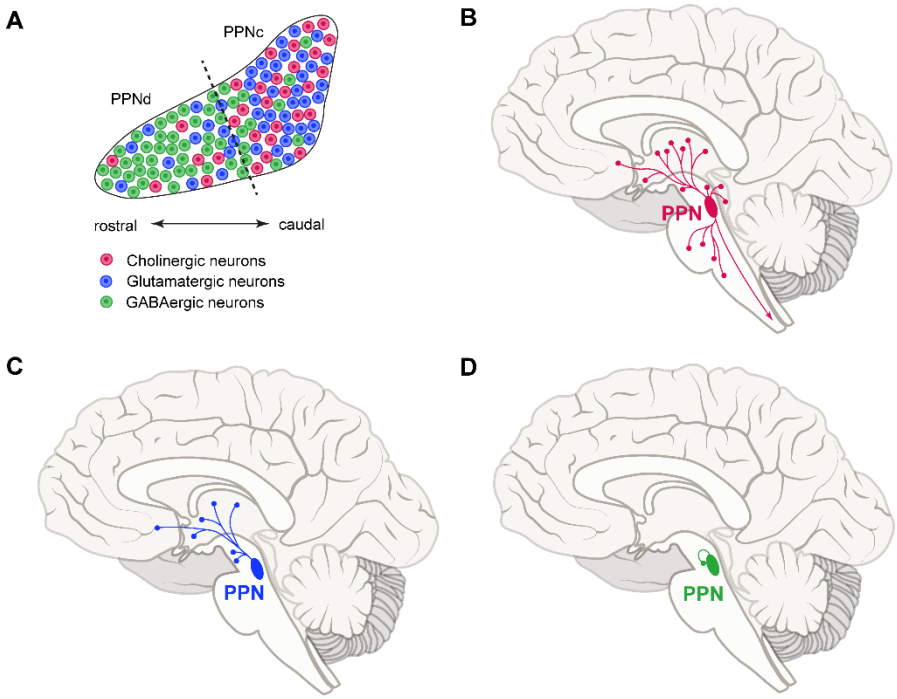

Figure 1.7 | The output projectome of the PPN.

- **A.** Rostro-caudal distribution of the distinct cellular subtypes in the PPN. Cholinergic and glutamatergic neurons are abundantly found in the compact subdivision of PPN laying caudally (PPNc), whereas GABAergic neurons are mostly found in the rostral portion called pars dissipatus (PPNd). Figure adapted from [227] based on [181].
- **B.** Output connectome of the cholinergic PPN based on two tracing studies [154, 196].
- **C.** Output connectome of the glutamatergic PPN based on [154].
- **D.** Output connectome of the GABAergic PPN based on [154].

The PPN receives direct projections from sensory areas such as the superior and inferior colliculi; motor areas such as the deep cerebellar nuclei, motor cortex, and basal ganglia structures; and from brain structures implicated in the regulation of the sleep/wake cycle such as the lateral hypothalamus, tuberomamillary nucleus, and laterodorsal tegmental nucleus [19, 105]. However, studies on the cell-type specific input connectomes of the PPN are sparse. Only recently a study investigated the input connectomes of the glutamatergic

and GABAergic PPN using a cell-type specific trans-synaptic rabies virus tracing technique [254]. According to this study, glutamatergic PPN neurons receive dense innervation from several basal ganglia structures such as the reticular part of the substantia nigra (SNr), STN, and dorsomedial striatum. Additionally, strong projections were observed from the central part of the amygdala, the oval nucleus of the bed nuclei of the stria terminalis, hypothalamic regions, and the superior colliculus. In contrast to this, GABAergic PPN neurons seemed to receive only sparse innervation from basal ganglia structures, whereas strong innervation from the superior colliculus, dorsal raphe nuclei, the oval nucleus of the bed nuclei of the stria terminalis, hypothalamic regions, and the preoptic area. To our knowledge, no cell-type specific tracing studies of cholinergic PPN neurons are available.

The PPN's extensive connections with functionally and anatomically diverse brain regions and its natural heterogeneity underpin that it is involved in several highly preserved brain functions [105, 227]. Projections from the PPN have been implicated in: (1) arousal and REM-sleep as a critical component of the ascending reticular arousal system (ARAS) via ascending pedunculo-thalamo-cortical pathways [154]; (2) modulation of motor activity over descending projections to brainstem motor regions and cortico-striatal circuits [254]; (3) generation of rapid responses as a result of integrating sensory input from different modalities [105]; and (4) making new action-outcome associations [2, 139].

1.4.2 Implications in Parkinson's disease

According to the neuropathological staging scheme of Braak, the PPN displays Lewy pathology in stage 3 of the disease, thus, the occurrence of LB in the PPN coincides with LB pathology in the SNc (see chapter 1.1.3) [30, 31]. Remarkably, despite the neurochemical heterogeneity of PPN neurons, the vast majority of aSYN aggregates are found in the cholinergic neuronal subpopulation [108, 346]. Additionally, several studies reported severe cell loss of cholinergic neurons ranging between 36 and 57% [117, 122, 137, 226, 249]. In stark contrast to this, stereological studies estimating degeneration of GABAergic PPN neurons reported an average loss 18% compared to 50% of loss of cholinergic PPN neurons in the same patients [226]. This suggests that cholinergic neurons are inherently more susceptible to the disease process.

The PPN provides the major source of cholinergic innervation to the thalamus via the pedunculo-thalamic pathway. As a consequence, neuroimaging of thalamic cholinergic innervation likely reflects the integrity, or, under pathological conditions, the dysfunction of PPN cholinergic pedunculo-thalamic efferents. Several studies reported thalamic cholinergic

denervation in PD patients implicating PPN cholinergic dysfunction and/or degeneration [28, 152, 201]. Additionally, thalamic cholinergic denervation seemed to correlate with the occurrence of gait disorders and falls [28, 201]. This finding is further supported by neuropathological studies observing a significantly greater reduction of cholinergic PPN neurons in PD patients with a history of falls compared to PD patients without falls or healthy controls [137]. This underpins the importance of PPN in the modulation of gait and locomotion.

The involvement of the PPN in the disease process and the resulting deafferentation of PPN output regions are implicated in the pathophysiology of several motor and non-motor symptoms of PD, including gait disorders, sleep disorders such as RBD, and certain cognitive deficits [19, 82].

1.5 The locus coeruleus-noradrenergic system

1.5.1 Functional neuroanatomy of the locus coeruleus

The locus coeruleus (LC) is a small, bilateral nucleus in the rostral pontine tegmentum, located in close vicinity to the 4th ventricle [18]. It mainly contains noradrenergic neurons, however, recent evidence indicates the existence of local GABAergic neurons [33]. It encompasses around 1500 neurons per hemisphere in rodents, and between 10 000 and 35 000 neurons in humans [24]. The LC-noradrenergic system possesses long, thinly or unmyelinated, hyperbranched axons [8]. In spite of the small cell number and owing to its extensively ramified axonal arborization, it represents the major source of noradrenaline to vast parts of the brain. Its axonal projections form three major pathways innervating various regions of the CNS spanning over the whole rostro-caudal extent of the neuroaxis: (1) the ascending pathway innervates all areas of the neocortex, midbrain structures (e.g. raphe nuclei, superior colliculus), the thalamus (mainly the intralaminar thalamic nuclei), and parts of the limbic system such as the amygdala and the hippocampus; (2) the cerebellar pathway innervates the deep cerebellar nuclei and the cerebellar cortex; and (3) the descending pathway innervates brainstem motor nuclei, such as the dorsal motor nucleus of the vagal nerve, and spinal neurons (Fig. 1.8) [298]. Remarkably, the only CNS regions devoid of LC-noradrenergic innervation are the caudate nucleus, the putamen, the internal and external divisions of the globus pallidus, the substantia nigra, and the nucleus accumbens [276].

The LC-noradrenergic system not only broadcasts information to wide array of brain regions, but it was shown to receive direct input from a just as large variety of structures. Highly

advanced rabies viral genetic tracing techniques revealed up to 111 brain regions directly innervating LC noradrenergic cells, where 9-15 different brain regions made monosynaptic contact with individual LC cells [33, 277]. The LC receives monosynaptic input from functionally diverse brain regions: (1) sensory areas, such as brainstem sensory nuclei or the dorsal horn neurons of the spinal cord; (2) motor areas, such as the substantia nigra, motor cortical areas, or deep cerebellar nuclei; (3) limbic regions, such as the amygdala or the bed nuclei of the stria terminalis; (4) brain regions implicated in sleep/arousal regulation, such as the periaqueductal gray; (5) autonomic regions, such as the paraventricular hypothalamic nucleus; and (5) brain regions implicated in cognitive functions, such as basal forebrain structures, and the prefrontal cortex [33, 277].

LC-noradrenergic neurons possess two distinct modes of chemical transmission: (1) synaptic or wiring transmission refers to highly organized connections between neurons, where point-to-point chemical neurotransmission between two cells takes place; and (2) volume or paracrine transmission implicates non-synaptic neurotransmitter release, were the released neurotransmitter (so called neuromodulator) diffuses through the interstitial space and cerebrospinal fluid, resulting in a diffuse, hormone-like modulation of nearby neuronal as well as glial cells [87, 120]. Remarkably, a few studies investigating the proportion of the two neurochemical transmission systems in cortical noradrenergic efferents revealed that synaptic contacts responsible for wiring neurotransmission were only seen in up to 20% of neurotransmitter release sites implicating that cortical noradrenergic neurotransmission relies mostly on a non-junctional system [51, 279].

The LC-noradrenergic system is engaged in several highly preserved brain functions such as the regulation of the sleep-wake cycle [301], enhancement of arousal [7, 23], facilitation of behavioral adaptions elicited by novel environmental stimuli, modulation of cognitive processes such as memory consolidation and –retrieval [265], and controlling autonomic functions [329]. LC-noradrenergic neurons display state-dependent activity: they are fully quiescent during rapid eye movement (REM) sleep, discharge at low rates during non-REM sleep, and at high rates during waking and wakefulness [81, 301]. Their neuronal activity closely correlates with the level of behavioral and cortical arousal and cognitive performance [38, 97, 266].

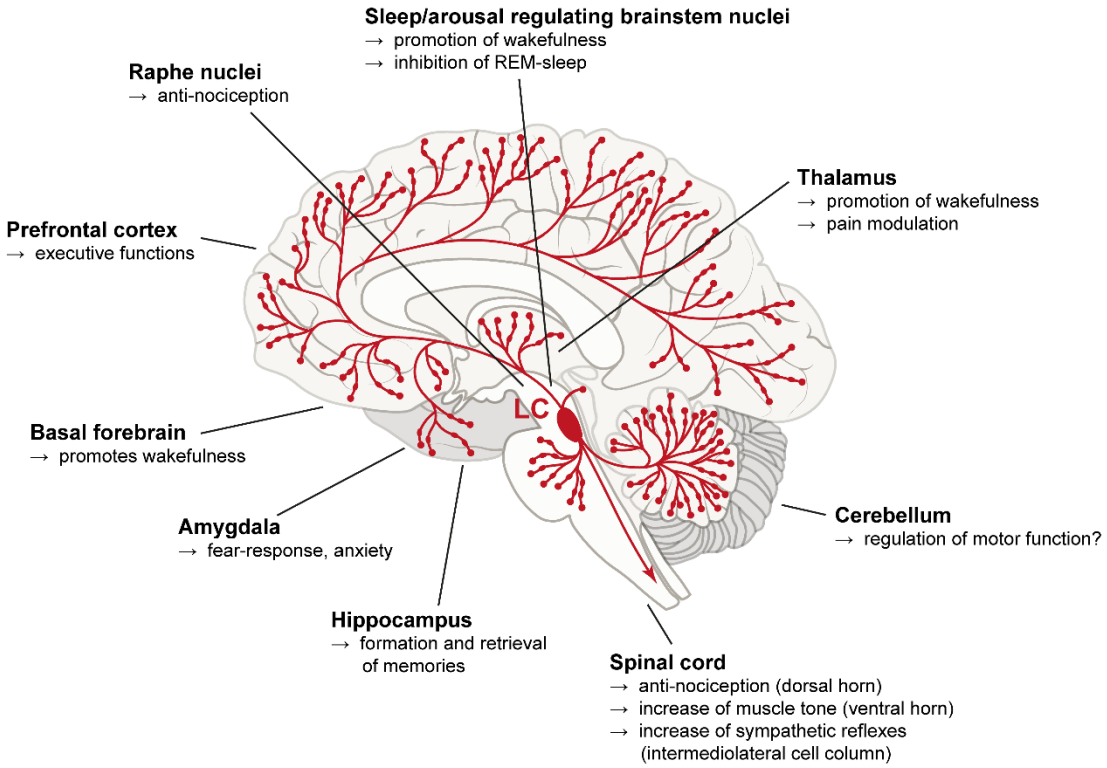

Figure 1.8 | Neuroanatomy of the LC-noradrenergic efferent pathways and their functions.

Interestingly, the LC noradrenergic fibers do not only make contact with neurons, but also with non-neuronal cells and structures by which they exert distinct neuromodulatory effects. It was shown that noradrenergic modulation of microglial cells decreases the production of pro-inflammatory cytokines thereby exerts anti-inflammatory effects; noradrenergic innervation of astroglial cells seems to promote the brain's metabolic responses to stress; and innervation of the blood vessels is implicated in the activity-dependent redistribution of cerebral blood volume promoting functional hyperemia in highly active brain regions [17, 76, 237, 298].

1.5.2 Implications in Parkinson's disease

A large body of evidence indicates that LB formation of noradrenergic LC neurons antedates the occurrence of Lewy pathology in and neurodegeneration of the dopaminergic SNc [30, 31, 132, 310]. According to the Braak staging hypothesis, the LC is affected in stage 2, just after the affection of the dorsal motor nucleus of the vagal nerve and the OB (see chapter 1.1.3) [30, 31]. Studies of neurodegenerative LC changes during the disease have reported 21 to 93% of neuronal cell loss in advanced PD stages, however, data of early PD stages are lacking [25, 41, 94, 108, 121, 221]. Neurodegeneration is usually distributed homogeneously

over the rostro-caudal extent of the LC, but in PD patients with dementia, the rostral portions of the LC display more severe cell loss [41]. Remarkably, although noradrenergic LC neurons display Lewy pathology earlier in the disease process than dopaminergic SNc neurons, they generally show less neurodegeneration than SNc neurons [41, 108, 109]. It is therefore tempting to speculate that LC neurons might have inherent properties which render them particularly vulnerable to pathophysiological processes underlying disease initiation, however, might have intrinsic features rendering them partially resilient against pathologic processes underlying disease progression.

Neuromelanin (NM)-sensitive magnetic resonance imaging (NM-MRI) allows the *in vivo* visualization of NM-content in neuromelanized brain nuclei, such as the LC and the SNc. Studies pursued in early and advanced stage PD patients observed significantly attenuated signal intensities in the LC region implicating loss of NM-containing LC neurons, a significant decrease of intracellular NM-content, or both [39, 199, 209, 267, 278]. Moreover, a study investigating NM-MRI signals in the LC region of patients with RBD, the most specific prodromal symptom of PD has revealed significantly diminished NM signal intensities in the LC region, indicating that the LC is already affected in prodromal PD [68].

The involvement of the LC in the disease process and the resulting noradrenergic deafferentation of LC output regions are implicated in the pathophysiology of several NMS of PD such as depression, anxiety, apathy, fatigue, cognitive impairment and dementia [61, 84, 240, 347].

2 Aims of the study

The aim of the present study was twofold.

Firstly, we wanted to investigate whether the selective vulnerability pattern of PPN neuronal subpopulations seen in human PD also translates into an animal model. Therefore, we aimed to establish a novel PD mouse model by targeted injection of PFF's into the PPN and analyze the induced local pathological alterations in a timely manner. The specific scientific questions were the following:

1. Does the local injection of PFF's induce aggregate formation in the PPN?
2. Does injection of aSYN PFF's induce α-synucleinopathy in all three neuronal subtypes, i.e. are cholinergic, GABAergic and glutamatergic neurons similarly affected?
3. Do all three neuronal subtypes degenerate in a comparable manner?
4. Does the local induction of α-synucleinopathy induce reactive microgliosis?

Currently, the two most popular animal models in the PD field rely on the focal induction of α-synucleinopathy either by targeted inoculation of PFF's or by loco-regional injection of aSYN-overexpressing viral vectors. Therefore, in a second set of experiments, we aimed to compare the brain-wide propagation pattern of two focally induced α-synucleinopathy mouse models, in which the initiation of the aSYN aggregation process and the site of α-synucleinopathy induction was different. To compare the aSYN propagation patterns in these two models, the following scientific questions were raised:

1. How does the brain-wide pattern of propagation look like in the different models?
2. Is the aSYN signal localized predominantly in axonal processes or perikarya?
3. Can a cell-to-cell transmission of aSYN be proven in the models?
4. What are the predominant aSYN species in distant brain regions?

3 Materials and methods

3.1 Experimental design

This study consists of two major parts.

In the first part of the study (Fig. 2.1A), PFF or monomeric aSYN (control) induced pathological changes were evaluated in a mouse model of PD. Therefore, PFF's or monomeric aSYN (control) were injected in the left PPN of wild-type mice. Subsequently, animals were consecutively sacrificed with transcardial perfusion 1, 6, and 12 weeks post-injection (wpi) for immunohistochemical analysis of: (1) locally induced pathology to delineate selective cellular vulnerability; and (2) brain-wide propagation of the PFF-induced pathology.

In the second part of the study (Fig. 2.1B), adeno-associated viral vectors containing the gene of human mutant A53T-aSYN or Luciferase (control) were injected into the right LC region of wild-type mice. Animals were sacrificed with transcardial perfusion 1, 3, 6, and 9 wpi for immunohistochemical analysis of brain-wide propagation of the locally induced pathology.

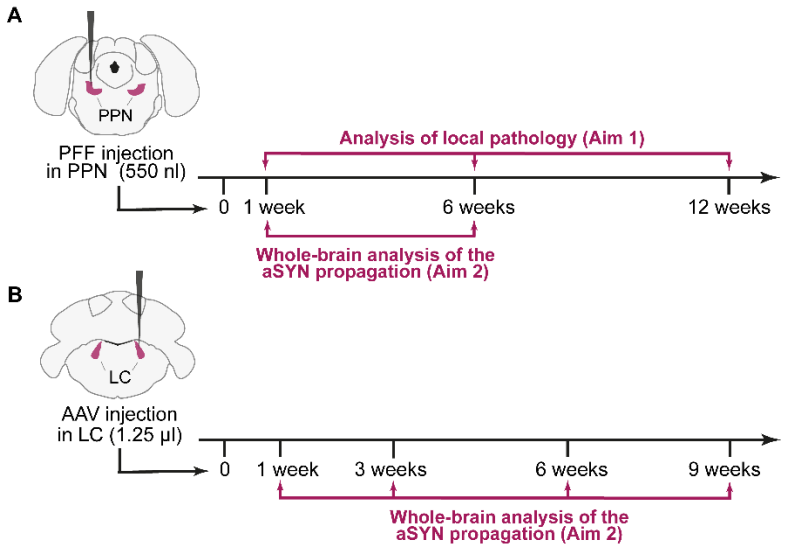

Figure 2.1 | Experimental design

A. Experimental design and schematic illustration of PFF injection into the left PPN of the mouse. Animals were consecutively sacrificed after 1, 6, and 12 weeks for immunohistochemical evaluation.

B. Experimental design and schematic depicting viral vector injection into the right LC of mouse. Animals were consecutively sacrificed after 1, 3, 6, and 9 weeks for immunohistochemical evaluation.

3.2 Materials and chemicals

3.2.1 Expendable supplies and materials

Bepanthen creme	Bayer
Bepanthen® eye ointment	Bayer
Combitips	Eppendorf
Costar® 12-well Clear TC-treated Well plates	Corning Incorporated
Cover slips	Menzel-Gläser GmbH
CryoPure tubes	Sarstedt
Ethibond Excel™ 3-0 USP, 19 mm 3/8c	Ethicon
Eukitt® Quick-hardening Mounting Medium	Sigma-Aldrich
Gloves (size M, powder free)	NOBA GmbH
Microscope glass slides	Menzel-Gläser GmbH
Nanofil stainless needle, 33G	World Precision Instruments (WPI)
Nanofil syringe	World Precision Instruments (WPI)
Netwell™ 12-well Carrier Kit for 15 mm Inserts	Corning Incorporated
Pasteur pipettes	Sarstedt
Pipette tips (10 µl, 100 µl, and 1000 µl)	Eppendorf AG
Pipettes (5 ml, 10 ml, 25 ml)	Sarstedt
ProLong Diamond Antifade Mountant	Thermofisher Scientific
Sterilin 100 mm Square Petri Dishes	Bibby Sterilin
Surgical instruments (scissors, forceps, etc.)	Bochem Instrumente
Tissue freezing medium	Leica

3.2.2 Stereotactic operations, perfusion, and brain processing

AAV1/2-CMV/CBA-A53T-aSYN vector	GeneDetect
AAV1/2-CMV/CBA-Luciferase	GeneDetect
Biotin tagged aSYN Monomers	Provided by Ted M. Dawson (John Hopkins University)
Carprophen	Zoetis
Glycerol (99.5+%)	Sigma-Aldrich
Ketamin	Intervet
Lidocain 5%	Serumwerk Bernburg
Na_2HPO_4	Merck Millipore

NaCl	Sigma-Aldrich
NaH_2PO_4	Merck Millipore
Paraformaldehyde (PFA)	Roth
Preformed aSYN fibrils (PFF's)	Provided by Ted Dawson (John Hopkins University)
Xylazine (2%)	Bayer
Sterile NaCl (0.9%) solution	Braun
Sucrose (99.95%)	Sigma-Aldrich

3.2.3 Immunohistochemistry

3.2.3.1 Solutions, chemicals, and kits

3,3'-diaminobenzidine (DAB)	Serva
DAPI	Sigma-Aldrich
Ethanol absolute (>99.8%)	Otto Fischar GmbH & Co.
H_2O_2 (30%)	Merck Millipore
Methanol (99.8%)	Sigma-Aldrich
Na-hypochlorite	Roth
Normal donkey serum	Millipore
Proteinase K	Invitrogen
SK-4700 SG Peroxidase Kit	Vector Laboratories
Triton X-100	Sigma-Aldrich
Vectastain® Elite® ABC HRP Kit	Vector Laboratories
Xylene	J.T.Baker

3.2.3.2 Primary antibodies

Antigen	Host	Cat. No.	Manufacturer	Dilution
Alpha-synuclein (p-S129)	Rabbit	ab51253	Abcam	1:2000
Choline Acetyltransferase (ChAT)	Goat	AB144P	Merck Millipore	1:100
IbA1	Rabbit	019-19741	Wako	1:500
Neuron N (NeuN)	Mouse	MAB377	Merck Millipore	1:1000
SQSTM1/p62	Mouse	ab56416	Abcam	1:2000
Human α-synuclein (Syn211)	Mouse	AH90261	ThermoFisher Scientific	1:1000
Luciferase	Goat	NB100-1677	Novus Biologicals	1:250
MAP2	Chicken	ab5392	Abcam	1:2000
Ubiquitin (Ubi-1)	Mouse	ab7254	Abcam	1:2000

3.2.3.3 Secondary antibodies

Antigen	Host	Cat. No.	Manufacturer	Dilution
Anti-chicken Cy3	Donkey	703-165-155	Jackson ImmunoResearch	1:1000
Anti-goat AlexaFluor405	Donkey	ab175664	Abcam	1:1000
Anti-goat AlexaFluor488	Donkey	A-11055	Invitrogen	1:1000
Anti-goat Cy3	Donkey	705-165-147	Jackson ImmunoResearch	1:1000
Anti-mouse AlexaFluor488	Donkey	A-2102	Invitrogen	1:1000
Anti-mouse Cy3	Donkey	715-165-150	Jackson ImmunoResearch	1:1000
Biotinylated anti-mouse	Donkey	715-065-151	Jackson ImmunoResearch	1:1000
Biotinylated anti-rabbit	Donkey	711-065-152	Jackson ImmunoResearch	1:1000
Biotinylated anti-goat	Donkey	705-065-147	Jackson ImmunoResearch	1:1000
Streptavidine AlexaFluor647	Donkey	016-600-084	Jackson ImmunoResearch	1:1000

3.2.4 Buffers and solutions

Antifreeze working solution (1 l):	NaH_2PO_4	1.57 g
	Na_2HPO_4	5.18 g
	H_2O dest.	400 ml
	ethylenglycol	300 ml
	glycerol	300 ml
0.1 M phosphate buffer (PB) working solution (10 l):	Na_2HPO_4	115 g
	NaH_2PO_4	26.22 g
	Adjust to pH 7.4 with NaOH (30%) and filter	
0.1 M PB with Triton X-100 (PBT) working solution (1 l):	0.1 M PB	1 l
	Triton X-100	3 ml
Phosphate buffered saline (PBS) working solution (1 l):	NaH_2PO_4	0.157 g
	Na_2HPO_4	0.518 g
	H_2O dest.	1 l
	NaCl	9 g

4% paraformaldehyde working solution (500 ml):	H_2O dest. (heat up to 60°C)	242 ml
	PFA (add while stirring)	20 g
	30% NaOH	5-7 drops
	0.2 M PB	242 ml
	If needed, adjust pH to 7.4 with NaOH (30%)	
30% sucrose working solution (100 ml):	Sucrose	30 g
	0.1 M PB	100 ml
DAB stock solution (5 mg/ml, 50 ml):	DAB	250 mg
	H_2O dest.	25 ml
	0.2 M PB	25 ml
DAB working solution (40 ml):	0.1 M PB	36 ml
	DAB (5 mg/ml) solution	4 ml
	H_2O_2 (1%)	0.8 ml
Peroxidase blocking solution (40 ml):	0.1 M PB	32 ml
	Methanol (100%)	4 ml
	H_2O_2 (30%)	4 ml
ABC-Kit working solution (10 ml):	0.1 M PB	9.9 ml
	Avidin (reagent A)	50 µl
	Biotin (reagent B)	50 µl
SK-4700 working solution (10 ml):	PBS	10 ml
	Chromogen	6 drops
	H_2O_2	6 drops

3.2.5 Equipment and software

3.2.5.1 Equipment

Equipment	Model	Manufacturer
Color camera	Axiocam 506	Zeiss
Confocal microscope	TCS SP8	Leica
Cryostat microtome	CM3050S	Leica
Digital Rat Stereotaxic Instrument	51900	Stoelting
Electric driller	Micromot 40/E+, NG 5/E	Proxxon
Homeothermic Blanket System	50305	Stoelting
Micro Syringe Pump Controller	Micro4™, UMC4	World Precision Instruments (WPI)
Microscope	AxioImager M2	Zeiss
Monochrome camera	C11440, Orca-flash4.0 LT	Hamamatsu
Mouse Adaptor	51624	Stoelting
Shaker	Polymax 2040	Heidolph
Shaker	Unimax 1010	Heidolph
Shaker	IKA-VIBRAX-VXR	Bachofer Laboratoriumsgeräte
Shaking water bath	GFL 1083	Kobe
Variable-speed tubing pump	Masterflex C/L	Novodirect

3.2.5.1 Software

Adobe Illustrator v21.1	Adobe Systems
FIJI	http://rsbweb.nih.gov/ij/
GraphPad Prism Software v7	GraphPad Software, La Jolla, California, USA
StereoInvestigator software v9	MicroBrightField Biosciences (MBF)

3.2.6 Animals and animal husbandry

For the viral vector injections, a total number of 48 C57Bl/6 mice (Charles River, Sulzfeld, Germany), 8 weeks old at the beginning of the experiment, were used. Animals were housed in individually ventilated cages with *ad libitum* access to food and water under a 12 h/12 h light-dark cycle. All procedures performed were in accordance with the ethical standards and approved by the appropriate institutional governmental agency (Regierungspräsidium Gießen, Germany).

For the PFF and monomeric aSYN injections, a total number of 14 C57Bl/6J mice (Stock JAX:000664, Jackson Laboratory, USA), 8 weeks old at the beginning of the experiment, were used. Animals were housed in standard cages with *ad libitum* access to food and water under a 12 h/12 h light-dark cycle. All experimental procedures performed were in accordance with ethical standards (NIH Guide for the Care and Use of Laboratory Animals) and approved by the Northwestern University Animal Care and Use Committee.

3.4 Methods

3.4.1 Production of mouse full length aSYN pre-formed fibrils

PFF's were produced at the John Hopkins University School of Medicine, Baltimore, USA according to protocols published elsewhere [228, 321], and provided by Ted M. Dawson. Briefly, thawed purified recombinant monomeric mouse full-length aSYN was centrifuged at 100 000*g* at 4 °C for 60 minutes to free the solution of any pelleted (aggregated) aSYN. The resulting supernatant was then pipetted into a sterile Eppendorf and diluted to a final protein concentration of 5 mg/ml. The Eppendorf was then placed into an Eppendorf Thermomixer R and shaken at 1 000 r.p.m. at 37 °C for 7 days to induce aSYN fibril formation. Next, aSYN PFF's were sonicated with 60 pulses at 10% power to fragment large fibrils into toxic, small aSYN seeds. To avoid repeated freeze-thaw cycles, PFF's were aliquoted and stored at -80 °C until use.

3.4.2 Unilateral microinjection of viral vectors or PFF's

Mice receiving PFF or monomeric aSYN injections into the left PPN were operated at the Northwestern University Chicago, USA by Martin T. Henrich. Mice receiving a viral vector injection into the right LC were operated by Fanni F. Geibl at the Philipps University Marburg, Germany.

For unilateral stereotactic injection into the LC, mice were deeply anesthetized with intraperitoneal injection of a mixture of ketamine (100 mg/kg bodyweight) and xylazine (5-10 m/kg bodyweight) diluted in sterile physiologic saline (0.9% NaCl), whereas for the injection into the PPN, mice were anesthetized with isoflurane. The depth of general anesthesia was assessed by testing the toe pinch reflex. When the level of surgical anesthesia was achieved, the head of the mouse was shaved and subsequently fixed in the stereotactic frame so that the surface of the skull paralleled the horizontal plane. The skin of the head was then opened sagitally in the median line over 1-1.5 cm and Bregma[2] and Lambda[3] were identified (Fig. 3.1A-C). Taking Bregma as a reference point, the following coordinates were used to localize the LC or the PPN (Fig. 3.1D,E):

Axis	Coordinates LC	Coordinates PPN
Antero-posterior	−5.4	− 4.6
Medio-lateral	−0.9	+1.15
Dorso-ventral	−3.65	−3.65

[2] Intersection of the coronal and sagittal sutures.

[3] Intersection of the sagittal and lambdoid sutures.

Subsequently, a small hole with 500-600 µm diameter was drilled into the skull with the help of an electric driller until the dura mater was exposed.

The injection of the viral vectors was performed using a microsyringe. A volume of 1.25 µl of rAAV-CMV-A53T-aSYN or rAAV-CMV-Luc was injected into the right LC with a velocity of 125 nl/min. The needle was kept for an additional 5 minutes in place after the injection to reduce efflux of the viral vector into the needle tract. The needle was thereafter retracted at a slow pace (1 mm/min).

Injection of the PFF's was performed using a glass pipette, pulled on a P-97 pipette puller. A volume of 500 nl of aSYN PFF's or monomeric aSYN was injected into the left PPN with a velocity of 100 nl/min. The glass pipette was kept for an additional 5 minutes in place after the injection to reduce PFF/monomeric aSYN efflux into the needle tract. The glass pipette was thereafter retracted at a slow pace (1 mm/min).

After successful stereotactic injection, the skin of the head was sutured with 4 to 5 individual stitches. The mouse was then warmed with an infrared lamp until awakening.

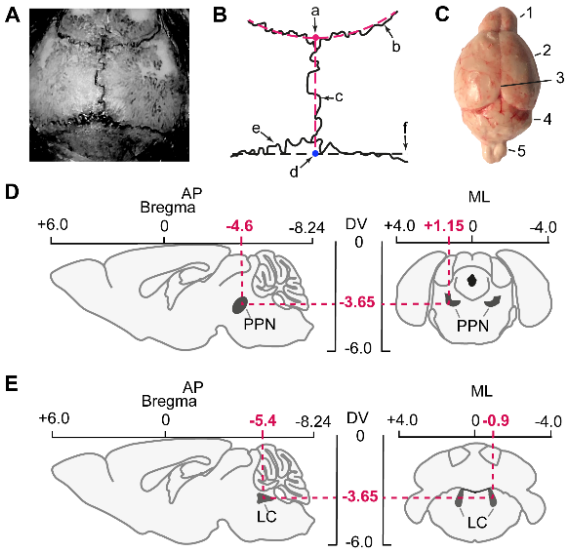

Figure 3.1 | Stereotactic operation

A. Surface of the mouse skull after incision of the skin. The different bone plates and their sutures are well identifiable.

B. Sutures of the mouse skull and identification of Bregma and Lambda reference points. *a* Bregma; *b* frontal or coronal suture; *c* sagittal suture; *d* lambda; *e* lambdoidal or occipital suture; *f* interaural line.

C. Mouse brain in the dorsal view. *1* olfactory bulbs; *2* cerebrum and cerebral neocortex; *3* fissura longitudinalis cerebri; *4* cerebellum and cerebellar cortex; *5* spinal cord.

D. Location of stereotactic injection of PFF's or monomeric aSYN into the left PPN in the sagittal (left) and coronal (right) view. Abbreviations: AP, antero-posterior axis; ML, medio-lateral axis; DV, dorso-ventral axis.

E. Location of stereotactic injection of viral vectors into the right LC in the sagittal (left) and coronal (right) view. Abbreviations: AP, antero-posterior axis; ML, medio-lateral axis; DV, dorso-ventral axis.

3.4.3 Transcardial perfusion, post-fixation, and microtomy

For reliable immunohistochemical analysis, brains have to be devoid of blood and fixed in a life-like state. As the intact brain (and mostly other intact organs as well) are too big for immersion fixation as the fixative (in our case 4% PFA) does not penetrate the tissue homogeneously, brains have to be fixed *in situ* by transcardial perfusion with 4% PFA [88]. For this purpose, mice were deeply anesthetized by intraperitoneal injection of a mixture of ketamine (100 mg/kg bodyweight) and xylazine (5-10 m/kg bodyweight) diluted in sterile physiologic saline (0.9% NaCl). The depth of the general anesthesia was assessed by testing the toe pinch reflex. Mice were subsequently fixed on their backs, and the thorax was opened with scissors to reveal a good view on the heart. A small incision was made in the right atrium and thereafter the left ventricle was punctured around the apex cordis with a needle connected to a perfusion pump. First, the blood was washed out of the vessels with ice-cold PBS solution for 5 to 10 minutes (15 ml/min rate, ~100 ml PBS), followed by ice-cold 4% PFA for 5 to 10 minutes to fix the brain *in situ* (15 ml/min rate, ~100 ml PFA). Subsequently, the brains were carefully removed and post-fixed in 4% PFA for 2-3 days and then transferred to 30% sucrose solution at 4 °C for 2-3 days for dehydration and cryoprotection. Brains were then frozen on dry ice and stored in -80°C until sectioning.

For sectioning, whole brains were embedded in tissue freezing medium and cut from the olfactory bulb to the spinal cord into 30 µm consecutive coronal sections at − 20 °C using a cryostat-microtome. A punctual mark was placed with a needle on the right side of the brains for later identification of the injected and non-injected sides. Sections were collected into eight equally spaced (240 µm) series and kept in antifreeze solution at 4 °C until further processing.

3.4.4 Immunohistochemistry – indirect immunofluorescence staining

For indirect immunofluorescence stainings, 30 µm thin free-floating sections were first washed four times five minutes in 0.1 M PB solution to remove the cryoprotectant. Thereafter, sections were blocked in 10% normal donkey serum (NDS) in PBT for one hour on a shaker at room temperature followed by overnight incubation at 4 °C with primary antibodies at the respective dilutions (see 3.2.3.2) in the same blocking solution. On the second day, sections were washed three times five minutes in 0.1 PB and one time five minutes in PBT, followed by incubation with fluorophore-conjugated, species-specific secondary antibodies at the respective dilutions (see 3.2.3.3) in the same blocking solution

for two hours at room temperature. Subsequently, sections were washed two times five minutes in PBT, followed by incubation with DAPI at a concentration of 0.5 µg/ml in 0.1 M PB solution for 10 minutes. Sections were then washed for three times five minutes in PBT before mounting them on glass slides and covering with ProLong Diamond Antifade Mountant.

Exceptions from this general protocol were made for staining microglial cells (IbA1) and phosphorylated aSYN (p-aSYN), where following the overnight incubation with the respective primary antibodies (see 3.2.3.2), sections were incubated for one hour in blocking solution with biotinylated, species-specific secondary antibodies directed against the primary antibody for IbA1 or p-aSYN (see 3.2.3.3). Sections were thereafter washed three times five minutes in PBT, followed by incubation with fluorophore-conjugated streptavidine and fluorophore-conjugated species-specific secondary antibodies at the respective dilutions (see 3.2.3.3) for two hours at room temperature. The following steps were identical with the general protocol described above.

3.4.5 Immunohistochemistry – DAB and SK-4700 double staining

For stereological analysis of cholinergic and non-cholinergic neurons of the PPN, an immunohistochemical double staining visualizing choline acetyltransferase (ChAT, rate-limiting enzyme in acetylcholine production and therefore marker of cholinergic neurons) and Neuron N (NeuN, pan-neuronal nuclear antigen, general marker for neuronal cells) was used. Therefore, 30 µm thin free-floating coronal sections containing the PPN region were washed four times five minutes in 0.1 M PB solution to remove cryoprotectant. Thereafter, endogenous peroxidase activity was quenched with peroxidase blocking solution (see 3.2.4) for fifteen minutes, followed by four times five minutes washing in 0.1 M PB solution. Sections were then blocked in 10% NDS in PBT for one hour at room temperature and incubated overnight at 4 °C with the primary antibody against NeuN (Merck Millipore, MAB377, 1:1000). On the second day, sections were washed four times five minutes in 0.1 M PB solution, followed by a one-hour incubation at room temperature with biotinylated anti-mouse secondary antibody (Jackson Immunoresearch, 715-065-151, 1:1000). This was followed by a one-hour incubation at room temperature in ABC-Kit working solution (see 3.2.4). Sections were then washed four times five minutes in 0.1 M PB-solution to remove unbound ABC-Kit solution and thereafter incubated for two minutes in DAB working solution (see 3.2.4) to induce the chromogenic reaction. This step, due to the high toxicity of DAB, was strictly performed under a hood. Sections were thereafter washed in 0.1 M PB

four times for five minutes and blocked in 10% NDS in PBT solution. Sections were then incubated overnight at 4 °C with a primary antibody directed against ChAT (Merck Millipore, AB144P, 1:100). On the third day, sections were washed four times five minutes in 0.1 M PB solution and incubated with a biotinylated anti-goat secondary antibody (Jackson ImmunoResearch, 705-065-147, 1:1000) for one hour at room temperature followed by a one-hour incubation in ABC-Kit working solution (see 3.2.4) at room temperature. Sections were then washed four times five minutes in 0.1 M PB solution and thereafter incubated for two minutes in SK-4700 working solution under the hood. Remaining SK-4700 solution was then removed in a four times five minutes washing step. Sections were then mounted on gelatinized glass slides and left to dry for two hours. This was followed by immersion of the tissue through a series of ethanol solutions of increasing concentrations (70%, 96%, 100%) for stepwise dehydration. The sections were finally passed twice through 100% xylene and coverslipped with Eukitt Quick-hardening Mounting Medium.

As both chromogens (DAB and SK-4700) are highly toxic, everything that was potentially contaminated with the chromogens (e.g. pipette tips, plates, gloves, beakers) was neutralized in 10% sodium hypochlorite (NaOCl) solution overnight and discarded in a biohazard box.

3.4.6 Proteinase K enzymatic digestion

One of the pathological hallmarks of PD is the intracellular accumulation of LBs and LNs consisting mainly of aSYN. A major characteristic and established marker of the aggregated state of aSYN is Proteinase K (PK) resistance [160, 203]. PK is a serine protease with a broad substrate specificity degrading most of the proteins, including aSYN in their native state. PK enzymatic digestion was performed as follows.

Sections were washed three times five minutes in 0.1 M PB solution and once for five minutes in PBT. Thereafter, sections were digested for ten minutes in 12 µg/ml PK diluted in PBT at 65 °C in a shaking water bath. Sections were then washed four times five minutes in 0.1 M PB solution at room temperature to remove PK. To visualize the PK-resistant (remaining) aSYN aggregates, the tissue was double stained for human aSYN, p-aSYN, p62, or Luc in combination with TH or ChAT (see 3.2.3.2) with the immunofluorescence staining protocol described above (see 3.4.4). The stainings for TH and ChAT served as controls: in case of complete digestion, immunoreactivity of the neurotransmitter systems were completely absent in the tissue. Sections with visible TH or ChAT immunoreactivity indicating incomplete digestion were excluded from the analysis.

3.4.7 Stereology

Unbiased stereology is a widely used method for the estimation of quantitative parameters of three-dimensional structures (brain regions, nuclei) from two-dimensional materials (planar histological tissue sections) [141, 272].

The analysis was performed using the *optical fractionator workflow* of the StereoInvestigator Software (MBF Biosciences, version 9). This method is based on the unbiased estimation of population number (in this case neuronal number) in the whole volume by unbiased analysis of a known fraction of volume. To achieve a uniform systematic sampling of the region of interest (ROI, the PPN), a known fraction of the serial sections containing the ROI with a known section thickness (z-axis) and known sectional area randomly assigned by the software (x-, and y-axes) was counted and the extrapolation of total neuronal number of the ROI was performed by the workflow.

The quantification of cholinergic and non-cholinergic neurons of the PPN was performed with ChAT and NeuN double stained sections (see 3.4.5) of five pre-defined Bregma coordinates (–4.24, –4.48, –4.72, –4.84, –4.96) (Fig. 3.2). The contours of the ROI were drawn according to the cytoarchitectonic distribution of cholinergic (ChAT-positive) neurons. ChAT- and NeuN-positive cells (cholinergic PPN neurons) and ChAT-negative but NeuN-positive (non-cholinergic neurons) were counted separately in the same sections. Parameters used for the counting were: grid size 100 × 100 µm, counting frame 85 × 85 µm, and 2 µm guard zones. Analysis was performed at 40× magnification. The investigator was blinded to treatment (PFF vs. monomeric aSYN), time-point, and injection side.

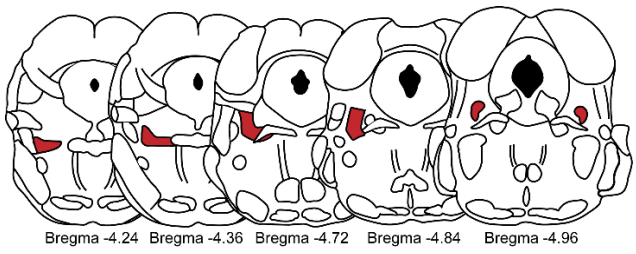

Figure 3.2 | Coronal sections of the PPN included into stereological assessment

Stereological quantification was performed of five distinct coronal serial sections of defined Bregma coordinates containing the whole rostro-caudal extent of the PPN (red). The contour of ROI was drawn according to the cytoarchitectonic distribution of ChAT-positive neurons. ChAT- and NeuN-positive and ChAT-negative but NeuN-positive cells were counted separately in the same sections of every animal.

3.4.8 Whole-brain analysis of p-aSYN pathology in the PFF model

For the whole brain analysis of p-aSYN pathology progression, equidistant sections with an interslice distance of 240 µm spanning the complete rostro-caudal extent of the mouse brain were stained against p-aSYN and DAPI following the immunofluorescence staining protocol described above (see 3.4.4). A semiquantitative grading system for p-aSYN neurite and soma pathology ranging from 0 to 4 was established. Neurite (*N*) and soma (*S*) pathology was graded separately as follows: *N1* sparse pathology (very few neurites), *N2* mild pathology (more neurites, but large areas uncovered), *N3* dense pathology (brain regions covered, but places spared), *N4* very dense pathology (brain region densely covered; and *S1* sparse pathology (1-3 soma), *S2* mild pathology (4 or more soma, but large areas uncovered), *S3* dense pathology (many aggregates, but places spared), *S4* very dense pathology (brain region densely covered by aggregates) (Fig. 3.3).

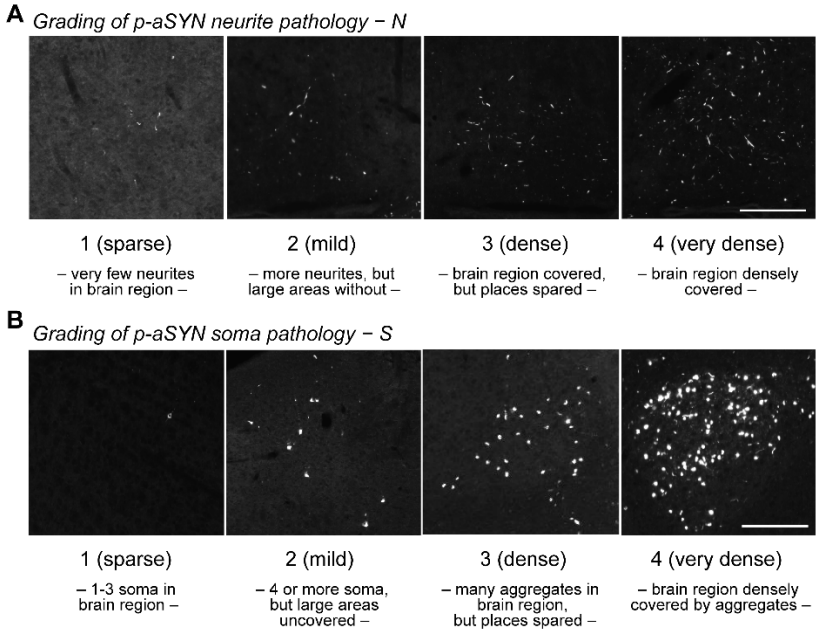

Figure 3.3 | Semiquantitative grading system for the whole-brain analysis of p-aSYN neurite and soma pathology

A. Template images used to assess the degree of p-aSYN neurite pathology (*N0-4*). The grading system ranged from 0 [very few neurites in brain region] to 4 [brain region densely covered by p-aSYN neurite pathology].

B. Template images used to assess the degree of p-aSYN soma pathology (*S0-4*). The grading system ranged from 0 [1-3 soma in brain region] to 4 [brain region densely covered by aggregates].

First, stained sections were scanned with the 10× objective lens of the AxioImager M2 microscope using the *Virtual Tissue (slide scanning) workflow* of the StereoInvestigator Software (MBF Biosciences, version 9). Thereafter, each tissue section was matched to the corresponding atlas image of the coronal reference atlas of the mouse brain by the Allen Institute, USA [3]. The degree of p-aSYN pathology was graded in every brain region using the template images of the grading system (Fig. 3.3). Brain regions were identified based on the DAPI signal and tissue autofluorescence. Mean score values were calculated for every brain region, treatment group (PFF vs. monomeric aSYN) and time-point. The investigator was blinded to treatment (PFF vs. monomeric aSYN) and time-point. Color coded heatmaps were generated with the Adobe Illustrator program.

3.4.9 Whole-brain analysis of human aSYN propagation in the rAAV model

For the whole-brain quantification of human aSYN propagation, coronal sections of pre-defined Bregma coordinates (+4.28, +2.86, +1.18, +0.38, –3.16, –7.56) covering the complete rostro-caudal extent of the brain were stained against human aSYN, or Luc in combination with DAPI following the immunofluorescence staining protocol described above (see 3.4.4). A semiquantitative grading system from 0 to 4 was established and template images for later assessment of the degree of aSYN transport were acquired.

First, stained sections were scanned with the 10× objective lens of the AxioImager M2 microscope using the *Virtual Tissue (slide scanning) workflow* of the StereoInvestigator Software (MBF Biosciences, version 9). Thereafter, each tissue section was matched to the corresponding atlas image of the coronal reference atlas of the mouse brain by the Allen Institute, USA [3]. The degree of human aSYN pathology/transport was assessed in every brain region using the template images of the grading system as follows: *0*, no positive axons; *1*, sparse (few positive axons); *2*, mild (more positive axons); *3*, moderate (many positive axons, covering almost the complete brain region); and *4*, severe pathology (large number of positive axons densely covering the complete brain region). Brain regions were identified based on the DAPI signal and tissue autofluorescence. Mean score values were calculated for every brain region, treatment group (A53T-aSYN vs. Luc) and time-point. The investigator was blinded to treatment and time-point. Color coded heatmaps were generated with the Adobe Illustrator program.

3.4.10 Quantification of reactive microgliosis

For the analysis of reactive microgliosis in the PPN region, coronal sections containing the whole rostro-caudal extent of the PPN were stained against ionized calcium binding adaptor molecule 1 (IbA1; microglial marker), ChAT, and DAPI following the immunofluorescence staining protocol described above (see 3.4.4). The quantification of the microgliosis was performed based on previously published protocols [220, 252]. First, images of the PPN region were captured using the 10× objective lens of the AxioImager M2 microscope (Zeiss, Germany). Images were then loaded into FIJI software [271], the IbA1 channel was isolated and the mean background of this channel was subtracted. The remaining background was measured, multiplied by four, and then this value was set as a threshold. All pixels with an intensity value higher than this threshold were interpreted as positive IbA1-signal and all pixels under this threshold value were considered as background labeling. The PPN region was outlined based on the cytoarchitectonic distribution of ChAT-positive cells using the ChAT-channel of the composite pictures and the IbA1-positive pixel count was quantified. This value was then normalized to the total pixel count of the sampled area. The investigator was blinded to treatment (PFF vs. monomeric aSYN), time-point, and injection side. For the analysis, the exact same five sections of pre-defined Bregma coordinates (–4.24, –4.48, –4.72, –4.84, –4.96) were used (Fig. 3.2).

3.4.11 Imaging

Fluorescent images were acquired with an AxioImager M2 microscope (Zeiss) equipped with an ORCA-Flash4.0 LT CMOS camera (Hamamatsu C11440-42 U). For confocal images, a TCS SP8 microscope (Leica) was used. Images were post-processed with FIJI image software to enhance signal-to-noise.

Brightfield images were acquired using an AxioImager M2 microscope (Zeiss) equipped with an Axiocam 506 color camera (Zeiss).

3.4.12 Statistical methods

All data were analyzed using GraphPad Prism (version 7.0 GraphPad Software, USA), Fiji [271], or Microsoft Excel 2016. In all experiments, sample size was based on prior studies using similar techniques and no statistical methods were used to predetermine sample size. Column bar graphs display mean and whiskers represent SD. Whisker plots show median, lower and upper quartiles and whiskers represent minimum and maximum of the data. Statistical significance of differences between two groups was analyzed by single or multiple Student's t-Tests and corrected with Holm-Sidak method for multiple testing. Differences between multiple groups were assessed by one-way or two-way ANOVA followed by Tukey's or Dunnett's multiple comparisons test. To calculate correlations, scatterplots and performed linear regression analysis was performed. Differences were considered significant at $P < 0.05$. Distribution of the data was assumed to be normal, but this was not formally tested. Significance indicators were kept constant in all figures (*$P < 0.05$, ** $P < 0.01$, *** $P < 0.001$) and exact P values are shown in the individual figure legends. All figures were created with Adobe Illustrator version 21.1 (Adobe Systems).

4 Results

4.1 The PFF model of Parkinson's disease

4.1.1 Experimental design

In the PFF mouse model of prodromal PD, we wanted to investigate the preferential vulnerability pattern of PPN neurons and the brain-wide propagation pattern of a focally induced α-synucleinopathy. Therefore, we injected murine aSYN PFF's unilaterally into the left PPN region of wild-type mice (Fig. 4.1A). As a control, monomeric murine aSYN was injected. Animals were consecutively sacrificed after 1, 6, and 12 wpi and local and brain-wide pathological patterns were investigated.

4.1.2 PFF's induced aggregate formation in the PPN region as soon as 1 wpi

Previous studies have proposed that murine aSYN PFF's possess prion-like properties: they act as seeds and thereby induce the self-perpetuating aggregation of primarily soluble endogenous aSYN when added to neuronal cell cultures or injected into the murine brain [179, 183, 189, 241]. To test whether local PFF injection into the left PPN resulted in aggregate formation in our mouse model, we stained brain sections containing the whole PPN region against phosphorylated aSYN (p-aSYN), an established marker for α-synucleinopathy in human PD brains and murine PD models [85, 116, 179, 241].

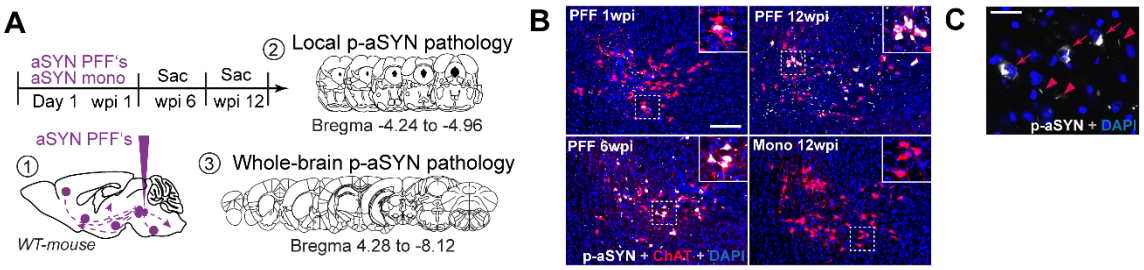

Figure 4.1 | PFF injection into the PPN induces aggregate formation.

A. Schematic depicting strategy for aSYN PFF injections and assessment of pathology.

B. Representative image showing aggregate formation in the PPN of PFF injected mice 1, 6, and 12 wpi. No aggregate formation was detected in monomeric aSYN injected animals. Scale bar, 250 µm

C. High magnification confocal images of p-aSYN-positive aggregates. Two types of aggregates could be distinguished: 1) large perinuclear inclusion bodies (arrows); and 2) smaller, filamentous aggregates (arrowheads). Scale bar, 50 µm

Our data revealed that injection of PFF's resulted in robust p-aSYN-positive aggregate formation in neurons of the left PPN (Fig. 4.1B). Accumulation of aggregates was progressive with first inclusions being observable as soon as 1 wpi. With high magnification confocal microscopy, two types of aggregates could be distinguished: (1) large perinuclear inclusion bodies (Fig. 4.1C, arrows); and (2) smaller, filamentous p-aSYN-positive aggregates in axons or neurites (Fig. 4.1C, arrowheads). The aggregates detected in our PFF animal model were highly reminiscent of LBs/LNs found in postmortem human brains. Interestingly, the inclusion bodies were not homogeneously distributed over the rostro-caudal extent of the PPN, but rather showed a gradient with p-aSYN-positive aggregates being significantly more abundant in the caudal PPN region (Fig. 4.2B). This distribution pattern highly resembled the gradient of cholinergic PPN neurons (Fig. 4.2A). No aggregate formation was detected in monomeric aSYN injected animals (Fig. 4.1B).

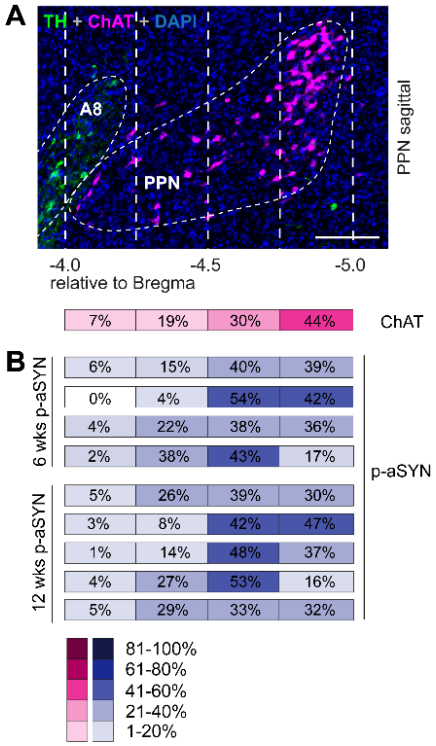

Figure 4.2 | Rostro-caudal distribution of p-aSYN harboring neurons following PFF injection.

A. Representative sagittal image of the cholinergic PPN of a wild-type mouse depicting the rostro-caudal distribution of ChAT-positive PPN neurons (magenta, n = 3). Scale bar, 250 µm.

B. Distribution of p-aSYN-positive aggregate harboring PPN neurons over the rostro-caudal extent of the PPN (blue, n= 4 for 6 wpi; n = 5 for 12 wpi). Aggregates were counted over the whole PPN region from Bregma –4.0 mm to Bregma –5.0 mm. Afterwards, aggregate count within the respective Bregma ranges was normalized to the total aggregate count.

4.1.3 p-aSYN-positive aggregates are PK resistant and p62-positive

Major hallmarks of LBs and LNs in PD are resistance to protease digestion (PK resistance) and SQSTM1/p62-positivity. Former is an indicator of the accumulation of insoluble proteinaceous aggregates, whereas latter implicates the dysregulation of the autophagic pathway, a common pathogenic event in neurodegenerative proteinopathies [156, 203, 245]. To test whether the aggregates found in our PFF mouse model share these characteristic

features with human LBs/LNs, we performed PK digestion and subsequently stained the sections for p-aSYN, p62, and ChAT.

PFF, but not monomeric aSYN injected mice showed accumulation of PK resistant and p-aSYN- and p62-positive inclusion bodies starting 6 wpi (Fig. 4.3). Aggregates were not restricted to the ipsilateral side but were also abundant in the contralateral PPN implicating that the propagation of the α-synucleinopathy to distant brain regions also results in the formation of PK-resistant aggregates (data not shown).

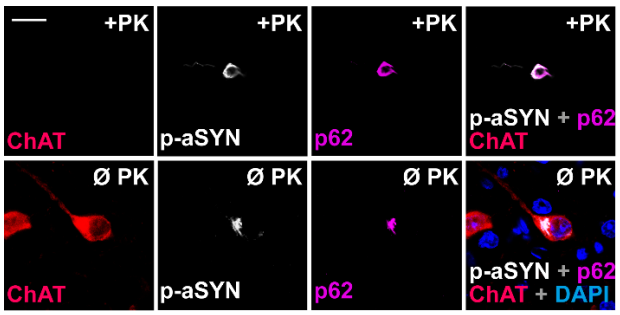

Figure 4.3 | PFF-induced aggregates are PK resistant and p62-positive.
Representative images of p-aSYN- and p62-positive aggregates after PK digestion (*upper row, +PK*), or without digestion (*lower row, Ø PK*). Inclusion bodies found in the injected PPN region are PK resistant. Scale bar, 25 µm.

4.1.4 Cholinergic PPN neurons bear the brunt of pathology

During the course of PD, the neuropathological process mostly affects the PPN cholinergic neurons, whereas the GABAergic and glutamatergic populations are relatively spared of the disease [89, 108, 122]. We wanted to test whether this selective vulnerability pattern found in human postmortem PD brains also translates into our PFF murine model. Hence, we stained coronal sections containing the complete rostro-caudal extent of the PPN against p-aSYN for aggregates, ChAT to visualize cholinergic neurons and MAP2 to stain all neuronal populations.

Our analysis revealed that although cholinergic neurons form the smallest subpopulation of the PPN accounting only for approximately 25% of all neurons [181, 327], they displayed the vast majority of p-aSYN-positive aggregates in the PPN region (89.0 ± 10.4% for 6 wpi; 76.9 ± 8.1% for 12 wpi) (Fig. 4.4A-C). At 6 wpi, approximately one-third of cholinergic neurons exhibited an aggregate (35.4 ± 8.4%), whereas at 12 wpi, the half of the cholinergic cells harbored an inclusion body (50.9 ± 2.8%) (Fig. 4.4D).

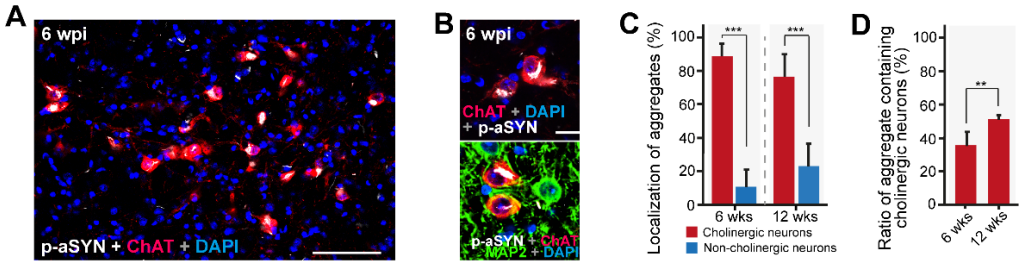

Figure 4.4 | The vast majority of the p-aSYN-positive aggregates co-localized with the cholinergic marker ChAT.

A. Representative image of the PPN region 6 wpi stained for p-aSYN (white), ChAT (red) and DAPI (blue). Scale bar, 100 µm.

B. High magnification confocal images of aggregate-containing cholinergic cells. Scale bar, 25 µm.

C. The vast majority of p-aSYN aggregates was found in cholinergic PPN neurons (89.0 ± 10.4% at 6 wpi; 76.9 ± 8.1% at 12 wpi; P < 0.001 for 6 wpi cholinergic versus non-cholinergic; *P* < 0.001 for 12 wpi cholinergic versus non-cholinergic; *n* = 4 at 6 wpi, *n* = 5 at 12 wpi; one-way ANOVA followed by Tukey's multiple comparisons test).

D. Quantification of the ratio of aggregate containing cholinergic PPN neurons on the injected (left) side (aggregate containing cholinergic neurons / all cholinergic neurons) reveals that around half of the PPN cholinergic neurons contain aSYN aggregates at 12 wpi (35.35 ± 8.44 at 6 wpi; 50.91 ± 2.8% at 12 wpi; *P* = 0,0057; *n* = 4 at 6 wpi; *n* = 5 at 12 wpi; unpaired t-test).

4.1.5 Reactive microgliosis is induced at the injection site

Profound reactive microgliosis is a common histopathological finding in brain regions affected by the PD disease process [84, 194]. Moreover, a growing body of evidence from epidemiological-, genome-wide association-, brain imaging-, postmortem histological-, and animal studies indicates that microglial activation is closely coupled to the neurodegenerative process [44, 90, 91, 93, 110, 127, 233, 295]. Therefore, we sought to investigate whether Lewy-like PPN pathology was accompanied by reactive microgliosis in our model.

Our analysis revealed that the injection of both aSYN PFF's and monomeric aSYN induced a similar degree of microglial activation at the injection site (Fig. 4.5A,B). Remarkably, there was also no difference in IbA1-positive pixel count in the contralateral (non-injected) PPN between PFF and monomeric aSYN injected animals, despite the fact that contralateral PPN neurons of PFF injected mice harbored p-aSYN-positive aggregates (Fig. 4.5B). This is an intriguing finding as it implicates that intraneuronal aggregation of aSYN *per se* does not induce a neuroinflammatory response in our model.

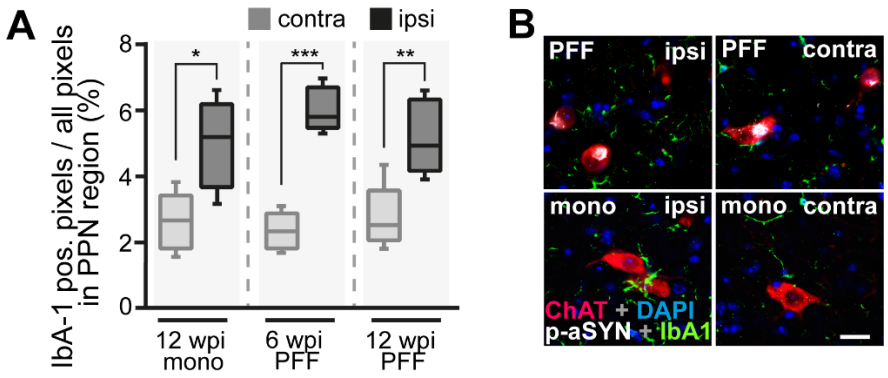

Figure 4.5 | Injection of different aSYN species leads to reactive microgliosis in the PPN region.

A. Graph showing percentage of IbA-1 positive pixels in PPN region. The amount of IbA-1 positive pixels was significantly higher on the injected side compared to the non-injected side for aSYN PFF injected animals but also for aSYN monomer injected mice ($P = 0.0260$ for 12 wpi mono contra versus 12 wpi mono ipsi; $P = 0.0003$ for 6 wpi PFF contra versus 6 wpi PFF ipsi; $P = 0.0095$ for 12 wpi PFF contra versus 12 wpi PFF ipsi; $n = 5$ for 12 wpi mono and 12 wpi PFF; $n = 4$ for 6 wpi PFF; one-way ANOVA followed by Tukey's multiple comparisons test). Whisker box plots show median, lower and upper quartiles, and whiskers represent minimum and maximum of the data.

B. High magnification images depicting different degrees of microglial (IbA1) activation. Scale bar, 25 µm.

4.1.6 Significant decrease of ChAT-positive neuronal cell count

The cascade of neuropathological events in human PD and animal models of PD lead to neuronal dysfunction and ultimately culminate in neuronal cell death. In postmortem PD brains, approximately 50% of large cholinergic neurons degenerate, whereas the GABAergic and glutamatergic neurons are relatively spared of the disease [89, 108, 122]. As we mainly observed pathological aSYN aggregation in the cholinergic PPN neurons, we sought to stereologically quantify cholinergic (ChAT- and NeuN-positive) and non-cholinergic, that is, GABAergic and glutamatergic (ChAT-negative but NeuN-positive) PPN neurons separately.

We observed a significant decrease of ChAT-positive neurons of the ipsilateral (injected) PPN 12 wpi in PFF injected animals (617.4 ± 70.49 cells in PFF injected animals 12 wpi vs 877 ± 94.89 cells in monomeric aSYN injected animals at 12 wpi; $P = 0.0071$) (Fig. 4.6A,C). The number of the contralateral (non-injected) cholinergic PPN neurons showed a decreasing tendency 6 and 12 wpi compared to monomeric aSYN injected animals, although this difference was not of statistical significance (717.8 ± 134.3 cells 6 wpi; 756.8 ± 80.85 cells 12 wpi in PFF injected animals vs 848.8 ± 125.6 cells 12 wpi in monomeric aSYN injected animals). The number of non-cholinergic PPN neurons did not show any alterations 6 and 12 wpi (5664 ± 590 cells 6 wpi ipsilaterally, 5435 ± 937 cells 6 wpi contralaterally, 5426 ± 448.6 cells 12 wpi ipsilaterally, 5203 ± 529 cells 12 wpi contralaterally in PFF injected animals vs 5143 ± 445.1 cells 12 wpi ipsilaterally, and 5331 ± 702.6 cells 12 wpi contralaterally in monomeric aSYN injected animals) (Fig. 4.6B).

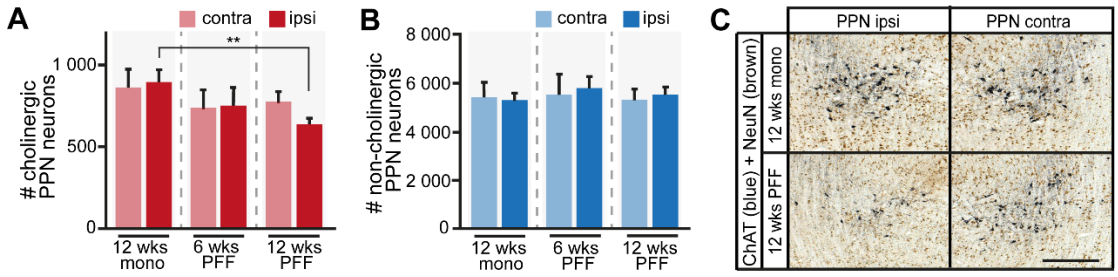

Figure 4.6 | PFF injection into the PPN region leads to a significant decrease of ChAT-positive neurons.

A. aSYN PFF treatment induces loss of ChAT pos. PPN neurons at 12 wpi (877 ± 94.89 vs 617.4 ± 70.49 cells; $P = 0.0071$ for 12 wpi mono ipsi versus 12 wpi PFF ipsi; for all other comparisons $P > 0.05$; $n = 5$ for 12 wpi mono and 12 wpi PFF; $n = 4$ for 6 wpi PFF; one-way ANOVA followed by Dunnett's multiple comparisons test).

B. The number of non-cholinergic neurons was not changed in any group or time point ($P > 0.05$ for all comparisons; $n = 5$ for 12 wpi mono and 12 wpi PFF; $n = 4$ for 6 wpi PFF; one-way ANOVA followed by Dunnett's multiple comparisons test).

C. Representative images of the PPN region for each group and time point. Scale bar, 500 µm.

4.1.7 Initial spreading of pathology occurs as soon as 1 wpi

Previous studies have demonstrated that PFF's initiate a cascade of pathological events mediated by seeding recruitment of primarily soluble endogenous aSYN [178, 320, 321]. *In vivo*, the induced pathology is not restricted to the close vicinity of the injection site but spreads over considerable distances to regions far beyond the initial inoculation in a stereotypical temporal and topological manner [179, 189, 190, 242, 243]. Mounting evidence suggests that this propagation of pathology occurs through synaptic connections and depends on the wiring architecture (connectome[4]) of the brain region in which the initial seeding took place. To investigate the neuroanatomical distribution of pathology in our murine PFF model, we sought to generate a highly comprehensive and quantitative map of the brain-wide Lewy-like pathology. Therefore, we stained p-aSYN in coronal brain sections with an interslice distance of 240 µm covering the complete rostro-caudal extent of the brain from the OB to the spinal cord. We thereafter generated a grading system distinguishing somal and axonal/neuritic pathology (see chapter 3.4.8 and Fig. 3.3) and systematically graded the observed p-aSYN pathology in distinct brain regions.

One-week post-injection, apart from the PPN, 16 regions stained positive for somal and/or neuritic Lewy-like pathology (Fig. 4.7A). Fifteen regions were located in the ipsilateral (left) hemisphere, whereas one region (tuberal nucleus) was affected bilaterally (Fig. 4.8). The observed pathology was most severe at the inoculation site, followed by the retrorubral field,

[4] Comprehensive map of the synaptic connections formed between neurons of the nervous system.

medial and lateral parts of the central amygdala, and parabrachial nucleus. Next, we wanted to examine whether and how strong neuritic and somal pathology were associated, i.e. how well the scores correlated with each other. Therefore, we plotted the neuritic and somal pathology scores and performed a linear regression analysis. We observed a strong correlation between the somal and neuritic pathology scores ($r^2 = 0.88$) (Fig. 4.7D). Thirteen out of the sixteen distant brain regions exhibited both neuritic and somal pathology, whereas only three regions displayed either somal or neuritic scores.

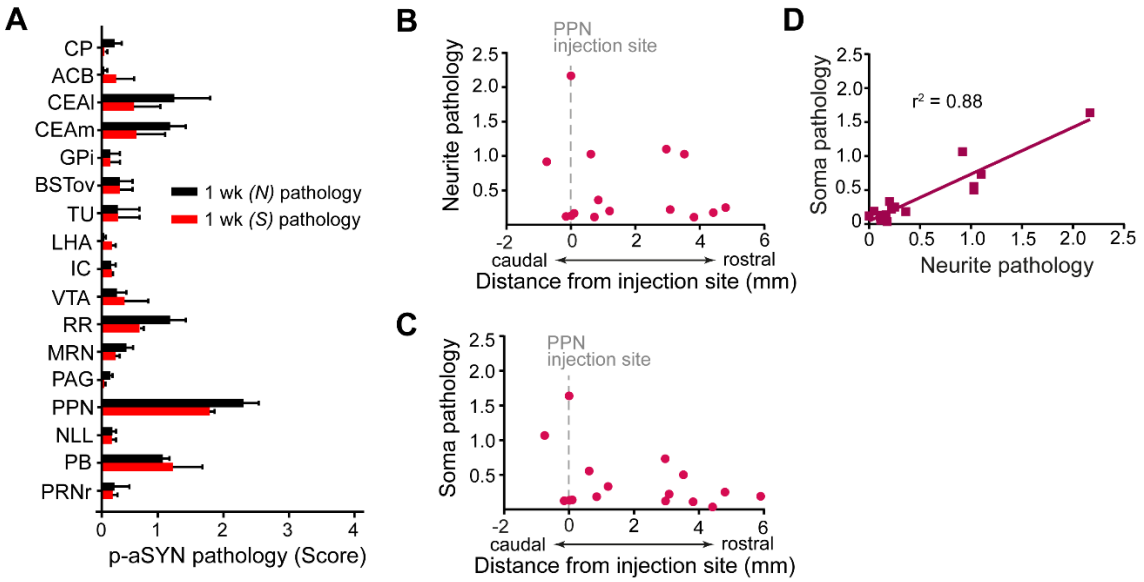

Figure 4.7 | Brain-wide propagation of the α-synucleinopathy 1 wpi

A. Whole-brain quantification of p-aSYN neurite (N) and soma (S) pathology at 1 wpi reveals aSYN pathology in 17 brain regions ($n = 3$).

B. Caudo-rostral distribution of brain regions relative to the injection site (left PPN, 0) showing neuritic pathology 1 wpi.

C. Caudo-rostral distribution of brain regions relative to the injection site (left PPN, 0) showing somal pathology 1 wpi.

D. p-aSYN soma pathology correlated strongly with p-aSYN neurite pathology 1 wpi ($r^2 = 0.88$, n=3).

Abbreviations: ACB, nucleus accumbens; BSTov, bed nuclei of the stria terminalis, anterior division, oval nucleus; CEAl, central amygdala, lateral part; CEAm, central amygdala, medial part; CP, caudoputamen; GPi, globus pallidus internus; IC, inferior colliculus; LHA, lateral hypothalamic area; MRN, midbrain reticular nucleus; NLL, nucleus of the lateral lemniscus; PAG, periaqueductal gray; PB, parabrachial nucleus; PPN, pedunculopontine nucleus; PRNr, pontine reticular nucleus, rostral part; RR, retrorubral field; TU, tuberal nucleus; VTA; ventral tegmental area.

To exclude the possibility of simple diffusion of the injected PFF's, we plotted the degree of p-aSYN pathology observed in individual brain regions with their caudo-rostral distances relative to the injection site (left PPN, Bregma −4.6, 0 mark on the graph) (Fig. 4.7B,C). We observed that the distribution of pathology over the rostro-caudal extent of the brain did not show any regularity. Brain regions far away from the injection site showed similar severity of p-aSYN pathology as did brain structures adjacent to the PPN. The distribution of pathology did not show characteristics of diffusion, i.e. the degree of induced pathology did not decrease with longer distances to the injection site (Fig. 4.7B,C). Remarkably, our analysis revealed that the initial propagation of Lewy-like pathology occurred in a clear caudo-rostral direction. While out of the sixteen regions, fifteen were rostral to the PPN, only one region (parabrachial nucleus) localized a bit caudally.

To clearly demonstrate the distribution and burden of α-synucleinopathy induced by focal PFF injection into the left PPN, we generated comprehensive heatmaps of both the brain-wide somal (Fig. 4.8A) and neuritic p-aSYN pathology (Fig. 4.8B). No p-aSYN pathology was seen in monomeric aSYN injected animals at any time-point (data not shown).

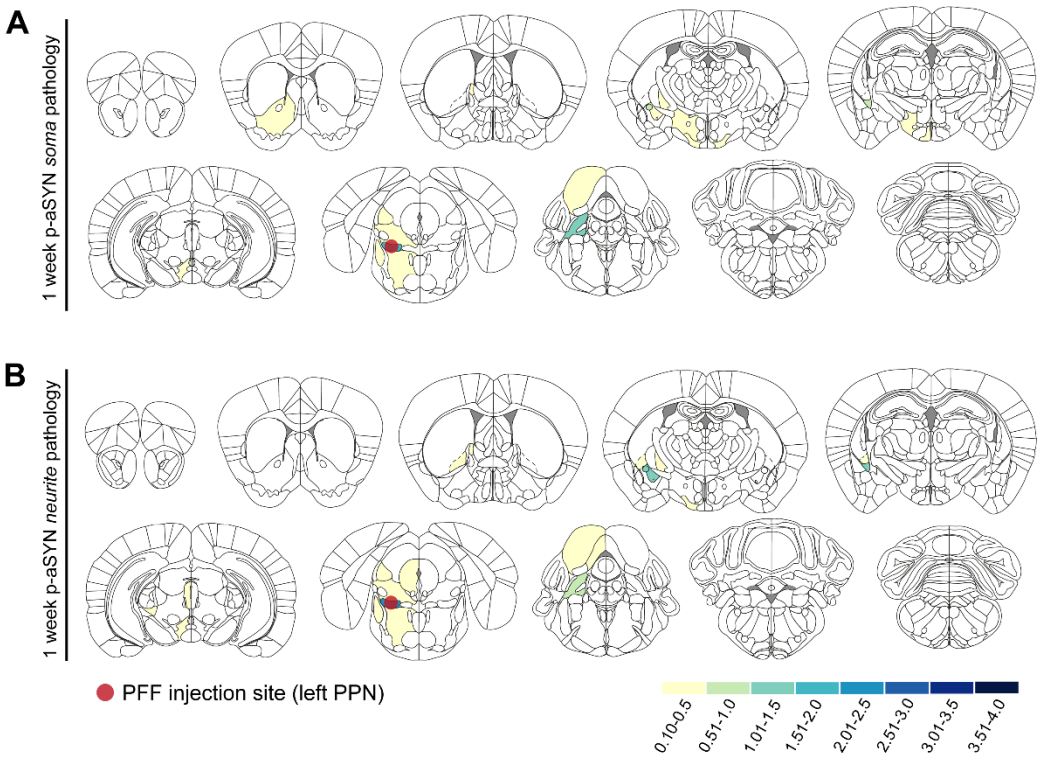

Figure 4.8 | Brain-wide distribution of Lewy-like pathology 1 wpi

A. Heatmaps depicting degree of somal p-aSYN pathology 1 week after PFF injection into the left PPN (red circle). For more information on the grading system see 2.3.8. $n = 3$

B. Heatmaps depicting degree of axonal/neuritic p-aSYN pathology 1 week after PFF injection into the left PPN (red circle). For more information on the grading system see 2.3.8. $n = 3$

4.1.8 Brain-wide p-aSYN pathology progresses in severity and distribution

To investigate the time-dependency of the pathological changes induced by focal PFF injection into the left PPN, we stained and analyzed coronal sections with an interslice distance of 240 μm of the whole murine brain at the 6 wpi time-point. The staining and grading protocols were identical to the 1-week time-point (see 4.1.7).

Systematic p-aSYN pathology mapping revealed 278 brain regions harboring somal p-aSYN pathology, and 286 regions exhibiting neuritic/axonal p-aSYN signal at 6 wpi (Fig. 4.9). The affected brain regions were distributed throughout the whole brain spanning from the OBs and prefrontal cortices to the spinal cord, the farthest region being as far as 7.19 mm from the inoculation site (medial and dorsal parts of the anterior olfactory nucleus, inoculation site: left PPN region, Bregma -4.6 mm). In spite of the unilateral injection of aSYN fibrils, the p-aSYN pathology appeared in both hemispheres, but was more abundant in the ipsilateral (left) hemisphere. The observed pathology was most severe at the inoculation site within the left PPN, followed by the lateral and medial parts of the central amygdala, laterodorsal tegmental nucleus, sublaterodorsal tegmental nucleus, anterolateral area and rhomboid nucleus in the anterior division of the bed nuclei of the stria terminalis, periaqueductal gray, midbrain reticular nucleus, and lateral hypothalamic area. Distant aggregates stained also positive for p62 indicating that these inclusions, such as the ones at the inoculation site, also share similarities with human LBs and LNs (Fig. 4.10D) [156].

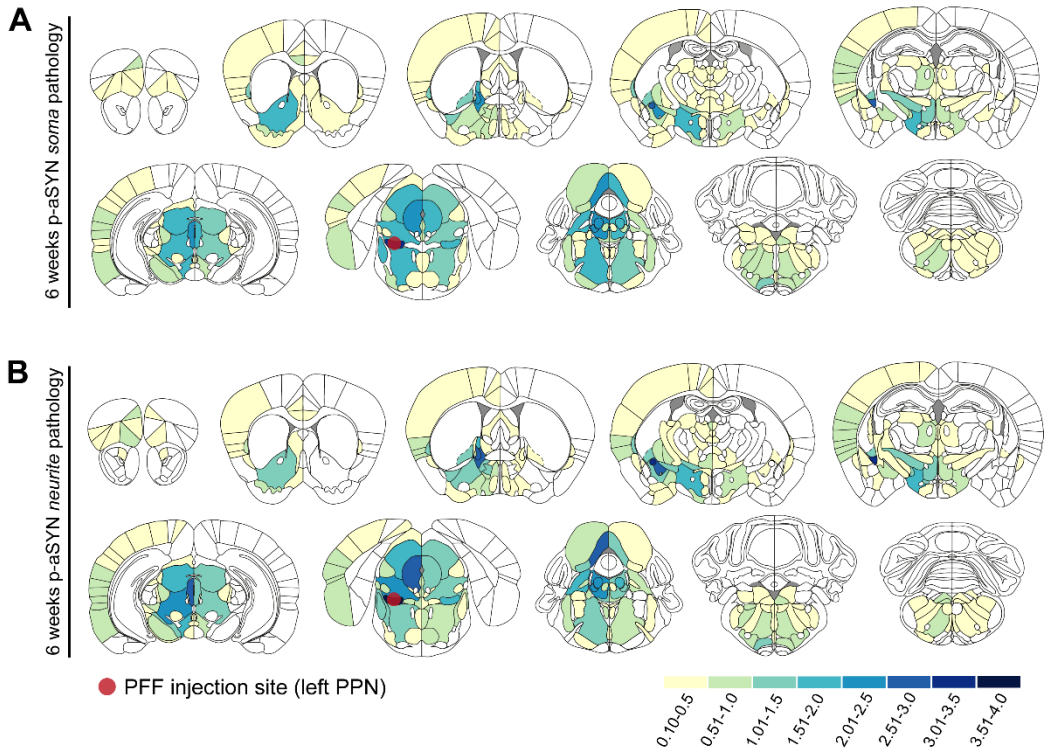

Figure 4.9 | Brain-wide distribution of Lewy-like pathology 6 wpi

A. Heatmaps depicting degree of somal p-aSYN pathology 6 weeks after PFF injection into the left PPN (red circle). For more information on the grading system see 2.3.8. $n = 4$

B. Heatmaps depicting degree of axonal/neuritic p-aSYN pathology 6 weeks after PFF injection into the left PPN (red circle). For more information on the grading system see 2.3.8. $n = 4$

Next, we wanted to test whether the strong correlation between the neuritic and somal pathology observed at the one-week time-point is still apparent at the six-week time-point. We therefore plotted the somal and neuritic p-aSYN pathology scores of the respective brain areas and performed a linear regression analysis (Fig. 4.10C). A strong correlation of the two pathology scores was observed at 6 wpi ($r^2 = 0.9082$, $n = 4$).

Next, we wanted to analyze the time-dependency of the brain-wide progression of pathological changes following unilateral aSYN fibril injection. Therefore, we compared both the whole brain distribution and the severity of the observed pathology at the respective brain regions 1 and 6 wpi.

Significantly more regions were affected by p-aSYN pathology at 6 wpi compared to 1 wpi (for somal pathology: 278 regions 6 wpi vs 15 regions 1 wpi; for neuritic pathology: 286 regions at 6 wpi vs 15 regions 1 wpi). At the six-week time-point, pathology also spread to caudal regions relative to the injection site, such as the gigantocellular nucleus, or the intermediate reticular nucleus (Fig. 4.9). Remarkably, all regions showing severe pathology were located rostral to the inoculation site, and structures caudal to the injection site showed milder pathology.

All 17 brain regions affected at 1 wpi showed considerable p-aSYN pathology also at 6 wpi. Comparison analysis revealed that all regions except three displayed a significantly more severe pathology 6 wpi than they did 1 wpi ($P < 0.05$; $n = 4$ for 6 wpi, $n = 3$ for 1 wpi; multiple *t*-tests adjusted with Holm-Sidak method). The only exceptions were the internal segment of the globus pallidus (GPi), tuberal nucleus of the hypothalamus (TU), and the parabrachial nucleus (PB), which showed similar degree of pathology at both time-points.

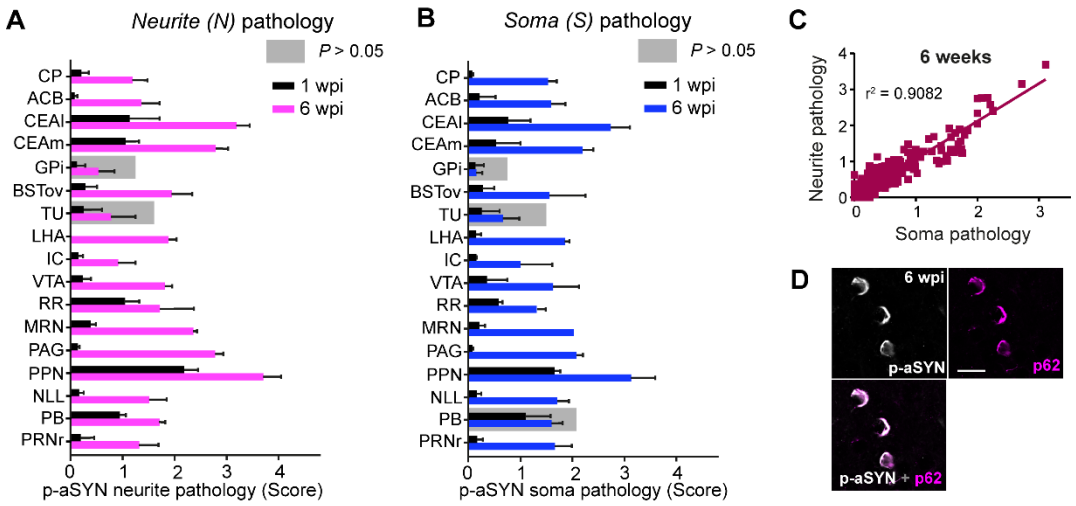

Figure 4.10 | Brain-wide p-aSYN pathology progresses over time

A. p-aSYN neurite scores 1 and 6 wpi of the 17 regions displaying p-aSYN pathology 1 wpi. Neurite pathology significantly increased 6 wpi in all depicted regions, except for those highlighted in grey (P = 0.0001, <0.0001, <0.0001, <0.0001, <0.0001, <0.0001, 0.0018, <0.0001, 0.0074, <0.0001, <0.0001, <0.0001, <0.0001, 0.0021, <0.0001 for CP, ACB, CEAl, CEAm, GPi, LHA, IC, VTA, RR, MRN, PAG, PPN, NLL, PB, and PRNr, respectively; $n = 3$ for 1 wpi; $n = 4$ for 6 wpi; multiple *t*-tests adjusted with Holm-Sidak method).

B. p-aSYN soma scores 1 and 6 wpi of the 17 regions displaying p-aSYN pathology 1 wpi. Neurite pathology significantly increased 6 wpi in all depicted regions, except for those highlighted in grey (P = <0.0001, <0.0001, <0.0001, <0.0001, <0.0001, <0.0001, 0.0010, <0.0001, 0.0044, <0.0001, <0.0001, <0.0001, <0.0001, <0.0001 for CP, ACB, CEAl, CEAm, BSTov, LHA, IC, VTA, RR, MRN, PAG, PPN, NLL, and PRNr, respectively; $n = 3$ for 1 wpi; $n = 4$ for 6 wpi; multiple *t*-tests adjusted with Holm-Sidak method).

C. p-aSYN neurite and soma pathology showed strong correlation 6 wpi ($n = 4$; $r^2 = 0.9082$).

D. Representative high magnification confocal images of the aggregates found in distant brain regions. Aggregates stained positive for both p-aSYN and p62. Scale bar, 25 µm.

Abbreviations: ACB, nucleus accumbens; BSTov, bed nuclei of the stria terminalis, anterior division, oval nucleus; CEAl, central amygdala, lateral part; CEAm, central amygdala, medial part; CP, caudoputamen; GPi, globus pallidus internus; IC, inferior colliculus; LHA, lateral hypothalamic area; MRN, midbrain reticular nucleus; NLL, nucleus of the lateral lemniscus; PAG, periaqueductal gray; PB, parabrachial nucleus; PPN, pedunculopontine nucleus; PRNr, pontine reticular nucleus, rostral part; RR, retrorubral field; TU, tuberal nucleus; VTA; ventral tegmental area.

4.3 The rAAV model of Parkinson's disease

4.3.1 Experimental design

The discovery that missense mutations and duplications/triplications of the aSYN gene (*SNCA*) cause familial forms of PD has prompted the development of animal models based on the overexpression of aSYN [145, 229, 285]. Two different approaches could be distinguished: 1) development of transgenic mouse lines overexpressing human/murine wild-type or mutated aSYN under several distinct promotors [79, 171, 184, 186, 197, 203, 246]; 2) targeted, viral vector mediated overexpression of aSYN in the nigrostriatal system [49, 72, 131, 142, 147, 148, 344]. Whereas former models exhibit aSYN accumulation and Lewy-like pathology in the central nervous system, but are mostly devoid of nigral and LC neurodegeneration [322], latter approach showed repeatedly high efficiency in replicating both the Lewy-like pathology and the cellular death of the dopaminergic SNc. However, up until now, no data exists on the effects of targeted aSYN overexpression in the noradrenergic LC.

To study the brain-wide effects of aSYN accumulation selectively induced in the noradrenergic LC region of wild-type mice, we chose to overexpress human mutated A53T-aSYN with a viral vector mediated approach. A chimeric rAAV vector of serotype 1/2 was used combining the advantages of rAAV serotype 1 (excellent brain penetration), and rAAV serotype 2 (high neuronal tropism). The chosen promotor was the CMV promotor (Fig. 4.11B), which belongs to the strongest known promotors to mediate transient and stable exogenous gene transcription. However, a considerable draw-back of this promotor is its unspecificity: it induces protein expression in neuronal cells as well as adjacent glial and endothelial cells.

To investigate the time-dependency of the brain-wide pathology progression, mice were consecutively sacrificed 1, 3, 6, and 9 wpi and their brains were processed for thorough immunohistochemical analysis (Fig. 4.11A).

4.3.2 Successful overexpression of human A53T-aSYN in the LC

Targeted overexpression of aSYN in the murine LC region is an until now unprecedented approach and the viral vectors used in this study have only been applied to the dopaminergic SNc region [131, 147, 148]. Therefore, we first sought to verify successful transduction[5] of the noradrenergic LC after loco-regional viral vector delivery. Therefore, we double stained coronal sections containing the whole rostro-caudal extent of the LC against tyrosine hydroxylase (TH), a common marker of noradrenergic neurons, and human aSYN (Syn211) or Luciferase (control).

Our analysis revealed successful transduction of the LC region by both the rAAV-A53T-aSYN vector, indicated by human aSYN overexpression (Fig. 4.11C), and the rAAV-Luc vector, indicated by Luciferase overexpression (data not shown). Due to the unspecificity of the CMV promotor, overexpression was not restricted to the TH-positive (noradrenergic) LC cells but was also evident in adjacent TH-negative brain regions, such as the parabrachial nucleus, Barrington's nucleus, mesencephalic trigeminal and vestibular nuclei (Fig. 11C). Robust human aSYN labeling was detectable in the cell bodies as well as axons and dendrites of the transduced cells indicating strong protein overexpression.

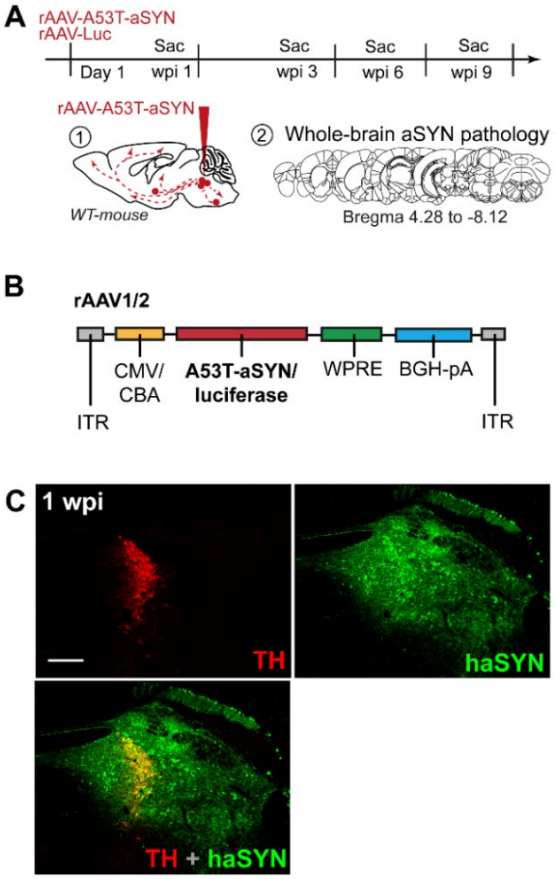

Figure 4.11 | Local viral vector driven overexpression of human A53T-aSYN in the LC region

A. Schematic depicting experimental design. rAAV-A53T-aSYN or –Luc vectors were iúnilaterally injected into the right LC region of wild-type mice. Animals were then consecutively sacrificed 1, 3, 6, and 9 wpi and their brains were processed for thorough immunohistochemical analysis.

B. Schematic of the viral vector map. ITR, inverted terminal repeat; CMV/CBA, chicken β-actin promotor hybridized with a CMV immediate early enhancer sequence; WPRE, woodchuck hepatitis virus posttranscriptional regulatory element; BGH-pA, bovine growth hormone polyadenylation sequence. Viral vector design published in [116].

C. Representative image of human A53T-aSYN overexpression in the noradrenergic LC region of mice at 1 wpi. Tyrosine hydroxylase (TH), red; human aSYN (haSYN), green. Scale bar, 100 µm.

[5] Introduction of foreign DNA-fragment (gene) via viral infection of targeted cells.

4.3.3 Brain-wide transport of human A53T-aSYN as soon as 1 wpi

A few previous studies utilizing viral vector mediated overexpression of aSYN to model PD in animals have described that regionally restricted expression of human aSYN leads to considerable neuron-to-neuron propagation of the protein in the central nervous system [115, 255, 311–313]. *In vivo* studies implicate that this spreading of human aSYN in the murine brain is an active process requiring intact and relatively healthy neurons and involves non-fibrillar forms of aSYN [115, 312]. To investigate whether restricted overexpression of A53T-aSYN in the LC region in our PD model led to brain-wide propagation of human aSYN, we stained eight coronal sections (Bregma: +4.28, +2.86, +1.18, +0.38, −0.58, −3.16, −6.96, and −7.56) covering the complete mouse brain against human aSYN (Syn211) or Luciferase (control). We thereafter generated a grading system (see chapter 3.4.9) and systematically graded the observed axonal and somal human aSYN burden in distinct brain regions.

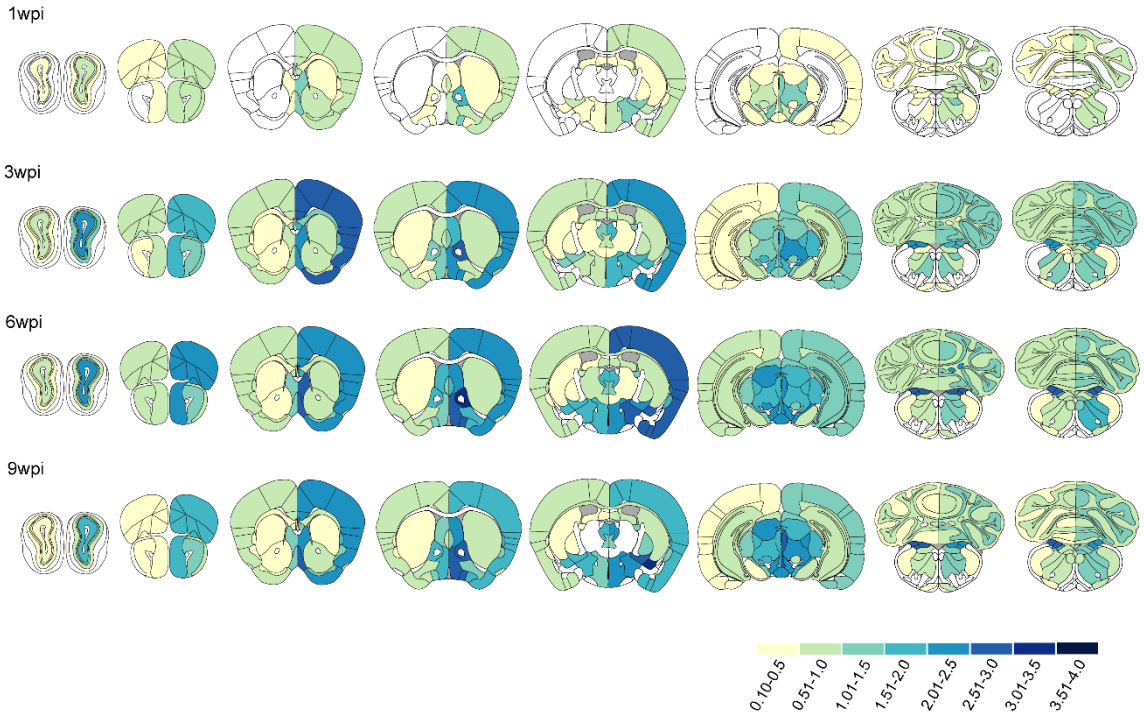

Figure 4.12 | Brain-wide distribution of human aSYN at the respective time-points.
Heatmaps depicting degree of axonal human aSYN-signal 1, 3, 6, and 9 wpi. For more information on the grading system see 3.4.9. *n* = 6 per time-point.

One-week post-injection, robust axonal human aSYN labeling was already observable in several brain regions (Fig. 4.12). Despite the unilateral injection of rAAVs, even at this early time-point, the axonal signal appeared bilaterally, however, the ipsilateral (right) hemisphere was affected more severely. The affected brain regions were distributed throughout the whole brain from the OBs (main olfactory bulb, granular layer) to the caudal medulla (gigantocellular and intermediate reticular nuclei) with the farthest positive region being as far as 8.83 mm away from the injection site (right LC, Bregma −5.4 mm). The most abundant human aSYN signal was detected in the lateral and medial septal nuclei, bed nuclei of the stria terminalis, lateral hypothalamic area, and the midbrain reticular nucleus. Remarkably, no aSYN signal was detected in cell bodies distant from the injection site.

At later time-points (3, 6, and 9 wpi), axonal human aSYN-signal was more abundantly distributed throughout the whole brain and more regions were affected bilaterally compared to 1 wpi. All regions displaying human aSYN-signal at 1 wpi also exhibited axonal pathology at later time-points. The most severely affected regions were the main olfactory bulb, lateral septal nucleus, diagonal band nucleus, bed nuclei of the stria terminalis, central amygdalar nucleus, periaqueductal gray, midbrain reticular nucleus, SNc, and the ventral tegmental area. Further statistical testing of 21 selected brain structures revealed that the vast majority of regions displayed a significant increase of pathology 3, 6, and 9 wpi compared to 1 wpi (Fig. 4.13).

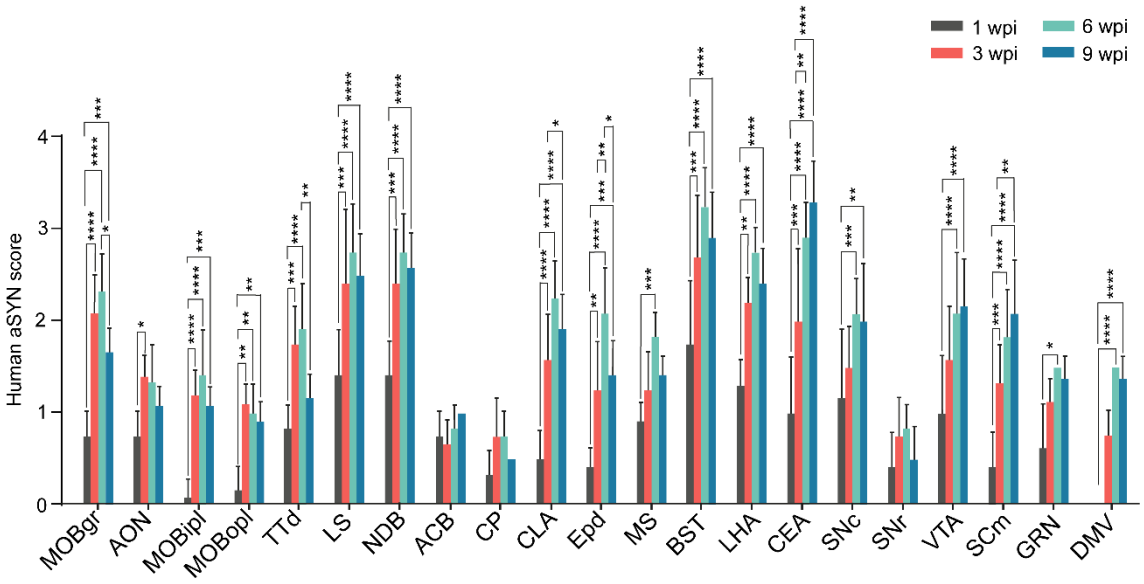

Figure 4.13 | Human aSYN score is significantly increased over time in a subset of brain regions ipsilateral from the injection site.

Graph depicting human aSYN score in preselected brain regions 1, 3, 6, and 9 wpi. gr: P <0.0001 for 1 vs 3 wpi and 1 vs 6 wpi, 0.0008 for 1 vs 9 wpi, 0.0282 for 6 vs 9 wpi; AON: P = 0.00483 for 1 vs 3 wpi; ipl: P = <0.0001 for 1 vs 3 wpi and 1 vs 6 wpi, 0.0002 for 1 vs 9 wpi; opl: P = 0.0013 for 1 vs 3 wpi, 0.0030 for 1 vs 6 wpi, 0.0099 for 1 vs 9 wpi; TTd: P = 0.0008 for 1 vs 3 wpi, P < 0.0001 for 1 vs 6 wpi, and 0.0099 for 1 vs 9 wpi; LS: P = 0.0002 for 1 vs 3 wpi, and < 0.0001 for 1 vs 6 and 1 vs 9 wpi; NDB: P = 0.0002 for 1 vs 3 wpi, and <0.0001 for 1 vs 3 and 1 vs 6 wpi; CLA: P = < 0.0001 for 1 vs 3, 1 vs 6, and 1 vs 9 wpi, and 0.0282 for 3 vs 6 wpi; Epd: P = 0.0030 for 1 vs 3 wpi, <0.0001 for 1 vs 6 wpi, 0.0002 for 1 vs 9 wpi, 0.0030 for 3 vs 6 wpi, and 0.0282 for 6 vs 9 wpi; MS: P = 0.0008 for 1 vs 6 wpi; BST: P = 0.0010 for 1 vs 3 wpi, and <0.0001 for 1 vs 6, and 1 vs 9 wpi; LHA: P = 0.0036 for 1 vs 3 wpi, and <0.0001 for 1 vs 6, and 1 vs 9 wpi; CEA: P = 0.0009 for 1 vs 3 wpi, <0.0001 for 1 vs 6, 1 vs 9, and 3 vs 9 wpi, and 0.0016 for 3 vs 6 wpi; SNc: P = 0.0008 for 1 vs 6 wpi, and 0.0030 for 1 vs 9 wpi; VTA: P < 0.0001 for 1 vs 6, and 1 vs 9 wpi; SCm: P = 0.0008 for 1 vs 3 wpi, <0.0001 for 1 vs 6, and 1 vs 9 wpi, and 0.0099 for 3 vs 9 wpi; GRN: P = 0.0157 for 1 vs 6 wpi; DMV: P < 0.0001 for 1 vs 6, and 1 vs 9 wpi. n = 6 per time-point. Two-way ANOVA with post-hoc Tukey's multiple comparisons tests.

Abbreviations: ACB, nucleus accumbens; AON, anterior olfactory nucleus; BST, bed nuclei of the stria terminalis; CEA, central amygdalar nucleus; CLA, claustrum; CP, caudoputamen; DMV, dorsal motor nucleus of the vagal nerve; Epd, endopiriform nucleus, dorsal part; GRN, gigantocellular nucleus; LHA, lateral hypothalamic area; LS, lateral septal nucleus; MOBgr, main olfactory bulb, granule layer; MOBipl, main olfactory bulb, inner plexiform layer; MOBopl, main olfactory bulb, outer plexiform layer; MS, medial septal nucleus; NDB, diagonal band nucleus; SCm, superior colliculus, motor related; SNc, substantia nigra, pars compacta; SNr, substantia nigra, pars reticulata; TTd, taenia tecta, dorsal part; VTA, ventral tegmental area.

Human aSYN signal was exclusively found in axons and synaptic boutons (Fig. 4.14A-D, high magnification images), and no human aSYN signal was detected in cell bodies apart from the injection site at any time-point. No Luciferase signal was found in in distant brain regions at any time-point (data not shown).

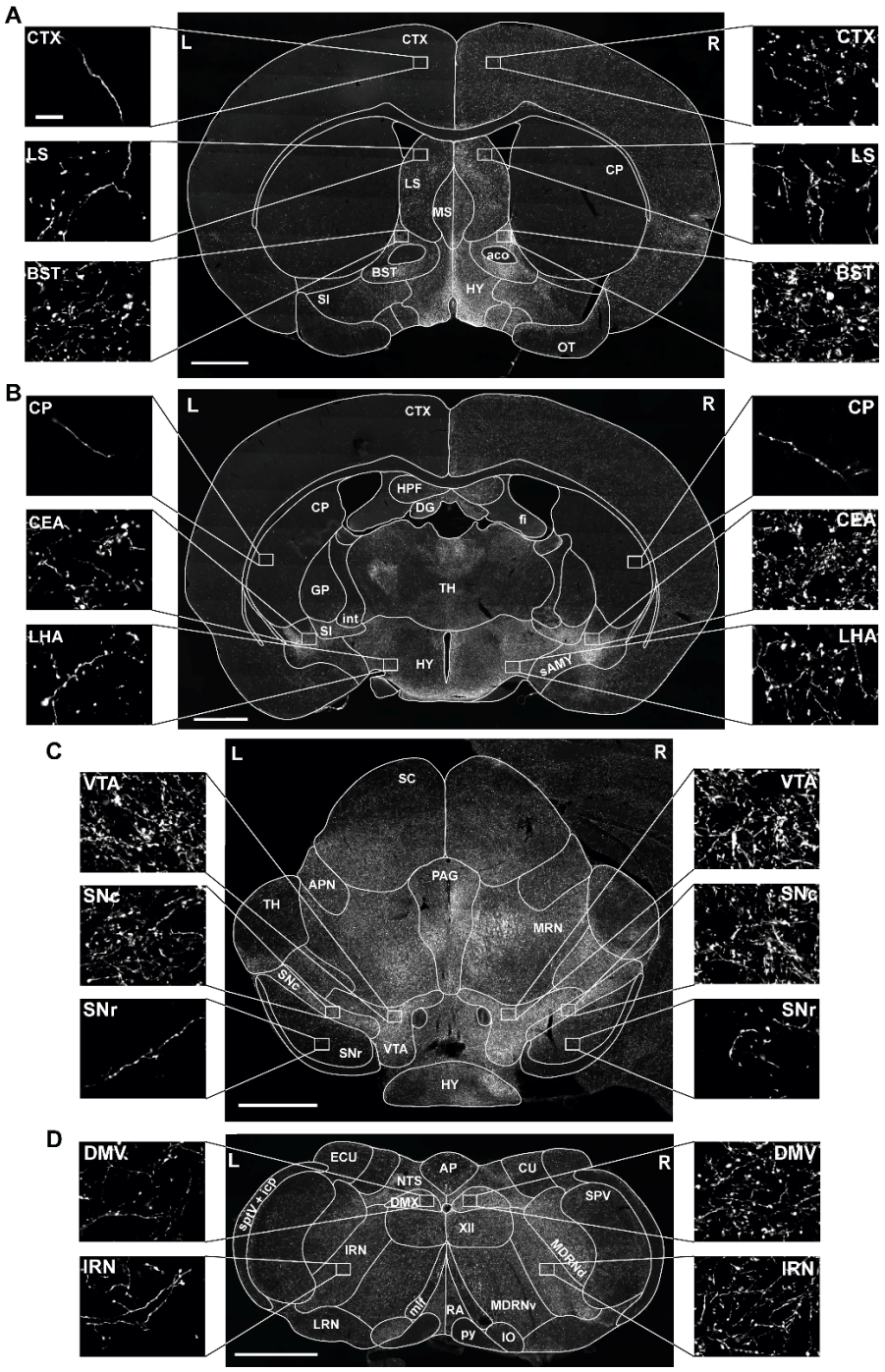

Figure 4.14 | Widespread axonal transport of human A53T-aSYN to distant brain regions.

A-D. Representative images of analyzed brain sections stained against human aSYN (Syn211) 6 wpi (A. Bregma +0.50 mm; B. Bregma −0.94 mm; C. Bregma −3.16 mm; D. −7.56 mm). Scale bar, 1 mm in overview images, 25 µm in high magnification images. Figure was published in [116].

Abbreviations: aco, anterior commissure; AP, area postrema; APN, anterior pretectal nucleus; BST, bed nuclei of stria terminalis; CEA, central amygdalar nucleus; CP, caudoputamen; CTX, cortex; CU, cuneate nucleus; DG, dentate gyrus; DMX, dorsal motor nucleus of the vagus nerve; ECU, external cuneate nucleus; fi, fimbria hippocampi; GP, globus pallidus; HPF, hippocampal formation; HY, hypothalamus; icp, inferior cerebellar peduncle; int, internal capsule; IO, inferior olivary complex; IRN, intermediate reticular nucleus; L, left (contralateral); LHA, lateral hypothalamic area; LRN, lateral reticular nucleus; LS, lateral septal nucleus; MDRNd, medullary reticular nucleus, dorsal part; MDRNv, medullary reticular nucleus, ventral part; mlf, medial longitudinal fascicle; MRN, midbrain reticular nucleus; MS, medial septal nucleus; NTS, nucleus of the solitary tract; OT, olfactory tubercle; PAG, periaqueductal gray; py, pyramid; R, right (ipsilateral); RA, raphe nuclei; sAMY, striatum-like amygdalar nuclei; SC, superior colliculus; SI, substantia innominata; SNc, substantia nigra pars compacta; SNr, substantia nigra pars reticulata; sptV, spinal tract of the trigeminal nerve; SPV, spinal nucleus of the trigeminal; TH, thalamus; VTA, ventral tegmental area; XII, hypoglossal nucleus.

4.3.4 Pathological forms of aSYN are not detectable in distant brain regions

Several previous studies indicate that the progression of Lewy-pathology in PD and PD animal models relies on the intercellular transport of toxic, aggregation-prone aSYN species [99]. According to this hypothesis, pathological forms of aSYN are formed within a subset of neuronal cells (donors), and then transported to synaptically connected neurons (recipients) where they act as seeds triggering the aggregation of endogenous, primarily soluble aSYN.

In our murine model of prodromal PD, we induced the overexpression of human aSYN in the noradrenergic LC region. Pathological, p-aSYN-, p62-, and Ubi-1-positive forms of aggregated aSYN were observable as soon as 1 wpi at the inoculation site [116]. We hypothesized, according to the above theory, that these aggregate harboring cells could act as donors of pathological aSYN and promote the transmission of aSYN aggregates to distant brain regions. As the aggregate formation in the recipient neurons involves endogenous *murine* aSYN, the antibody against human aSYN (Syn211) used in the previous analysis (chapter 4.3.3) would only detect the artificially overexpressed aSYN and not the induced pathology in distant brain regions. Therefore, to test whether pathological aSYN species are observable in distant neurons, we stained coronal sections with an interslice distance of 240 µm of the whole murine brain against common markers of pathological aSYN, namely p-aSYN, p62, and Ubi-1.

In contrast to the above proposed hypothesis, our whole-brain analysis revealed that brain regions distant from the injection site were devoid of pathological forms of aSYN even at the longest, nine-week time-point (data not shown). None of the regions displaying high axonal human aSYN burden (e.g. bed nuclei of the stria terminalis, central amygdalar nucleus, periaqueductal gray) did exhibit p-aSYN, p62, or Ubi-1 positive aSYN species. Signal was neither observed axonally nor in perikarya.

4.3.5 No degeneration of the dopaminergic SNc was detectable 9 wpi

Previous studies have demonstrated that loco-regional viral vector mediated overexpression of human aSYN leads to propagation of aSYN through neuronal connections and progressive neurodegeneration of secondary brain regions [255, 311]. We wanted to investigate whether this also translates into our mouse model. Therefore, we stereologically quantified dopaminergic, TH-positive neurons of the SNc 9 wpi in A53T-aSYN and Luciferase overexpressing animals.

Despite the unilateral injection of rAAV vectors, transport of human aSYN was observed bilaterally, although the ipsilateral (right) SNc displayed more abundant human aSYN-signal. Human aSYN-positive axons were observable as soon as 1 wpi in the SNc region, and at 9 wpi, the region was densely covered (Fig. 4.15A). However, no human aSYN-signal was detectable in TH-positive dopaminergic SNc somata at any time-point.

Unbiased stereological quantification revealed no significant difference in the number of TH-positive neurons of A53T-aSYN overexpressing animals compared to Luciferase overexpressing mice (Fig. 4.15B). Difference was neither present ipsi-, nor contralaterally to the injection site.

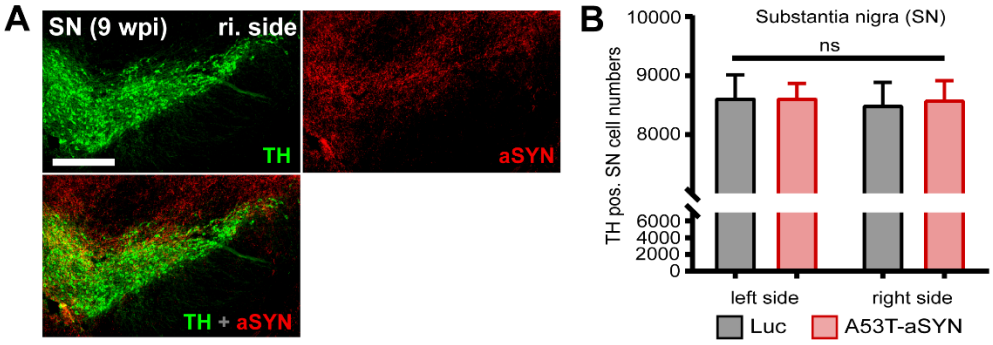

Figure 4.15 | No degeneration of dopaminergic SNc neurons 9 wpi. Figure published in [116].

A. Representative overview image of the right SNc region of wild-type mice overexpressing human A53T-aSYN in the LC region. Scale bar, 250 µm

B. Quantification of TH-positive SNc neurons revealed to significant difference between A53T-aSYN (red bars) and Luciferase (black bars) overexpressing animals 9 wpi. Values are presented as mean ± SEM, one-way ANOVA analysis, $n = 8$ per group.

5 Discussion

The purpose of the herein presented study was twofold: (1) we wanted to establish a new PFF-induced mouse model of PD at the level of the mesopontine PPN and investigate whether the selective vulnerability pattern of this nucleus in human PD also translates into a PFF mouse model; (2) we wanted to compare the aSYN propagation pattern in two distinct aSYN-based animal models.

In the first part of the study we showed that loco-regional PFF injection led to intraneuronal aggregate formation in the PPN. Inclusion bodies were immunoreactive to p-aSYN and p62, and were proteinase resistant thereby recapitulating several key features of human LBs. Remarkably, despite representing only around 25% of PPN neurons, cholinergic cells harbored the brunt of p-aSYN pathology, and also displayed significant cell loss 12 wpi. Interestingly, reactive microgliosis was observed both in PFF and monomeric aSYN (control) injected animals, although no other pathology was observed in control animals. Additionally, injection of PFF's led to widespread transneuronal propagation of p-aSYN to brain regions far beyond the injection site. Pathology was found in perikarya (somal pathology) reminiscent of LBs as well as in axons reminiscent of human LNs.

In the second part of the study we showed that targeted, viral vector mediated overexpression of human mutated A53T-aSYN in the noradrenergic LC led to widespread axonal transport of human aSYN to distant brain regions. Interestingly, signal was exclusively found axonally and no cell bodies were positive outside the primarily transduced LC region. No pathological forms of aSYN were detected in distant brain regions. Additionally, unbiased stereological quantification of the dopaminergic SNc revealed no significant cell loss at the relatively short time-frame of 9 weeks.

5.1 The fibril model of Parkinson's disease

5.1.1 PFF's lead to Lewy body-like aggregate formation

One of the major neuropathological hallmarks of PD are intraneuronal aSYN-containing proteinaceous inclusion bodies called LBs or LNs, based on the predominant location in perikarya or axons [30]. Postmortem studies of PD patients revealed that approximately 90% of aSYN found in LBs is phosphorylated at serine 129 (S129-phosphorylation), whereas only 4% of soluble monomeric aSYN is phosphorylated at this residue indicating that this

posttranslational modification of aSYN occurs during the pathogenic process of PD and might increase the aggregation propensity of the protein [5, 85, 114, 230, 262, 275]. Therefore, the detection of S129-phosphorylated aSYN serves as a common aggregation marker both in human neuropathological studies as well as in animal models of PD [16, 177, 179, 242, 259]. In our model, a single inoculation of pathological PFF into the PPN region of mice induced progressive accumulation of aSYN inclusions at the injection site as evidenced by p-aSYN staining. As the exogenously injected PFF's are unphosphorylated, detection of S129-phosphorylation in our model reflects an intracellular modification. Based on their location and shape, two types of aggregates could be distinguished: (1) large somal, located in the perinuclear region of the neuronal cell bodies; and (2) small, thread-like aggregates most likely located in axonal processes. The aggregates were highly reminiscent of human LBs and LNs found in postmortem PD brain tissues.

Several studies have raised doubts whether the mere detection of p-aSYN truly proves the presence of high molecular weight aSYN aggregates [116, 275, 303]. Therefore, we investigated additional aggregation markers used in postmortem neuropathological studies: p62-positivity and PK resistance.

The cell possesses several distinct pathways to get rid of toxic, misfolded, or unnecessary proteins. The two major pathways are: (1) ubiquitin-proteasome system, which is used to degrade small or intermediate forms of pathological aSYN, such as oligomers; and (2) the autophagy-lysosomal pathway, a catabolic cellular process in which higher molecular weight aSYN forms are removed [318]. p62, also called sequestosome-1 (SQSTM1) is a stress-inducible protein which acts as an autophagy receptor: it binds to cargos such as ubiquitinated aggregates and directs them toward selective autophagy [146]. In neurodegenerative proteinopathies, including PD, the accumulating aggregates display p62-positivity, which is therefore commonly used to screen for aggregated forms of various proteins [157, 158]. In our model, almost all the p-aSYN-positive aggregates stained also positive for p62 indicative of an overloaded or dysfunctional autophagy-lysosomal pathway. p62-positivity was observed in both large perinuclear as well as thread-like axonal inclusions.

A common method to prove (or disprove) insolubility of protein aggregates is by digestion of the tissue with broad-spectrum proteases such as Proteinase K (PK), which was used in several postmortem neuropathological studies to demonstrate the insolubility of aSYN aggregates in PD brains [131, 203, 275]. Therefore, we performed PK digestion on our brain tissue samples and thereafter stained for p-aSYN in combination with p62. We could show

that the vast majority of the developing p-aSYN- and p62-positive aggregates at the injection site were truly insoluble protein inclusions.

Taken together, PFF injection into the PPN region induced aSYN inclusion formation recapitulating several key features of human LBs and LNs, such as p-aSYN- and p62-positivity and PK resistance. Our results prove that PFF's possess prion-like properties *in vivo* by templating and seeding the misfolding of endogenous murine aSYN thereby triggering the aggregation of primarily native and soluble aSYN.

5.1.2 Cholinergic PPN neurons are selectively vulnerable to PFF's

The PPN is a neurochemically heterogeneous structure composed of three distinct neuronal subtypes: cholinergic, GABAergic, and glutamatergic [327]. In neuropathological studies of PD brains, despite this inherent heterogeneity, the occurrence of LBs predominates in cholinergic neurons [108]. Additionally, cholinergic neurons seem to be more susceptible to the disease process than GABAergic neurons, as the loss of cholinergic neurons is reported to be up to 57%, whereas only around 18% of GABAergic neurons are lost during the disease process [117, 122, 137, 226, 249].

We found that the specific pattern of pathology distribution seen in human PD brains also translates into our PFF model. Although all neuronal subtypes were exposed to the same extracellular PFF concentration, the distribution of p-aSYN aggregates between the three neuronal subtypes did not follow the natural proportional composition of PPN: in spite of representing the smallest cell group of the PPN (up to 25% of neurons) [181], the vast majority of aggregates localized to cholinergic neurons (up to 89% 6 wpi, and 77% 12 wpi). Additionally, we detected selective and significant loss of ChAT-positive (cholinergic) neurons, whereas neuronal counts of non-cholinergic neurons did not show any alterations within the observational period of 12 weeks. The loss of ChAT-positive neuronal count can implicate loss of acetyl choline transferase (ChAT) expression, cholinergic neuronal cell death, or a mixture of both.

The finding that cholinergic PPN neurons are particularly susceptible to PFF induced pathology is intriguing. Currently, due to the sparse knowledge and data on PPN neurons, we can only speculate the underlying cellular factors for this differential susceptibility. In the following paragraphs, we will give a brief list of factors which might contribute to the observed vulnerability of cholinergic, and partial resistance of non-cholinergic neurons to PFF induced pathology.

1. Expression of fibril receptors

The prerequisite for pathological aSYN seeding by exogenously inoculated PFF's is their internalization into cellular compartments where soluble endogenous aSYN is present. A large body of evidence indicates that aSYN PFF's are taken up by neurons via receptor mediated endocytosis [124, 169, 183]. Several cell-surface molecules have been found to bind aSYN PFF's, including heparin sulfate proteoglycans, neurexin 1β, amyloid β precursor-like protein 1 (APLP1), or lymphocyte-activation gene 3 (LAG3) [124, 126, 183]. *In vitro* experiments by Mao and colleagues implicated a dose-dependent effect of LAG3 receptors on the rate of PFF internalization, as LAG3 overexpression significantly enhanced PFF internalization, whereas LAG3 knockout cells exhibited only minimal PFF endocytosis [183]. Additionally, deletion of LAG3 significantly attenuated PFF-induced neuropathology in the CNS of LAG3 knockout mice, however, did not fully abolish intracerebral aggregate formation [183]. This suggests that LAG3 is a significant, but not exclusive mediator of PFF internalization.

Data on the different expression level of LAG3 and potentially other receptors mediating PFF internalization by different neuronal subtypes are not existing. However, different level of fibril-receptor expression might significantly contribute to the vulnerability neurons.

2. Endogenous aSYN-levels

Multiplication of the *SNCA* (aSYN gene) leads to autosomal dominantly inherited PD. A clear relationship between the level of aSYN expression (copy number of the gene) and the age of onset, distribution of neuropathology, severity of disease, and pace of progression could be observed, implicating a dose-dependent effect of aSYN [42, 128]. PFF's, similar to prion proteins, serve as templates and trigger the misfolding and aggregation of endogenous aSYN *in vitro* and *in vivo* (homologous seeding). The seeding capacity of PFF's depends on the presence and concentration of their endogenous counterparts [138, 179, 190, 320].

Although a comprehensive map of aSYN expression levels in distinct brain regions and neuronal subtypes is lacking, a few studies investigated key brain areas in the development of PD. The level of aSYN expression significantly differed between neuronal subtypes. Generally, GABAergic neurons and interneurons showed the least immunoreactivity to aSYN, whereas catecholaminergic neurons showed a rather robust labeling [22, 299, 300]. The level of aSYN expression in glutamatergic synapses varied considerably between different brain regions [300].

Studies specifically investigating aSYN expression levels in distinct PPN neuronal subtypes are lacking. However, it is tempting to speculate that the observed resilience to PFF induced pathology of GABAergic neurons in the PPN might partly be due to their low aSYN expression levels.

3. aSYN phosphorylation capacity

Around 4% of aSYN is phosphorylated at serine 129 physiologically, whereas over 90% of aSYN found in LBs is phosphorylated at this residue [85]. The exact pathophysiological relevance of this post-translational modification, however, is still controversial.

In vitro studies showed that phosphorylation of monomeric aSYN increases its propensity to self-assemble into fibrils and aggregates [85, 262, 287]. Moreover, targeted injection of primarily phosphorylated PFF's induced more severe aggregate formation and neurodegeneration *in vivo* than did non-phosphorylated or phosphorylation deficient PFF's implicating that S129-phosphorylation enhances the aggregation propensity and neurotoxicity of the fibrils [138]. However, reports on unaltered toxicity, or even neuroprotective effects of S129-phosphorylation exist [10, 159, 193, 216].

The cell possesses several kinases to phosphorylate aSYN at S129 including but not limited to polo-like kinases 1-3 (PLK), G protein-coupled receptor kinases (GRK), or leucine-rich repeat kinase 2 (LRRK2) [230]. Differential expression of these kinases between neuronal subtypes could influence their general vulnerability to PFF induced pathology. The significance of aSYN phosphorylation in the pathogenesis of PD needs further clarification.

4. Extensive axonal arborization and rate of oxidative phosphorylation

Neurons which are predominantly affected by LB formation in PD such as the dopaminergic SNc or the noradrenergic LC possess long, thinly or unmyelinated axons which show extensive arborization in their target regions [31, 191, 297]. Thus, axonal hyperbranching has been proposed as a key vulnerability factor in PD.

A recent study by Pacelli and colleagues compared the axonal arborization and oxidative phosphorylation capacity of SNc, ventral tegmental, and OB dopaminergic neurons [217]. They showed that the most vulnerable SNc neurons have the most extensively arborizing axonal tree, whereas the least vulnerable OB neurons have the smallest axonal arbor size [217]. They also observed a considerably higher basal oxidative phosphorylation rate of SNc neurons compared to OB and ventral tegmental neurons. Remarkably, a reduction of axonal arborization of SNc neurons significantly decreased their basal oxidative phosphorylation

rate and their vulnerability to the neurotoxin MPP^+ indicating that the degree of axonal arborization is a key contributor to the vulnerability of neurons [217].

Mena-Segovia and colleagues have demonstrated in single-cell tracing studies that cholinergic PPN neurons have a highly collaterizing axonal arborization which might contribute to their selective vulnerability observed in our PFF model [195]. Studies on GABAergic and glutamatergic neurons are to our knowledge not available. However, as GABAergic cells seem to function as local interneurons and their axonal projections do not leave the PPN region [154], their axonal collateralization is assumably lower.

5.1.3 Aggregate formation *per se* does not induce reactive microgliosis

Since the first description of apparent microgliosis in the SNc of PD patients in 1988 [194], the number of studies addressing the role of neuroinflammatory processes in disease initiation and progression is ever growing.

Microglia are the resident immune cells of the CNS making up around 10-20% of adult glial cells [168, 289, 293]. Postmortem studies of PD brains have observed the presence of activated microglia in various brain regions including but not limited to the SNc, putamen, LC, and hippocampus [55, 84, 129, 144, 194]. Additionally, positron emission tomography (PET) studies of microglia activation using the translocator protein (TSPO) radioligand ^{11}C-PK11195 demonstrated early and long-lasting microglial activation in the pons, basal ganglia, putamen, and midbrain of PD patients [14, 93, 215]. Remarkably, activation of microglia seemed to better correlate with the presence of α-synucleinopathy than neuronal cell loss [78, 264], which was also confirmed by neuropathological studies [55].

In our model, injection of PFF's was accompanied by significant microgliosis at the injection site as evidenced by an increase of IbA1-positive pixel count. Microgliosis was already evident at the earliest 6-week time-point (Fig. 4.5A), even before significant cholinergic cell loss was present (Fig. 4.6A), and persisted without further progression until 12 wpi. Remarkably, injection of monomeric aSYN (control) induced a comparable degree of microgliosis at the injection site, despite the absence of aggregate formation, and neurodegeneration. In contrast to human studies implicating a correlation of the presence of intraneuronal aSYN aggregates (LBs) and activated microglia [55], we did not detect microgliosis in the contralateral PPN region of PFF injected mice, in spite of p-aSYN aggregate formation in cholinergic neurons (Fig. 4.5B). This implicates that in our model, intraneuronal aggregate formation *per se* does not induce activation of microglial cells.

In vitro studies showed that extracellular aSYN can act as chemoattractant and damage-associated molecular pattern (DAMP) inducing activation and recruitment of microglia resulting in pro-inflammatory cytokine production (IL-1β, IL-6, TNF-α), elevated expression of COX-2 and inducible nitric oxide synthase (iNOS), and elevated free radical production [ROS, reactive nitrogen species (RNS)] [170, 253, 295, 328]. The rate of microglial activation strongly depended on the structure of aSYN: fibrillar forms of aSYN induced the highest level of pro-inflammatory cytokine production and secretion compared to monomeric or oligomeric aSYN [123].

In our model, inoculation of monomeric aSYN or PFF's into brain parenchyma primarily results in high levels of extracellular monomeric aSYN or PFF's, which, based on the above mentioned *in vitro* studies, likely act as chemoattractants and activators of microglial cells *in vivo* resulting in reactive microgliosis at the injection site. However, in contrast to the *in vitro* studies describing a structure-dependent activity level of microglial cells, we did not detect any differences between monomeric aSYN and PFF injected animals in the level of microglia activation. Importantly, as the method utilized in this study to investigate microglial activation solely measured IbA1-positive pixel count reflecting microglial morphological changes (ramified → amoeboid) and microglial proliferation, we might have missed different levels of cytokine production in PFF injected animals compared to controls.

In vivo studies of aSYN overexpression in predetermined neuronal populations either in transgenic mouse lines or via rAAV-mediated approaches showed that aSYN overexpression alone, even in the absence of overt neurodegeneration, was enough to elicit reactive microgliosis [295, 305, 330]. The proposed mechanism of microglial activation in these models is neuronal secretion of different forms of aSYN, which then leads to microglial recruitment and activation. Neuronal secretion of aSYN is supported by *in vitro* as well as *in vivo* studies demonstrating that aSYN can be secreted by neurons in an activity-dependent manner [4, 69, 70, 345].

Remarkably, despite the suggested correlation of α-synucleinopathy and regional activation of microglia in human PD brains and aSYN overexpression-based animal models of PD [55, 100, 263, 295, 305, 330], we did not detect any activation of microglia cells in the contralateral, aggregate-containing PPN region of PFF injected mice. Currently, we can only speculate about the underlying cause of this discrepancy. The induction of α-synucleinopathy in aSYN overexpression and PFF models is substantially different. Whereas overexpression-based animal models induce supraphysiological aSYN levels, PFF's trigger the misfolding of physiological levels of endogenous aSYN and result in a rather decreased cytoplasmic aSYN

level due to the relocalization of the protein to intraneuronal aggregates [213, 322]. Thus, neurons overexpressing high amounts of aSYN most likely secrete considerably higher amounts of the protein compared to neurons with physiological levels of aSYN. As the activation level of microglia correlates with extracellular aSYN concentrations [295], this might lead to a differential activity level of microglia in overexpression- and PFF-based animal models.

5.1.4 PFF induced pathology spreads over considerable distances

A better understanding of the mechanisms and routes of disease progression would provide key opportunities to develop disease-modifying (neuroprotective) strategies. Several lines of evidence, including the Braak staging scheme and studies of PFF animal models indicate that PD pathology spreads in a predictable manner between brain regions sharing considerable interconnections [30, 31, 188, 190, 205, 242].

Our whole-brain analysis of the propagation pattern of p-aSYN pathology revealed that PFF induced pathology was not restricted to the close vicinity of the inoculation site but was observed in brain regions far beyond the left PPN region. First p-aSYN aggregates in distant brain regions were observable as soon as 1 wpi. At this early time-point, aggregates were confined to the ipsilateral (left) hemisphere with only one region being affected bilaterally. Thereafter, pathology progressed both in severity and distribution affecting up to 286 brain regions at the 6-week time-point. Despite the unilateral injection, aggregates were found bilaterally, although the ipsilateral (left) hemisphere was affected more severely. Aggregates were distributed throughout the whole brain spanning from the olfactory bulb to the spinal cord with the farthest positive region being as far as 7.19 mm away from the injection site. We found a strong correlation between the degree of somal and neuritic pathology at 1 as well as 6 wpi, indicating that the neuritic Lewy-like pathology most likely represents axonal p-aSYN pathology of those neurons who exhibit somatic inclusions. Monomeric aSYN injected animals were devoid of p-aSYN aggregates indicating that the conformational difference of monomeric (soluble) aSYN and PFF is crucial in the induction of pathology.

Simple diffusion of the injected PFF's in the brain parenchyma and cerebrospinal fluid is an unlike explanation of the seeding effect in distant brain regions. Upon simple diffusion, due to the dose-dependency of the aggregative potential of PFF's [102], one would expect severe pathology in close proximity to the injection site, which would gradually decrease with longer distances from the primary inoculation. This expected gradient of pathology was not evident in our analysis as we did not observe any regularity in the severity of p-aSYN pathology and

the distance from the injection site (Fig. 4.7B,C). A confounding factor is certainly the selective vulnerability pattern of different neuronal populations which would likely influence this expected gradient of pathology (see chapter 5.1.2). However, the dopaminergic SNc, which lays in close proximity to the injection site (0.56 mm rostral from the PPN), and shows considerable vulnerability to PFF induced pathology in animal models [179, 189, 223], did not display any pathology 1 wpi and only moderate pathology 6 wpi. Additionally, affection of the contralateral hemisphere cannot be explained by simple diffusion of PFF's.

A more likely explanation of the observed brain-wide pathology is axonal transport and cell-to-cell transmission of PFF's within interconnected neuronal circuits. *In vitro*, microfluidic chambers can be used to separate axonal projections from perikarya of cultured neurons and additionally prevent diffusion of PFF's between chambers. Studies utilizing this system showed that PFF's can be transported in the anterograde and retrograde direction and second-order neurons primarily not exposed to exogenous PFF's can readily acquire aggregates indicative of cell-to-cell transmission of pathological aSYN species within neuronal interconnections [83, 102, 320]. Under *in vivo* conditions, injection of human monomeric aSYN into the OB of mice resulted in fast transport of the protein to brain regions sharing strong interconnections with the primary inoculation site in less than one hour [241]. Additionally, further *in vivo* studies evidenced interneuronal transmission of pathogenic aSYN species as a likely event in disease progression. Animal studies modeling intrastriatal dopaminergic cell transplantation observed the transfer of host-derived aSYN to engrafted neurons which can only be explained by cell-to-cell transmission of the protein [6, 62, 111, 150].

In an elegant set of experiments, Okuzumi and colleagues demonstrated that propagation of PFF's in the murine brain strongly depends on the integrity of axonal interconnections [210]. They performed corpus callosotomy[6] prior to unilateral PFF injection into the dorsal striatum and compared the brain-wide propagation pattern of p-aSYN pathology in mice with and without callosotomy [210]. They observed significant reduction of p-aSYN aggregates in the contralateral hemisphere in animals that underwent callosotomy prior to PFF inoculation compared to animals without callosotomy [210]. As the corpus callosum comprises the major commissural fiber tract connecting the two hemispheres, this highly indicates that propagation of PFF pathology depends on intact neuronal interconnections.

[6] Corpus callosotomy: surgical intervention in which the corpus callosum is cut through.

Our results of the brain-wide propagation pattern of PFF induced pathology is consistent with the proposed progression of pathology within given neuronal circuits as regions developing p-aSYN aggregate pathology lay all within the known anterograde- or retrograde connectomes of the PPN. However, it must be noted that not all interconnected regions developed pathology indicating that factors other than synaptic interconnectivity may also play a crucial role in determining the route of pathological aSYN progression. For example, the thalamus is a major output structure of both the cholinergic and glutamatergic PPN [59, 154, 196], nevertheless, no or only sparse pathology was observed 1 and 6 wpi. Similarly, although the SNr strongly innervates glutamatergic PPN neurons [254], it was almost devoid of pathology at all examined time-points.

Currently, we can only speculate about the additional factors determining pathology spread in our model. These certainly include the selective vulnerability factors mentioned in chapter 5.1.2, which might influence the degree of evolving pathology due to extracellular and intracellular PFF exposure. Additionally, further factors might impact the acquisition and degree of pathology in interconnected brain regions. These include: (1) strength of synaptic interconnectivity; (2) the firing frequency of the interconnected neuron, as higher firing frequencies might lead to increased PFF endocytosis due to increased rate of vesicle membrane recycling [29]; (3) the degree of myelination of PFF exposed axons, as the myelin sheath might act as a physical barrier against PFF's [205].

5.2 The rAAV-model of Parkinson's disease

In this part of the study we showed that targeted, viral vector mediated overexpression of human mutated A53T-aSYN in the noradrenergic LC led to widespread axonal transport of human aSYN to distant brain regions.

5.2.1 Human aSYN progression is consistent with axonal transport

Our whole-brain analysis of human aSYN progression following successful viral vector mediated protein expression in the LC region revealed widespread axonal human aSYN signal in A53T-aSYN overexpressing animals as soon as 1 wpi, which progressed significantly to later time-points. Despite the unilateral vector injection, signal was also abundantly found in the contralateral hemisphere. However, aSYN-positive axons were more abundantly found ipsilaterally. Human aSYN was solely found in axons and synaptic boutons, no cells (neurons or glia) showed somatic human aSYN immunoreactivity distant from the injection

site. Remarkably, no p-aSYN, p62, or Ubi-1-positive pathological forms of aSYN were detectable at any examined time-point. Additionally, no axonal labeling of the control protein Luciferase was found at any time-point distant from the injection site, which might be due to its significantly higher molecular weight (Luciferase 62 kDa vs. aSYN 15 kDa), or due to the physiological presynaptic localization of aSYN.

The distribution of axonal signal in our model is consistent with intra-axonal, anterograde transport of human aSYN to the respective output regions of the primarily transduced LC, and partly parabrachial and vestibular nuclei. This finding is consistent with previous studies reporting human aSYN transport within the axonal fields of the mesencephalic dopaminergic system following successful transduction of SNc and ventral tegmental neurons [60, 131, 142, 147].

Previous studies report a cell-to-cell transmission of overexpressed aSYN in the murine brain. One study showed that striatal engrafted fetal rat ventral mesencephalic neurons acquired human aSYN following viral vector mediated overexpression of the protein in adjacent brain regions [150]. Additionally, Ulusoy and colleagues reported neuron-to-neuron transmission of human aSYN following targeted overexpression of human aSYN in the cholinergic vagal nerve and its neuronal cell bodies (dorsal motor nucleus of the vagal nerve, and nucleus ambiguus) [255, 311]. We did not detect any human aSYN-immunoreactivity in cell bodies outside the primarily transduced LC region at any investigated time-point, which argues against interneuronal transport of aSYN in our overexpression-based animal model. This is in line with the finding that despite abundant axonal human aSYN-pathology in the SNc region of A53T-aSYN overexpressing mice, we did not detect any alterations of dopaminergic neuronal cell counts between aSYN and Luciferase injected animals. To detect spread of human aSYN and consequent cellular loss in target regions in the model, longer observational periods might be needed.

Interestingly, no p-aSYN signal was found in distant brain regions, neither axonally nor in cell bodies. This is especially intriguing as the LC region showed abundant and progressive intraneuronal accumulation of p-aSYN in primarily transduced neurons [116]. The underlying cause of this discrepancy is not known. However, as phosphorylation at specific residues of proteins might change their axonal transport rates [57, 250], the disparity between the p-aSYN labeling of the cell body and the axons might therefore stem from different efficacy in axonal transport of non-phosphorylated and phosphorylated aSYN, which was already reported in cell culture systems [258]. Therefore, axonal p-aSYN might be apparent at later observational time-point, which is in line with a previous study of a nigral

overexpression model showing p-aSYN immunoreactivity in a subset of human aSYN-positive axons 13 wpi [344].

5.3 Comparison of the spreading pattern of two PD models

In this study, the propagation pattern of induced pathology was investigated in two different types of PD animal models.

In the PFF model of PD, PFF's were injected unilaterally into the left PPN region of mice inducing progressive recruitment of endogenous, primarily soluble aSYN into p-aSYN- and p62-positive, PK resistant aggregates. PFF-induced pathology was not confined to the injection site but also spread over considerable distances to brain regions far beyond the left PPN region. P-aSYN-positive inclusions were found bilaterally, both in perikarya of neurons reminiscent of human LBs (somal pathology), and in axons reminiscent of human LNs (neuritic pathology). The propagation pattern of pathology was consistent with trans-neuronal transport of pathological aSYN species within interconnected neuronal circuits.

In the rAAV mediated overexpression based animal model of PD, human A53T-aSYN expressing rAAV vectors were injected into the right LC region of mice inducing robust human aSYN overexpression at the injection site. The supraphysiological levels of aSYN resulted in severe aSYN pathology at the injection site in form of progressive accumulation of p-aSYN, and p62- and Ubi-1-positive aggregates [116]. However, in stark contrast to the PFF model of PD, distant brain regions were devoid of p-aSYN immunoreactivity. Moreover, although robust human aSYN signal was found in brain regions distant from the injection site, immunoreactivity was confined to axons most likely of the primarily transduced pontine tegmental neurons, and was not found in cell bodies apart from the inoculation site. This finding implicates that in the human aSYN overexpression based model, trans-neuronal transport of human aSYN did not take place or remained under the detection threshold in the time-frame of 9 weeks.

The reason for this difference in the two models most likely lies within the high dissimilarity of the approaches by which α-synucleinopathy was induced *in vivo*. In the PFF model, nucleation-dependent aggregation of endogenous aSYN is triggered by addition of exogenous protein seeds (PFF's). In this scenario, the templated misfolding of physiological levels of intracellular aSYN takes place most likely resulting in lower aSYN concentration due to its relocalization to aggregates [213]. *In vitro* experiments with microfluidic neuronal cultures reported efficient anterograde and retrograde transport of both oligomeric aSYN

and aSYN fibrils [32, 83]. Moreover, second order neurons in the axonal chamber acquired exogenously added PFF's which seeded the recruitment of endogenous aSYN [83, 183]. This highly implicates that the seeding potential of PFF's is maintained even after axonal- and interneuronal transport.

In the viral vector mediated model, loco-regionally injected rAAV vectors induce the overexpression of human aSYN resulting in supraphysiological levels of intracellular aSYN. The exact mechanisms of aSYN aggregate formation in these models are unknown, but might include concentration-dependent aggregation of aSYN, and overburden and disruption of the protein degradation systems, i.e. the proteasomal and autophagy-lysosomal systems. Cell culture models of inducible overexpression of aSYN showed that soluble monomeric and oligomeric aSYN are readily detectable in the supernatant indicating secretion of cell-produced aSYN [69]. Interestingly, purified fractions of the secreted aSYN could only be internalized by proliferating, but not by differentiated SH-SY5Y cells or primary cortical neurons [69]. Additionally, even after cellular uptake of extracellular aSYN species, no aggregate formation was detected in these cells [69]. These results translate well into our *in vivo* model of aSYN overexpression, where no pathological aggregates were found distant from the injection site. Although highly speculative, but the results might indicate that the aSYN species formed within overexpressing neurons are not readily transmissible between neuronal populations and that they do not possess prion-like properties and therefore cannot induce the templated misfolding of endogenous aSYN [309].

5.4 Limitations of the study

A number of limitations of this study have to be considered. First, the primary induction site of the focal α-synucleinopathy was different in the two investigated animal models of PD. Whereas PFF's were injected into the neurochemically heterogeneous ponto-mesencephalic PPN, viral vector mediated overexpression of A53T-aSYN was induced in the mainly noradrenergic LC. These two brain nuclei, although sharing some common features, exhibit significant differences including neurochemical properties, wiring architecture, and electrophysiological properties. One might hypothesize that the essentially different propagation pattern of α-synucleinopathy in the two PD models might be partly or even entirely attributable to the inherent differences of PPN and LC neurons. This limits the generalizability of the results, and therefore, the results should be interpreted as preliminary. Further investigations are needed to confirm the significantly different propagation pattern

of PFF and rAAV induced focal α-synucleinopathy. Accordingly, we plan to inject PFF's into the noradrenergic LC region, and rAAV-A53T-aSYN into the PPN region of mice in a follow-up study to confirm our preliminary results.

Second, we used different aSYN species in the two parts of the study. In the LC, overexpression of *human* mutant A53T-aSYN was induced via viral vector mediated overexpression, whereas PFF's were generated from *mouse* aSYN. Human wild-type and mouse aSYN differ in only six out of 140 amino acid residues and are therefore 95.7% homologous [167]. The amino acid alanine is found at position 53 in wild-type human aSYN, and a subtitution of alanine to threonine causes autosomal dominantly inherited PD (A53T-aSYN) [229]. Remarkably, threonine is the naturally occurring amino acid at position 53 in rodents, hence, A53T-aSYN and mouse aSYN differ in only five amino acids and therefore share a 96.4% homology [167]. Despite this high homology, partial species barrier was evidenced by several studies which showed that injection of PFF's generated from human aSYN showed less efficiency in inducing local and brain-wide pathology in wild-type mice compared to PFF's generated from mouse aSYN [180, 189, 242]. The lack of intercellularly transmitted pathological aSYN species in the rAAV model of PD might therefore stem from the partial species barrier between mice and humans. Hence, further studies are required in which endogenous mouse aSYN is overexpressed in the LC and/or the PPN to confirm our preliminary results.

5.5 Conclusions and outlook

PD is a highly debilitating disorder significantly decreasing the quality of life of patients and their caregivers. The ultimate goal of both preclinical and clinical research is to finally be able to prevent disease initiation, or, if the disease has been already initiated, to slow down or even halt the disease progression.

The long-term objectives of the establishment of new disease models are multiple: (1) studying mechanisms underlying disease initiation, or disease progression to provide new targets for the development of disease-modifying therapy; (2) testing of newly developed compounds concerning efficacy and toxicity.

The most intriguing finding of the herein presented study is the selective vulnerability pattern of distinct PPN neuronal subpopulations. We showed that cholinergic PPN neurons were significantly more vulnerable to extracellular PFF's compared to GABAergic or glutamatergic PPN neurons, as most of the intracellular p-aSYN inclusion bodies were

located in cholinergics leading to their selective degeneration. Further research is needed to determine the factors which render cholinergic neurons particularly susceptible to the disease process, or, on the contrary, render GABAergic and glutamatergic neurons partially resilient to extracellular PFF's. The mechanisms underlying differential vulnerability might include:

- heterogeneity at the molecular level, which could be elucidated via comparative expression profiling at the single-cell level;
- differential electrophysiological properties, which could be investigated with single-cell patch clamp recordings;
- distinct bioenergetic requirements, which could be elucidated via measurements of basal oxidative phosphorylation, reserve capacity, and mitochondrial density;
- morphological features, e.g. the degree of axonal arborization.

Elucidation of the exact mechanisms underlying the differential vulnerability pattern of neuronal subpopulations holds great potential for the identification of novel drug targets for the development of disease-modifying therapy.

Analysis of the brain-wide spreading pattern of PFF induced pathology implicated that pathological aSYN species do not propagate indiscriminately. One of the major determinants of the propagation pattern is the wiring architecture, i.e. the connectome of the primarily targeted brain region, since all the structures developing p-aSYN inclusions lay within the known synaptic connections of the PPN. However, connectivity *per se* cannot explain the full extent of pathology as brain regions sharing strong synaptic interconnectivity, such as the SNr or the thalamus showed only sparse pathology, whereas brain regions loosely connected to the PPN, such as the bed nuclei of the stria terminalis or the central amygdala showed severe pathology. Further research is needed to resolve additional determinants of pathology progression as understanding the mechanisms underlying pathology propagation would provide valuable knowledge for the development of neuroprotective therapies aimed at decelerating disease progression.

The comparison of the PFF-induced and rAAV-mediated overexpression based PD animal models revealed fundamental differences in the brain-wide propagation patterns in the two models. Whereas in the PFF model, trans-synaptic, cell-to-cell transmission of aggregation-prone aSYN species could be undoubtedly observed, in the targeted overexpression-based model, no pathological aSYN could be observed apart from the injection site. Although trans-synaptic transport of human, non-aggregated aSYN has been reported in previous studies [311], this could not be definitely proven (or disproven) in our model.

Both models recapitulate several features of human PD, however, based on the differences of available outcome measures in the two models, their eligibility for preclinical testing of potentially disease-modifying compounds is different. For example, as in the PFF model aggregation-prone aSYN species are transported trans-synaptically, the model is appropriate to test antibody therapies targeting extracellular aSYN, as opposed to the rAAV-based model, which, due to the lack of pathological aSYN propagation, is not suited in its present form.

Taken together, this study provides a valuable starting point for further research on cellular vulnerability factors and mechanisms of disease progression, which hold great potential for the identification of novel drug targets aimed at disease-modification rather than symptom alleviation. Additionally, both animal models provide valuable tools for testing of newly developed neuroprotective compounds.

6 Summary

6.1 Summary

Parkinson's disease is a highly debilitating disorder classically characterized by the degeneration of dopaminergic midbrain neurons of the substantia nigra. The resulting nigrostriatal dopamine deficiency is thought to be responsible for the onset of the cardinal Parkinson's motor symptomtomatology; bradykinesia, rigidity, and resting tremor. However, recent studies show that Parkinson's disease is a multisystem disorder. Thus, it comes not only to degeneration in the nigrostriatal system, but also to pronounced cell loss in many other brain regions. Histopathologically, Parkinson's disease is characterized by the presence of so-called Lewy bodies or neurites. These are intracytoplasmic proteinaceous inclusions consisting mainly of aggregated α-synuclein. Two neuronal structures that both have pronounced Lewy pathology in Parkinson's disease and prominent neurodegeneration are the noradrenergic locus coeruleus and the neurochemically heterogeneous pedunculopontine nucleus. Remarkably, in the pedunculopontine nucleus Lewy pathology and neurodegeneration are predominantly restricted to the cholinergic cell population, while the GABAergic and glutamatergic cell groups exhibit only minor Lewy pathology and are largely spared of neurodegeneration.

The present dissertation pursued two main goals. On the one hand, we investigated whether the selective vulnerability pattern of the cholinergic subpopulation of the pedunculopontine nucleus could be reproduced in a mouse model based on the intracerebral injection of preformed α-synuclein fibrils. Second, the brain-spreading pattern of two focal-induced α-synucleinopathy mouse models were compared with respect to the methodology used to initiate the aggregation process (vector-mediated overexpression vs. α-synuclein fibril model).

In the first part of the study, we used a targeted intracerebral injection of preformed α-synuclein fibrils to induce a focal α-synucleinopathy in the pedunculopontine nucleus. Our data show that the injection of α-synuclein fibrils resulted in the recruitment and misfolding of endogenous α-synuclein leading to formation of Lewy body-like aggregates in neuronal perikarya and axons. Interestingly, the observed inclusion bodies were immunoreactive for S129-phosphorylated α-synuclein, p62 positive and resistant to proteinase K digestion. We thereby showed that the experimentally induced α-synuclein pathology possessed several key features of human Lewy pathology. Remarkably, the major burden of Lewy-like pathology

and quantified cell loss was limited to the cholinergic subpopulation of the pedunculopontine nucleus, while the non-cholinergic neurons were largely spared of Lewy pathology and degeneration at any investigated time-point. Interestingly, in both fibril and monomer-α-synuclein (control) injected animals, induction of reactive microgliosis occurred, although no α-synuclein pathology was observed in the control group. Our analysis also showed that the formation of α-synuclein pathology was not limited to the immediate vicinity of the site of injection, but propageted over considerable distances to other interconnected brain regions. Since α-synuclein positive aggregates were found in neuronal cell bodies of distant brain regions, which lay all within the neuronal network of the pedunculopontine nucleus, it can be concluded that the α-synucleinopathy spread only within the neural network of the pedunculopontine nucleus.

In the second part of the thesis, focal α-synucleinopathy was induced in the locus coeruleus by intracerebral injection of adeno-associated viral vectors containing the gene for human mutant A53T-α-synuclein or luciferase (control protein). The obtained data showed that local overexpression of human α-synuclein led to widespread propagation of the protein consistent with anterograde axonal transport. Analysis of the α-synuclein propagation pattern demonstrated that the brain-wide α-synucleinopathy was confined to the output regions of the noradrenergic locus coeruleus. Furthermore, there was no evidence of cell-to-cell transmission of human α-synuclein. Based on these findings we concluded that the induced Lewy-like pathology did not leave the noradrenergic locus coeruleus system in the studied time frame of 9 weeks. In addition, unbiased stereological quantification of the dopaminergic substantia nigra revealed no significant cell loss at the relatively short time-frame of 9 weeks. In conclusion, the studies presented in this dissertation show that cholinergic pedunculopontine neurons are significantly more vulnerable to α-synuclein fibril-induced α-synucleinopathy than non-cholinergic neurons. In addition, we were able to show that the brain-wide progression pattern of Lewy-like pathology is significantly different between the two studied α-synucleinopathy models. While in the fibril model the α-synucleinopathy pattern was consistent with cell-to-cell transmission of pathological α-synuclein species, we only observed axonal transport of α-synuclein but not cell-to-cell transmission in the overexpression-based model. The studies carried out within this dissertation therefore provide a valuable starting point for the further investigation of cellular vulnerability factors and mechanisms of disease progression.

6.2 Zusammenfassung

Die Parkinson-Krankheit ist eine hochgradig einschränkende Erkrankung, die klassischerweise durch die Degeneration dopaminerger Mittelhirnneurone der Substantia nigra gekennzeichnet wird. Der daraus resultierende Mangel an striatonigralem Dopamin wird als ursächlich für das Entstehen der kardinalen Parkinson-Symptomatik – Bradykinesie, Rigidität und Ruhezittern – aufgefasst. Neuere Untersuchungen belegen jedoch, dass es sich bei der Parkinson-Krankheit um eine Multisystemerkrankung handelt. So kommt es nicht nur zur Degeneration im striatonigralen System, sondern auch zu ausgeprägten Zellverlussten in vielen weiteren Hirnregionen. Histopathologisch ist die Parkinson-Krankheit durch das Vorhandensein sogenannter Lewy-Körperchen oder –Neurite gekennzeichnet. Es handelt sich hierbei um intrazytoplasmatische proteinhaltige Einschlüsse, die hauptsächlich aus aggregiertem α-Synuclein bestehen. Zwei neuronale Strukturen, die im Rahmen der Parkinson-Krankheit sowohl eine ausgeprägte Lewy-Pathologie besitzen, wie auch eine prominente Neurodegeneration aufweisen, sind der noradrenerge locus coeruleus und der neurochemisch heterogene pedunculopontine Kern. Bemerkenswerterweise beschränken sich im pedunculopontinen Kern Lewy-Pathologie und Neurodegeneration jedoch überwiegend auf die cholinerge Zellpopulation, so weisen die GABAergen und glutamatergen Zellgruppen kaum Lewy-Pathologie auf und bleiben auch von der neurodegeneration weitestgehend verschont.

Die hier vorliegende Dissertation verfolgte zwei Hauptziele. Zum einen sollte untersucht werden, ob das selektive Vulnerabilitätsmuster der cholinergen Subpopulation des pedunculopontinen Kerns in einem Mausmodell, welches auf der intrazerebralen Injektion von präformierten α-Synuclein-Fibrillen basiert, reproduziert werden kann. Zweitens sollte das hirnweite Ausbreitungsmuster von zwei fokal induzierten α-Synucleinopathie-Mausmodellen im Hinblick auf die verwendete Methodik zur Initiierung des Aggregationsprozesses (vektor-vermittelte Überexpression vs. α-Synuclein-Fibrillenmodell) verglichen werden.

Im ersten Teil der Studie wurde durch gezielte intrazerebrale Injektion von präformierten α-Synuclein-Fibrillen eine fokale α-Synucleinopathie im pedunculopontinen Kern induziert. Die gewonnenen Daten zeigen, dass es durch die Injektion der α-Synuclein-Fibrillen zu einer Rekrutierung und Fehlfaltung von endogenem α-Synuclein kam, was zu Lewy-Körperchen artigen Aggregaten in neuronalen Perikarya und Axonen führte. Interessanterweise waren die beobachteten Einschlusskörperchen immunreaktiv gegen S129-phosphoryliertes α-

Synuclein, p62 positiv und resistent gegen Proteinase K Verdauung. Es konnte hierdurch gezeigt werden, dass die experimentell induzierte α-Synuclein-Pathologie mehrere Schlüsselmerkmale der humanen Lewy-Pathologie besaß. Bemerkenswerterweise war die Hauptlast der Lewy-ähnlichen Pathologie und der quantifizierte Zellverlust auf die cholinerge Subpopulation des pedunculopontinen Kerns beschränkt. Die nicht-cholinergen Neurone blieben größtenteils von der Aggregatbildung verschont und wiesen zu keinem untersuchten Zeitpunkt einen Zellverlust auf. Interessanterweise kam es sowohl bei Fibrillen injezierten als auch bei monomer α-Synuclein (Kontrolle) injizierten Tieren zur Induktion einer reaktiven Mikrogliose, obwohl in der Kontrollgruppe keine α-Synuclein-Pathologie beobachtet wurde. Unsere Analysen zeigten weiterhin, dass die Bildung der α-Synuclein-Pathologie nicht nur auf die unmittelbare Nähe der Injektionsstelle beschränkt war, sondern sich sich über beträchtliche Entfernungen in andere Hirnregionen ausbreitete. Da die Aggregate nur in neuronalen Zellkörpern entfernter Gehirnregionen gefunden wurden, die alle innerhalb des neuronalen Netzwerkes des Pedunculopontinen Kerns lagen, kann aus den Daten geschlossen werden, dass sich die α-Synucleinopathie innerhalb des Konnektoms des Pedunculopontinen Kerns ausbreitet.

Im zweiten Teil der Dissertation wurde erstmals eine fokale α-Synucleinopathie im Locus coeruleus durch intrazerebrale Injektion von Adeno-assoziierten viralen Vektoren induziert, die das Gen für humanes mutiertes A53T-α-Synuclein oder Luciferase (Kontrollprotein) enthielten. Die hierdurch gewonnenen Daten zeigten, dass es im Rahmen einer lokalen Überexpression von humanem α-Synuclein zu einer raschen axonalen Ausbreitung des Proteins kommt. Die Analyse des Ausbreitungsmusters konnte aufzeigen, dass die gehirnweite α-Synucleinopathie auf die Outputregionen des noradrenergen locus coeruleus beschränkt war und gleichzeitig keine Hinweise auf eine Zell-zu-Zell-Übertragung von menschlichem α-Synuclein vorlagen. Hieraus schlussfolgerten wir, dass die induzierte Pathologie das noradrenerge locus coeruleus System im untersuchten Zeitrahmen von 9 Wochen nicht verließ. Desweiteren zeigte sich im Rahmen der stereologischen Quantifizierung der dopaminergen Substantia nigra Neurone, in dem relativ kurzen Zeitraum von 9 Wochen, kein signifikanter Zellverlust.

Zusammengefasst belegen die hier vorgestellten Studien, dass cholinerge pedunculopontine Neurone signifikant vulnerabler gegenüber einer mittels α-Synuclein-Fibrillen induzierten α-Synucleinopathie sind als nicht-cholinerge Neurone. Zusätzlich konnten wir zeigen, dass das hirnweite Progressionsmuster der Pathologie in den zwei untersuchten α-Synucleinopathie-Modellen signifikant unterschiedlich ist. Während im Fibrillenmodell das α-

Synucleinopathiemuster mit einer Zell-zu-Zell-Übertragung von pathologischen α-Synuclein-Spezies vereinbar war, konnte im überexpressionsbasierten Modell lediglich ein axonaler Transport von α-Synuclein, aber nicht eine Zell-zu-Zell-Übertragung nachgewiesen werden. Die innerhalb dieser Dissertation durchgeführten Studien stellen daher einen wertvollen Ausgangspunkt für die weitere Erforschung von zellulären Vulnerabilitätsfaktoren und Mechanismen des Krankheitsverlaufs dar.

7 List of abbreviations

7.1 Abbreviations in the main text

6-OHDA	6-hydroxydopamine
AON	anterior olfactory nucleus
ARAS	ascending reticular arousal system
aSYN	α-synuclein
ATP	adenosine triphosphate
CBA	chicken β-actin
ChAT	choline acetyltransferase
CMV	cytomegalovirus
CNS	central nervous system
COMT	catechol-O-methyltransferase
DA	dopamine
DAB	3,3'-diaminobenzidine
DAT	dopamine transporter
DBS	deep brain stimulation
dsDNA	double-stranded DNA
GABA	γ-aminobutyric acid
GI	gastrointestinal
GPi	globus pallidus internus
GRK	G protein-coupled receptor kinase
GRN	gigantocellular nucleus
LAG3	lymphocyte-activation gene 3
LB	Lewy-body
LC	locus coeruleus
LN	Lewy-neurite
LRRK2	leucine-rich repeat kinase 2
LV	lentivirus
MAO	monoamine oxidase
MDS	Movement Disorders Society
mfb	media forebrain bundle
MIBG	metaiodobenzylguanidine
$MPDP^+$	1-methyl-4-phenyl-2,3-dihydropyridinium
MPP^+	neurotoxic 1-methyl-4-phenylpyridinium
MPPP	1-methyl-4-phenyl-4-propionoxypiperidine
MPTP	1-methyl-4-phenyl-1,2,3,6-tetrahydropyridine
MRI	magnetic resonance imaging
NDS	normal donkey serum
NET	noradrenaline transporter
NeuN	neuron N
NHP	non-human primate
NM	neuromelanin
NMS	non-motor symptoms
OB	olfactory bulb
p-aSYN	phosphorylated α-synuclein
PB	phosphate buffer
PB	parabrachial nucleus
PBS	phosphate buffered saline
PBT	phosphate buffered saline with Triton X-100
PD	Parkinson's disease
PET	positron emission tomography
PFA	paraformaldehyde
PFF	preformed fibril
PK	proteinase K
PLK	polo-like kinase
PPN	pedunculopontine nucleus
PrP^C	native form of the prion protein
PrP^{Sc}	misfolded prion protein
rAAV	recombinant adeno-associated virus
RBD	REM sleep behavior disorder
RNS	reactive nitrogen species
ROI	region of interest
ROS	reactive oxygen species
SNc	substantia nigra pars compacta
SNr	substantia nigra pars reticulata
ssDNA	single-stranded DNA
STN	subthalamic nucleus
STR	striatum
TH	tyrosine hydroxylase
TU	tuberal nucleus
VTA	ventral tegmental area
wpi	weeks post-injection
WT	wild-type

7.2 Abbreviations in the figures

ACB	nucleus accumbens
aco	anterior commissure
AP	area postrema
APN	anterior pretectal nucleus
BST	bed nuclei of the stria terminalis
BSTov	bed nuclei of the stria terminalis, anterior division, oval nucleus
CEA	central amygdala
CEAl	central amygdala, lateral part
CEAm	central amygdala, medial part
CLA	claustrum
contra	contralateral
CP	caudoputamen
CTX	cortex
CU	cuneate nucleus
DG	dentate gyrus
DMV	dorsal motor nucleus of the vagal nerve
ECU	external cuneate nucleus
Epd	endopiriform nucleus, dorsal part
fi	fimbria hippocampi
GP	globus pallidus
HPF	hippocampal formation
HY	hypothalamus
IC	inferior colliculus
icp	inferior cerebellar peduncle
int	internal capsule
IO	inferior olivary complex
ipsi	ipsilateral
IRN	intermediate reticular nucleus
L	left
LHA	lateral hypothalamic area
LRN	lateral reticular nucleus
LS	lateral septal nucleus
MDRNd	medullary reticular nucleus, dorsal part
MDRNv	medullary reticular nucleus, ventral part
mlf	medial longitudinal fascicle
MOBgr	main olfactory bulb, granule layer
MOBipl	main olfactory bulb, inner plexiform layer
MOBopl	main olfactory bulb, outer plexiform layer
mono	monomeric α-synuclein
MRN	midbrain reticular nucleus
MRN	midbrainr eticular nucleus
MS	medial septal nucleus
NDB	diagonal band nucleus
NLL	nucleus of the lateral lemniscus
OT	olfactory tubercle
PAG	periaqueductal gray
PB	parabrachial nucleus
PRNr	pontine reticular nucleus, rostral part
py	pyramid
R	right
RA	raphe nuclei
RR	retrorubral field
sAMY	striatumlike amygdalar nuclei
SC	superior colliculus
SCm	superior colliculus, motor related
SI	substantia innominata
sptV	spinal tract of the trigeminal nerve
SPV	spinal nucleus of the trigeminal
TH	thalamus
TTd	taenia tecta, dorsal part
TU	tuberal nucleus
XII	hypoglossal nucleus

8 Table of figures

9 List of tables

10 Own publications related to the dissertation

10.1 Scientific presentations

Congress of the German Society of Neurology, September 2017, Leipzig, Germany:
"Mouse models of prodromal Parkinson's disease"

27th European Congress of Psychiatry, in a joint symposium with the European Brain Council, April 2019, Warsaw, Poland:
"Neuropsychiatric symptoms in prodromal and early phase Parkinson's disease"

10.2 Peer reviewed original and review articles

Oertel WH, Henrich MT, Janzen A, **Geibl FF**: The locus coeruleus – another vulnerability target in Parkinson's disease. Mov Disord. 2019 Jul 10. doi: 10.1002/mds.27785.

*__Geibl FF__, *Henrich MT, Oertel WH: Mesencephalic and extramesencephalic dopaminergic systems in Parkinson's disease. (*shared first authors). J Neural Transm (Vienna). 2019 Apr;126(4):377-396. doi: 10.1007/s00702-019-01970-9

*Henrich MT, *__Geibl FF__ Lee B, Chiu W-H, Koprich JB, Brotchie JM, Timmermann L, Decher N, Matschke LA, Oertel WH: A53T-α-synuclein overexpression in murine locus coeruleus induces Parkinson's disease-like pathology in neurons and glia. (*shared first authors). Acta Neuropathol Commun. 2018 May 10;6(1):39. doi: 10.1186/s40478-018-0541-1

10.3 Abstracts

*__Geibl FF__, *Henrich MT, Lee B, Matschke L, Koprich J, Decher N, Oertel WH. Targeted overexpression of human A53T-α-synuclein in the locus coeruleus causes widespread transport of α-synucein to interconnected brain regions. (2018) 20th α-synuclein Meeting, Athens, Greece.

Lee B, Henrich MT, **Geibl FF**, Chiu WH, Matschke L, Decher N, Oertel WH. Relationship between the locus coeruleus and nucleus ambiguus in the recombinant adeno-associated viral vector-mediated α-synuclein overexpression mouse models of Parkinson's disease. (2018) 20th α-synuclein Meeting, Athens, Greece.

Henrich MT, Matschke LA, Stoehr A, Chiu WH, Lee B, **Geibl FF**, Koprich J, Decher N, Oertel WH. Overexpression of A53T-α-synuclein via rAAV in the locus coeruleus – A prodromal mouse model of Parkinson's disease. (2017) 11th Göttingen Meeting of the German Neuroscience Society, Göttingen, Germany.

11 Appendix

11.1 Verzeichnis der akademischen Lehrer

Meine akademischen Lehrer waren die Damen/Herren…

…an der Semmelweis Universität, Budapest, Ungarn

Alföldy Ferenc; Bánvölgyi András; Bokodi Miklós Géza; Csukly Gábor; Forgács Gábor; Ghidán Ágoston; Hagymási Krisztina; Heinzelmann Andrea; Holnapy Gergely; Hornyák Csilla; Magyar Attila; Miklós Zsuzsanna; Molnár Miklós; Nagy Péter; Pós Zoltán; Rózsavölgyi Éva; Szabó Arnold; Szabó Balázs; Terebessy András; Tretter László; Varjú Imre; Vojnisek Zsuzsanna.

…an der Philipps Universität Marburg, Marburg, Deutschland

Wolfgang H. Oertel.

11.2 Danksagung

Zuerst möchte ich mich bei meinem Doktorvater, Prof. Wolfgang Oertel bedanken, der mir die Möglichkeit gegeben hat, in seiner Arbeitsgruppe zu promovieren. Ich bedanke mich für die kontinuierliche wissenschaftliche Betreuung und die motivierende Unterstützung.

Ganz herzlich bedanke ich mich bei Frau Sabine Anfimov, die mich in die Kunst der Immunhistochemie eingearbeitet hat und mir auch bei bürokratischen Angelegenheiten stets zur Hand ging.

Des Weiteren möchte ich mich bei meinen Kollegen aus der Klinik für Neurologie bedanken, die mich in dieser Zeit unterstützt haben. Besonders möchte ich mich bei Frau Anna Stegmann bedanken.

Bei Frau Dr. Katrin Roth möchte ich mich für die Einarbeitung und Unterstützung bei der Konfokalmikroskopie bedanken.

Ich möchte mich auch bei Herrn Prof. Heinrich J. Dingeldein bedanken, der mich in Marburg und Deutschland unterstützt hat, und mir bei Problemen immer weitergeholfen hat. Danke!

Ich möchte mich auch bei Martin T. Henrich ganz herzlich bedanken. Er hat mich sowohl wissenschaftlich, als auch privat die ganze Zeit lang unterstützt und motiviert. Danke Dir dafür!

Abschließend möchte ich mich ganz besonders bei meiner Familie bedanken. Meine Eltern, Maria Erb und József Geibl, die mich von klein auf immer bedingungslos unterstützt haben meinen eigenen Weg zu gehen. Die mir meine Promotion in Deutschland ermöglicht haben, mir beim Umzug geholfen haben, und mich über Skype stets unterstützt und motiviert haben. Vielen lieben Dank an Euch!

12 References

1. Ahn T-B, Langston JW, Aachi VR, Dickson DW (2012) Relationship of neighboring tissue and gliosis to α-synuclein pathology in a fetal transplant for Parkinson's disease. Am J Neurodegener Dis 1(1):49–59

2. Alderson HL, Latimer MP, Blaha CD, Phillips AG, Winn P (2004) An examination of d-amphetamine self-administration in pedunculopontine tegmental nucleus-lesioned rats. Neuroscience 125(2):349–358. doi:10.1016/j.neuroscience.2004.02.015

3. Allen Institute for Brain Science. (2004) Allen Mouse Brain Atlas. http://mouse.brain-map.org/

4. Alvarez-Erviti L, Seow Y, Schapira AH, Gardiner C, Sargent IL, Wood MJA, Cooper JM (2011) Lysosomal dysfunction increases exosome-mediated alpha-synuclein release and transmission. Neurobiol Dis 42(3):360–367. doi:10.1016/j.nbd.2011.01.029

5. Anderson JP, Walker DE, Goldstein JM, Laat R de, Banducci K, Caccavello RJ, Barbour R, Huang J, Kling K, Lee M, Diep L, Keim PS, Shen X, Chataway T, Schlossmacher MG, Seubert P, Schenk D, Sinha S, Gai WP, Chilcote TJ (2006) Phosphorylation of Ser-129 is the dominant pathological modification of alpha-synuclein in familial and sporadic Lewy body disease. J Biol Chem 281(40):29739–29752. doi:10.1074/jbc.M600933200

6. Angot E, Steiner JA, Lema Tomé CM, Ekström P, Mattsson B, Björklund A, Brundin P (2012) Alpha-synuclein cell-to-cell transfer and seeding in grafted dopaminergic neurons in vivo. PLoS ONE 7(6):e39465. doi:10.1371/journal.pone.0039465

7. Aston-Jones G, Cohen JD (2005) An integrative theory of locus coeruleus-norepinephrine function: adaptive gain and optimal performance. Annu Rev Neurosci 28:403–450. doi:10.1146/annurev.neuro.28.061604.135709

8. Aston-Jones G, Segal M, Bloom FE (1980) Brain aminergic axons exhibit marked variability in conduction velocity. Brain Res 195(1):215–222. doi:10.1016/0006-8993(80)90880-X

9. Attems J, Jellinger KA (2008) The dorsal motor nucleus of the vagus is not an obligatory trigger site of Parkinson's disease. Neuropathol Appl Neurobiol 34(4):466–467. doi:10.1111/j.1365-2990.2008.00937.x

10. Azeredo da Silveira S, Schneider BL, Cifuentes-Diaz C, Sage D, Abbas-Terki T, Iwatsubo T, Unser M, Aebischer P (2009) Phosphorylation does not prompt, nor prevent, the formation of alpha-synuclein toxic species in a rat model of Parkinson's disease. Hum Mol Genet 18(5):872–887. doi:10.1093/hmg/ddn417

11. Bae E-J, Lee H-J, Rockenstein E, Ho D-H, Park E-B, Yang N-Y, Desplats P, Masliah E, Lee S-J (2012) Antibody-aided clearance of extracellular α-synuclein prevents cell-to-cell aggregate transmission. J Neurosci 32(39):13454–13469. doi:10.1523/JNEUROSCI.1292-12.2012

12. Barbeau A, Roy M, Bernier G, Campanella G, Paris S (1987) Ecogenetics of Parkinson's Disease: Prevalence and Environmental Aspects in Rural Areas. Can. j. neurol. sci. 14(1):36–41. doi:10.1017/S0317167100026147

13. Barone P, Poewe W, Albrecht S, Debieuvre C, Massey D, Rascol O, Tolosa E, Weintraub D (2010) Pramipexole for the treatment of depressive symptoms in patients with Parkinson's disease: a randomised, double-blind, placebo-controlled trial. The Lancet Neurology 9(6):573–580. doi:10.1016/S1474-4422(10)70106-X

14. Bartels AL, Willemsen ATM, Doorduin J, Vries EFJ de, Dierckx RA, Leenders KL (2010) 11C-PK11195 PET: quantification of neuroinflammation and a monitor of anti-inflammatory treatment in Parkinson's disease? Parkinsonism Relat Disord 16(1):57–59. doi:10.1016/j.parkreldis.2009.05.005

15. Beach TG, Adler CH, Lue L, Sue LI, Bachalakuri J, Henry-Watson J, Sasse J, Boyer S, Shirohi S, Brooks R, Eschbacher J, White CL, Akiyama H, Caviness J, Shill HA, Connor DJ, Sabbagh MN, Walker DG (2009) Unified staging system for Lewy body disorders: correlation with nigrostriatal degeneration, cognitive impairment and motor dysfunction. Acta Neuropathol 117(6):613–634. doi:10.1007/s00401-009-0538-8

16. Beach TG, Adler CH, Sue LI, Vedders L, Lue L, White Iii CL, Akiyama H, Caviness JN, Shill HA, Sabbagh MN, Walker DG (2010) Multi-organ distribution of phosphorylated alpha-synuclein histopathology in subjects with Lewy body disorders. Acta Neuropathol 119(6):689–702. doi:10.1007/s00401-010-0664-3

17. Bekar LK, Wei HS, Nedergaard M (2012) The locus coeruleus-norepinephrine network optimizes coupling of cerebral blood volume with oxygen demand. J Cereb Blood Flow Metab 32(12):2135–2145. doi:10.1038/jcbfm.2012.115

18. Benarroch EE (2009) The locus ceruleus norepinephrine system: functional organization and potential clinical significance. Neurology 73(20):1699–1704. doi:10.1212/WNL.0b013e3181c2937c

19. Benarroch EE (2013) Pedunculopontine nucleus: functional organization and clinical implications. Neurology 80(12):1148–1155. doi:10.1212/WNL.0b013e3182886a76

20. Benito-León J, Bermejo-Pareja F, Rodríguez J, Molina J-A, Gabriel R, Morales J-M (2003) Prevalence of PD and other types of parkinsonism in three elderly populations of central Spain. Mov Disord 18(3):267–274. doi:10.1002/mds.10362

21. Berg D, Postuma RB, Adler CH, Bloem BR, Chan P, Dubois B, Gasser T, Goetz CG, Halliday G, Joseph L, Lang AE, Liepelt-Scarfone I, Litvan I, Marek K, Obeso J, Oertel W, Olanow CW, Poewe W, Stern M, Deuschl G (2015) MDS research criteria for prodromal Parkinson's disease. Mov Disord 30(12):1600–1611. doi:10.1002/mds.26431

22. Bernstein H-G, Johnson M, Perry RH, LeBeau FEN, Dobrowolny H, Bogerts B, Perry EK (2011) Partial loss of parvalbumin-containing hippocampal interneurons in dementia with Lewy bodies. Neuropathology 31(1):1–10. doi:10.1111/j.1440-1789.2010.01117.x

23. Berridge CW (2008) Noradrenergic modulation of arousal. Brain Res Rev 58(1):1–17. doi:10.1016/j.brainresrev.2007.10.013

24. Berridge CW, Waterhouse BD (2003) The locus coeruleus–noradrenergic system. Modulation of behavioral state and state-dependent cognitive processes. Brain Res Rev 42(1):33–84. doi:10.1016/S0165-0173(03)00143-7

25. Bertrand E, Lechowicz W, Szpak GM, Dymecki J (1997) Qualitative and quantitative analysis of locus coeruleus neurons in Parkinson's disease. Folia Neuropathol 35(2):80–86

26. Betarbet R, Sherer TB, MacKenzie G, Garcia-Osuna M, Panov AV, Greenamyre JT (2000) Chronic systemic pesticide exposure reproduces features of Parkinson's disease. Nat Neurosci 3(12):1301–1306. doi:10.1038/81834

27. Betarbet R, Sherer TB, Greenamyre JT (2002) Animal models of Parkinson's disease. Bioessays 24(4):308–318. doi:10.1002/bies.10067

28. Bohnen NI, Müller MLTM, Koeppe RA, Studenski SA, Kilbourn MA, Frey KA, Albin RL (2009) History of falls in Parkinson disease is associated with reduced cholinergic activity. Neurology 73(20):1670–1676. doi:10.1212/WNL.0b013e3181c1ded6

29. Bowen S, Ateh DD, Deinhardt K, Bird MM, Price KM, Baker CS, Robson JC, Swash M, Shamsuddin W, Kawar S, El-Tawil T, Roos J, Hoyle A, Nickols CD, Knowles CH, Pullen AH, Luthert PJ, Weller RO, Hafezparast M, Franklin RJM, Revesz T, King RHM, Berninghausen O, Fisher EMC, Schiavo G, Martin JE (2007) The phagocytic capacity of neurones. Eur J Neurosci 25(10):2947–2955. doi:10.1111/j.1460-9568.2007.05554.x

30. Braak H, Del Tredici K, Rüb U, De Vos, Rob A I, Jansen Steur, Ernst N H, Braak E (2003) Staging of brain pathology related to sporadic Parkinson's disease. Neurobiol Aging 24(2):197–211

31. Braak H, Ghebremedhin E, Rub U, Bratzke H, Del Tredici K (2004) Stages in the development of Parkinson's disease-related pathology. Cell Tissue Res 318(1):121–134. doi:10.1007/s00441-004-0956-9

32. Brahic M, Bousset L, Bieri G, Melki R, Gitler AD (2016) Axonal transport and secretion of fibrillar forms of alpha-synuclein, Abeta42 peptide and HTTExon 1. Acta Neuropathol 131(4):539–548. doi:10.1007/s00401-016-1538-0

33. Breton-Provencher V, Sur M (2019) Active control of arousal by a locus coeruleus GABAergic circuit. Nat Neurosci 22(2):218–228. doi:10.1038/s41593-018-0305-z

34. Brundin P, Melki R (2017) Prying into the Prion Hypothesis for Parkinson's Disease. J Neurosci 37(41):9808–9818. doi:10.1523/JNEUROSCI.1788-16.2017

35. Burger C, Gorbatyuk OS, Velardo MJ, Peden CS, Williams P, Zolotukhin S, Reier PJ, Mandel RJ, Muzyczka N (2004) Recombinant AAV viral vectors pseudotyped with viral capsids from serotypes 1, 2, and 5 display differential efficiency and cell tropism after delivery to different regions of the central nervous system. Mol Ther 10(2):302–317. doi:10.1016/j.ymthe.2004.05.024

36. Carlsson A (1959) The occurrence, distribution and physiological role of catecholamines in the nervous system. Pharmacol Rev 11(2, Part 2):490–493

37. Carlsson A, Lindqvist M, Magnusson T (1957) 3,4-Dihydroxyphenylalanine and 5-hydroxytryptophan as reserpine antagonists. Nature 180(4596):1200

38. Carter ME, Yizhar O, Chikahisa S, Nguyen H, Adamantidis A, Nishino S, Deisseroth K, Lecea L de (2010) Tuning arousal with optogenetic modulation of locus coeruleus neurons. Nat Neurosci 13(12):1526–1533. doi:10.1038/nn.2682

39. Castellanos G, Fernández-Seara MA, Lorenzo-Betancor O, Ortega-Cubero S, Puigvert M, Uranga J, Vidorreta M, Irigoyen J, Lorenzo E, Muñoz-Barrutia A, Ortiz-de-Solorzano C, Pastor P, Pastor MA (2015) Automated neuromelanin imaging as a diagnostic biomarker for Parkinson's disease. Mov Disord 30(7):945–952. doi:10.1002/mds.26201

40. Castle MJ, Turunen HT, Vandenberghe LH, Wolfe JH (2016) Controlling AAV Tropism in the Nervous System with Natural and Engineered Capsids. Methods Mol Biol 1382:133–149. doi:10.1007/978-1-4939-3271-9_10

41. Chan-Palay V, Asan E (1989) Alterations in catecholamine neurons of the locus coeruleus in senile dementia of the Alzheimer type and in Parkinson's disease with and without dementia and depression. J Comp Neurol 287(3):373–392. doi:10.1002/cne.902870308

42. Chartier-Harlin M-C, Kachergus J, Roumier C, Mouroux V, Douay X, Lincoln S, Levecque C, Larvor L, Andrieux J, Hulihan M, Waucquier N, Defebvre L, Amouyel P, Farrer M, Destée A (2004) α-synuclein locus duplication as a cause of familial Parkinson's disease. The Lancet 364(9440):1167–1169. doi:10.1016/S0140-6736(04)17103-1

43. Chaudhuri KR, Healy DG, Schapira AHV (2006) Non-motor symptoms of Parkinson's disease: diagnosis and management. The Lancet Neurology 5(3):235–245. doi:10.1016/S1474-4422(06)70373-8

44. Chen H, Jacobs E, Schwarzschild MA, McCullough ML, Calle EE, Thun MJ, Ascherio A (2005) Nonsteroidal antiinflammatory drug use and the risk for Parkinson's disease. Ann Neurol 58(6):963–967. doi:10.1002/ana.20682

45. Cheng H-C, Ulane CM, Burke RE (2010) Clinical progression in Parkinson disease and the neurobiology of axons. Ann Neurol 67(6):715–725. doi:10.1002/ana.21995

46. Chesselet M-F, Richter F (2011) Modelling of Parkinson's disease in mice. The Lancet Neurology 10(12):1108–1118. doi:10.1016/S1474-4422(11)70227-7

47. Chiba K, Trevor A, Castagnoli N (1984) Metabolism of the neurotoxic tertiary amine, MPTP, by brain monoamine oxidase. Biochem Biophys Res Commun 120(2):574–578. doi:10.1016/0006-291X(84)91293-2

48. Chiken S, Nambu A (2016) Mechanism of Deep Brain Stimulation: Inhibition, Excitation, or Disruption? Neuroscientist 22(3):313–322. doi:10.1177/1073858415581986

49. Chung CY, Koprich JB, Siddiqi H, Isacson O (2009) Dynamic changes in presynaptic and axonal transport proteins combined with striatal neuroinflammation precede dopaminergic neuronal loss in a rat model of AAV alpha-synucleinopathy. J Neurosci 29(11):3365–3373. doi:10.1523/JNEUROSCI.5427-08.2009

50. Clavería LE, Duarte J, Sevillano MD, Pérez-Sempere A, Cabezas C, Rodríguez F, Pedro-Cuesta J de (2002) Prevalence of Parkinson's disease in Cantalejo, Spain: a door-to-door survey. Mov Disord 17(2):242–249

51. Cohen Z, Molinatti G, Hamel E (1997) Astroglial and vascular interactions of noradrenaline terminals in the rat cerebral cortex. J Cereb Blood Flow Metab 17(8):894–904. doi:10.1097/00004647-199708000-00008

52. Collins SJ, Lawson VA, Masters CL (2004) Transmissible spongiform encephalopathies. The Lancet 363(9402):51–61. doi:10.1016/S0140-6736(03)15171-9

53. Combs B, Kneynsberg A, Kanaan NM (2016) Gene Therapy Models of Alzheimer's Disease and Other Dementias. In: Manfredsson FP (Hrsg) Gene Therapy for Neurological Disorders: Methods and Protocols. Springer New York, New York, NY, S 339–366

54. Conway KA, Harper JD, Lansbury PT (2000) Fibrils formed in vitro from alpha-synuclein and two mutant forms linked to Parkinson's disease are typical amyloid. Biochemistry 39(10):2552–2563. doi:10.1021/bi991447r

55. Croisier E, Moran LB, Dexter DT, Pearce RKB, Graeber MB (2005) Microglial inflammation in the parkinsonian substantia nigra: relationship to alpha-synuclein deposition. J Neuroinflammation 2:14. doi:10.1186/1742-2094-2-14

56. Crowther RA, Jakes R, Spillantini MG, Goedert M (1998) Synthetic filaments assembled from C-terminally truncated α-synuclein. FEBS Letters 436(3):309–312. doi:10.1016/S0014-5793(98)01146-6

57. Cuchillo-Ibanez I, Seereeram A, Byers HL, Leung K-Y, Ward MA, Anderton BH, Hanger DP (2008) Phosphorylation of tau regulates its axonal transport by controlling its binding to kinesin. FASEB J 22(9):3186–3195. doi:10.1096/fj.08-109181

58. Dauer W, Przedborski S (2003) Parkinson's disease: mechanisms and models. Neuron 39(6):889–909

59. Dautan D, Hacioğlu Bay H, Bolam JP, Gerdjikov TV, Mena-Segovia J (2016) Extrinsic Sources of Cholinergic Innervation of the Striatal Complex: A Whole-Brain Mapping Analysis. Front Neuroanat 10:1. doi:10.3389/fnana.2016.00001

60. Decressac M, Mattsson B, Lundblad M, Weikop P, Björklund A (2012) Progressive neurodegenerative and behavioural changes induced by AAV-mediated overexpression of α-synuclein in midbrain dopamine neurons. Neurobiol Dis 45(3):939–953. doi:10.1016/j.nbd.2011.12.013

61. Del Tredici K, Braak H (2013) Dysfunction of the locus coeruleus-norepinephrine system and related circuitry in Parkinson's disease-related dementia. J Neurol Neurosurg Psychiatr 84(7):774–783. doi:10.1136/jnnp-2011-301817

62. Desplats P, Lee H-J, Bae E-J, Patrick C, Rockenstein E, Crews L, Spencer B, Masliah E, Lee S-J (2009) Inclusion formation and neuronal cell death through neuron-to-neuron transmission of alpha-synuclein. Proc Natl Acad Sci U S A 106(31):13010–13015. doi:10.1073/pnas.0903691106

63. Deutsche Gesellschaft für Neurologie (2016) S3-Leitlinie: Idiopatisches Parkinson-Syndrom. https://www.dgn.org/leitlinien/3219-030-010-idiopathisches-parkinson-syndrom. Zugegriffen: 22. Juli 2019

64. Dhillon AS, Tarbutton GL, Levin JL, Plotkin GM, Lowry LK, Nalbone JT, Shepherd S (2008) Pesticide/environmental exposures and Parkinson's disease in East Texas. J Agromedicine 13(1):37–48. doi:10.1080/10599240801986215

65. Dickson DW (2012) Parkinson's disease and parkinsonism: neuropathology. Cold Spring Harb Perspect Med 2(8). doi:10.1101/cshperspect.a009258

66. Díez-Cirarda M, Ojeda N, Peña J, Cabrera-Zubizarreta A, Lucas-Jiménez O, Gómez-Esteban JC, Gómez-Beldarrain MÁ, Ibarretxe-Bilbao N (2017) Increased brain connectivity and activation after cognitive rehabilitation in Parkinson's disease: a randomized controlled trial. Brain Imaging Behav 11(6):1640–1651. doi:10.1007/s11682-016-9639-x

67. Duffy MF, Collier TJ, Patterson JR, Kemp CJ, Fischer DL, Stoll AC, Sortwell CE (2018) Quality Over Quantity: Advantages of Using Alpha-Synuclein Preformed Fibril Triggered Synucleinopathy to Model Idiopathic Parkinson's Disease. Front Neurosci 12:621. doi:10.3389/fnins.2018.00621

68. Ehrminger M, Latimier A, Pyatigorskaya N, Garcia-Lorenzo D, Leu-Semenescu S, Vidailhet M, Lehericy S, Arnulf I (2016) The coeruleus/subcoeruleus complex in idiopathic rapid eye movement sleep behaviour disorder. Brain 139(Pt 4):1180–1188. doi:10.1093/brain/aww006

69. Emmanouilidou E, Melachroinou K, Roumeliotis T, Garbis SD, Ntzouni M, Margaritis LH, Stefanis L, Vekrellis K (2010) Cell-produced alpha-synuclein is secreted in a calcium-dependent manner by exosomes and impacts neuronal survival. J Neurosci 30(20):6838–6851. doi:10.1523/JNEUROSCI.5699-09.2010

70. Emmanouilidou E, Minakaki G, Keramioti MV, Xylaki M, Balafas E, Chrysanthou-Piterou M, Kloukina I, Vekrellis K (2016) GABA transmission via ATP-dependent K+ channels regulates α-synuclein secretion in mouse striatum. Brain 139(Pt 3):871–890. doi:10.1093/brain/awv403

71. Engelender S, Isacson O (2017) The Threshold Theory for Parkinson's Disease. Trends Neurosci 40(1):4–14. doi:10.1016/j.tins.2016.10.008

72. Eslamboli A, Romero-Ramos M, Burger C, Bjorklund T, Muzyczka N, Mandel RJ, Baker H, Ridley RM, Kirik D (2007) Long-term consequences of human alpha-synuclein overexpression in the primate ventral midbrain. Brain 130(Pt 3):799–815. doi:10.1093/brain/awl382

73. Fall PA, Axelson O, Fredriksson M, Hansson G, Lindvall B, Olsson JE, Granérus AK (1996) Age-standardized incidence and prevalence of Parkinson's disease in a Swedish community. J Clin Epidemiol 49(6):637–641

74. Farrer M, Chan P, Chen R, Tan L, Lincoln S, Hernandez D, Forno L, Gwinn-Hardy K, Petrucelli L, Hussey J, Singleton A, Tanner C, Hardy J, Langston JW (2001) Lewy bodies and parkinsonism in families withparkin mutations. Ann Neurol 50(3):293–300. doi:10.1002/ana.1132

75. Fearnley JM, Lees AJ (1991) Ageing and Parkinson's disease: substantia nigra regional selectivity. Brain 114 (Pt 5):2283–2301

76. Feinstein DL, Kalinin S, Braun D (2016) Causes, consequences, and cures for neuroinflammation mediated via the locus coeruleus. Noradrenergic signaling system. J Neurochem 139 Suppl 2:154–178. doi:10.1111/jnc.13447

77. Fernagut P-O, Chesselet M-F (2004) Alpha-synuclein and transgenic mouse models. Neurobiol Dis 17(2):123–130. doi:10.1016/j.nbd.2004.07.001

78. Ferreira SA, Romero-Ramos M (2018) Microglia Response During Parkinson's Disease: Alpha-Synuclein Intervention. Front Cell Neurosci 12:247. doi:10.3389/fncel.2018.00247

79. Fleming SM, Salcedo J, Fernagut P-O, Rockenstein E, Masliah E, Levine MS, Chesselet M-F (2004) Early and progressive sensorimotor anomalies in mice overexpressing wild-type human alpha-synuclein. J Neurosci 24(42):9434–9440. doi:10.1523/JNEUROSCI.3080-04.2004

80. Fleming SM, Tetreault NA, Mulligan CK, Hutson CB, Masliah E, Chesselet M-F (2008) Olfactory deficits in mice overexpressing human wildtype alpha-synuclein. Eur J Neurosci 28(2):247–256. doi:10.1111/j.1460-9568.2008.06346.x

81. Foote SL, Aston-Jones G, Bloom FE (1980) Impulse activity of locus coeruleus neurons in awake rats and monkeys is a function of sensory stimulation and arousal. Proc Natl Acad Sci U S A 77(5):3033–3037

82. French IT, Muthusamy KA (2018) A Review of the Pedunculopontine Nucleus in Parkinson's Disease. Front Aging Neurosci 10:99. doi:10.3389/fnagi.2018.00099

83. Freundt EC, Maynard N, Clancy EK, Roy S, Bousset L, Sourigues Y, Covert M, Melki R, Kirkegaard K, Brahic M (2012) Neuron-to-neuron transmission of alpha-synuclein fibrils through axonal transport. Ann Neurol 72(4):517–524. doi:10.1002/ana.23747

84. Frisina PG, Haroutunian V, Libow LS (2009) The neuropathological basis for depression in Parkinson's disease. Parkinsonism Relat Disord 15(2):144–148. doi:10.1016/j.parkreldis.2008.04.038

85. Fujiwara H, Hasegawa M, Dohmae N, Kawashima A, Masliah E, Goldberg MS, Shen J, Takio K, Iwatsubo T (2002) alpha-Synuclein is phosphorylated in synucleinopathy lesions. Nat Cell Biol 4(2):160–164. doi:10.1038/ncb748

86. Furlong M, Tanner CM, Goldman SM, Bhudhikanok GS, Blair A, Chade A, Comyns K, Hoppin JA, Kasten M, Korell M, Langston JW, Marras C, Meng C, Richards M, Ross GW, Umbach DM, Sandler DP, Kamel F (2015) Protective glove use and hygiene habits modify the associations of specific pesticides with Parkinson's disease. Environ Int 75:144–150. doi:10.1016/j.envint.2014.11.002

87. Fuxe K, Dahlström AB, Jonsson G, Marcellino D, Guescini M, Dam M, Manger P, Agnati L (2010) The discovery of central monoamine neurons gave volume transmission to the wired brain. Prog Neurobiol 90(2):82–100. doi:10.1016/j.pneurobio.2009.10.012

88. Gage GJ, Kipke DR, Shain W (2012) Whole animal perfusion fixation for rodents. J Vis Exp (65). doi:10.3791/3564

89. Gai WP, Halliday GM, Blumbergs PC, Geffen LB, Blessing WW (1991) Substance P-containing neurons in the mesopontine tegmentum are severely affected in Parkinson's disease. Brain 114 (Pt 5):2253–2267. doi:10.1093/brain/114.5.2253

90. Gao H-M, Kotzbauer PT, Uryu K, Leight S, Trojanowski JQ, Lee VM-Y (2008) Neuroinflammation and oxidation/nitration of alpha-synuclein linked to dopaminergic neurodegeneration. J Neurosci 28(30):7687–7698. doi:10.1523/JNEUROSCI.0143-07.2008

91. Gao H-M, Zhang F, Zhou H, Kam W, Wilson B, Hong J-S (2011) Neuroinflammation and α-synuclein dysfunction potentiate each other, driving chronic progression of neurodegeneration in a mouse model of Parkinson's disease. Environ Health Perspect 119(6):807–814. doi:10.1289/ehp.1003013

92. Garcia L, D'Alessandro G, Bioulac B, Hammond C (2005) High-frequency stimulation in Parkinson's disease: more or less? Trends Neurosci 28(4):209–216. doi:10.1016/j.tins.2005.02.005

93. Gerhard A, Pavese N, Hotton G, Turkheimer F, Es M, Hammers A, Eggert K, Oertel W, Banati RB, Brooks DJ (2006) In vivo imaging of microglial activation with 11C(R)-PK11195 PET in idiopathic Parkinson's disease. Neurobiol Dis 21(2):404–412. doi:10.1016/j.nbd.2005.08.002

94. German DC, Manaye KF, White CL, Woodward DJ, McIntire DD, Smith WK, Kalaria RN, Mann DM (1992) Disease-specific patterns of locus coeruleus cell loss. Ann Neurol 32(5):667–676. doi:10.1002/ana.410320510

95. Giasson BI, Uryu K, Trojanowski JQ, Lee VM (1999) Mutant and wild type human alpha-synucleins assemble into elongated filaments with distinct morphologies in vitro. J Biol Chem 274(12):7619–7622. doi:10.1074/jbc.274.12.7619

96. Giasson BI, Duda JE, Quinn SM, Zhang B, Trojanowski JQ, Lee VM-Y (2002) Neuronal α-Synucleinopathy with Severe Movement Disorder in Mice Expressing A53T Human α-Synuclein. Neuron 34(4):521–533. doi:10.1016/S0896-6273(02)00682-7

97. Glennon E, Carcea I, Martins ARO, Multani J, Shehu I, Svirsky MA, Froemke RC (2019) Locus coeruleus activation accelerates perceptual learning. Brain Res 1709:39–49. doi:10.1016/j.brainres.2018.05.048

98. Glinka YY, Youdim MBH (1995) Inhibition of mitochondrial complexes I and IV by 6-hydroxydopamine. European Journal of Pharmacology: Environmental Toxicology and Pharmacology 292(3-4):329–332. doi:10.1016/0926-6917(95)90040-3

99. Goedert M (2015) Neurodegeneration. Alzheimer's and Parkinson's diseases: The prion concept in relation to assembled Aβ, tau, and α-synuclein. Science 349(6248):1255555. doi:10.1126/science.1255555

100. Gomez-Isla T, Irizarry MC, Mariash A, Cheung B, Soto O, Schrump S, Sondel J, Kotilinek L, Day J, Schwarzschild MA, Cha J-HJ, Newell K, Miller DW, Uéda K, Young AB, Hyman BT, Ashe KH (2003) Motor dysfunction and gliosis with preserved dopaminergic markers in human α-synuclein A30P transgenic mice. Neurobiol Aging 24(2):245–258. doi:10.1016/S0197-4580(02)00091-X

101. Greffard S, Verny M, Bonnet A-M, Beinis J-Y, Gallinari C, Meaume S, Piette F, Hauw J-J, Duyckaerts C (2006) Motor score of the Unified Parkinson Disease Rating Scale as a good predictor of Lewy body-associated neuronal loss in the substantia nigra. Arch Neurol 63(4):584–588. doi:10.1001/archneur.63.4.584

102. Gribaudo S, Tixador P, Bousset L, Fenyi A, Lino P, Melki R, Peyrin J-M, Perrier AL (2019) Propagation of α-Synuclein Strains within Human Reconstructed Neuronal Network. Stem Cell Reports 12(2):230–244. doi:10.1016/j.stemcr.2018.12.007

103. Groiss SJ, Wojtecki L, Südmeyer M, Schnitzler A (2009) Deep brain stimulation in Parkinson's disease. Ther Adv Neurol Disord 2(6):20–28. doi:10.1177/1756285609339382

104. Gurevich E (1999) Distribution of Dopamine D3 Receptor Expressing Neurons in the Human Forebrain Comparison with D2 Receptor Expressing Neurons. Neuropsychopharmacology 20(1):60–80. doi:10.1016/S0893-133X(98)00066-9

105. Gut NK, Winn P (2016) The pedunculopontine tegmental nucleus-A functional hypothesis from the comparative literature. Mov Disord 31(5):615–624. doi:10.1002/mds.26556

106. Halliday G, Hely M, Reid W, Morris J (2008) The progression of pathology in longitudinally followed patients with Parkinson's disease. Acta Neuropathol 115(4):409–415. doi:10.1007/s00401-008-0344-8

107. Halliday G, Lees A, Stern M (2011) Milestones in Parkinson's disease--clinical and pathologic features. Mov Disord 26(6):1015–1021. doi:10.1002/mds.23669

108. Halliday GM, Li YW, Blumbergs PC, Joh TH, Cotton RGH, Howe PRC, Blessing WW, Geffen LB (1990) Neuropathology of immunohistochemically identified brainstem neurons in Parkinson's disease. Ann Neurol 27(4):373–385. doi:10.1002/ana.410270405

109. Halliday GM, Ophof A, Broe M, Jensen PH, Kettle E, Fedorow H, Cartwright MI, Griffiths FM, Shepherd CE, Double KL (2005) Alpha-synuclein redistributes to neuromelanin lipid in the substantia nigra early in Parkinson's disease. Brain 128(Pt 11):2654–2664. doi:10.1093/brain/awh584

110. Hamza TH, Zabetian CP, Tenesa A, Laederach A, Montimurro J, Yearout D, Kay DM, Doheny KF, Paschall J, Pugh E, Kusel VI, Collura R, Roberts J, Griffith A, Samii A, Scott WK, Nutt J, Factor SA, Payami H (2010) Common genetic variation in the HLA region is associated with late-onset sporadic Parkinson's disease. Nat Genet 42(9):781–785. doi:10.1038/ng.642

111. Hansen C, Angot E, Bergström A-L, Steiner JA, Pieri L, Paul G, Outeiro TF, Melki R, Kallunki P, Fog K, Li J-Y, Brundin P (2011) α-Synuclein propagates from mouse brain to grafted dopaminergic neurons and seeds aggregation in cultured human cells. J Clin Invest 121(2):715–725. doi:10.1172/JCI43366

112. Hartmann A (2004) Postmortem studies in Parkinson's disease. Dialogues Clin Neurosci 6(3):281–293

113. Hasegawa E, Takeshige K, Oishi T, Murai Y, Minakami S (1990) 1-Methyl-4-phenylpyridinium (MPP+) induces NADH-dependent superoxide formation and enhances NADH-dependent lipid peroxidation in bovine heart submitochondrial particles. Biochem Biophys Res Commun 170(3):1049–1055. doi:10.1016/0006-291X(90)90498-C

114. Hasegawa M, Fujiwara H, Nonaka T, Wakabayashi K, Takahashi H, Lee VM-Y, Trojanowski JQ, Mann D, Iwatsubo T (2002) Phosphorylated alpha-synuclein is ubiquitinated in alpha-synucleinopathy lesions. J Biol Chem 277(50):49071–49076. doi:10.1074/jbc.M208046200

115. Helwig M, Klinkenberg M, Rusconi R, Musgrove RE, Majbour NK, El-Agnaf OMA, Ulusoy A, Di Monte DA (2016) Brain propagation of transduced α-synuclein involves non-fibrillar protein species and is enhanced in α-synuclein null mice. Brain 139(3):856–870. doi:10.1093/brain/awv376

116. Henrich MT, Geibl FF, Lee B, Chiu W-H, Koprich JB, Brotchie JM, Timmermann L, Decher N, Matschke LA, Oertel WH (2018) A53T-alpha-synuclein overexpression in murine locus coeruleus induces Parkinson's disease-like pathology in neurons and glia. Acta Neuropathol Commun 6(1):39. doi:10.1186/s40478-018-0541-1

117. Hepp DH, Ruiter AM, Galis Y, Voorn P, Rozemuller AJM, Berendse HW, Foncke EMJ, van de Berg WDJ (2013) Pedunculopontine cholinergic cell loss in hallucinating Parkinson disease patients but not in dementia with Lewy bodies patients. J Neuropathol Exp Neurol 72(12):1162–1170. doi:10.1097/NEN.0000000000000014

118. Hernandez-Baltazar D, Mendoza-Garrido ME, Martinez-Fong D (2013) Activation of GSK-3β and caspase-3 occurs in Nigral dopamine neurons during the development of apoptosis activated by a striatal injection of 6-hydroxydopamine. PLoS ONE 8(8):e70951. doi:10.1371/journal.pone.0070951

119. Hertzman C, Wiens M, Snow B, Kelly S, Calne D (1994) A case-control study of Parkinson's disease in a horticultural region of British Columbia. Mov Disord 9(1):69–75. doi:10.1002/mds.870090111

120. Hirase H, Iwai Y, Takata N, Shinohara Y, Mishima T (2014) Volume transmission signalling via astrocytes. Philos Trans R Soc Lond B Biol Sci 369(1654). doi:10.1098/rstb.2013.0604

121. Hirsch E, Graybiel AM, Agid YA (1988) Melanized dopaminergic neurons are differentially susceptible to degeneration in Parkinson's disease. Nature 334:345 EP -. doi:10.1038/334345a0

122. Hirsch EC, Graybiel AM, Duyckaerts C, Javoy-Agid F (1987) Neuronal loss in the pedunculopontine tegmental nucleus in Parkinson disease and in progressive supranuclear palsy. Proc Natl Acad Sci U S A 84(16):5976–5980. doi:10.1073/pnas.84.16.5976

123. Hoffmann A, Ettle B, Bruno A, Kulinich A, Hoffmann A-C, Wittgenstein J von, Winkler J, Xiang W, Schlachetzki JCM (2016) Alpha-synuclein activates BV2 microglia dependent on its aggregation state. Biochem Biophys Res Commun 479(4):881–886. doi:10.1016/j.bbrc.2016.09.109

124. Holmes BB, DeVos SL, Kfoury N, Li M, Jacks R, Yanamandra K, Ouidja MO, Brodsky FM, Marasa J, Bagchi DP, Kotzbauer PT, Miller TM, Papy-Garcia D, Diamond MI (2013) Heparan sulfate proteoglycans mediate internalization and propagation of specific proteopathic seeds. Proc Natl Acad Sci U S A 110(33):E3138-47. doi:10.1073/pnas.1301440110

125. Holmqvist S, Chutna O, Bousset L, Aldrin-Kirk P, Li W, Björklund T, Wang Z-Y, Roybon L, Melki R, Li J-Y (2014) Direct evidence of Parkinson pathology spread from the gastrointestinal tract to the brain in rats. Acta Neuropathol 128(6):805–820. doi:10.1007/s00401-014-1343-6

126. Horonchik L, Tzaban S, Ben-Zaken O, Yedidia Y, Rouvinski A, Papy-Garcia D, Barritault D, Vlodavsky I, Taraboulos A (2005) Heparan sulfate is a cellular receptor for purified infectious prions. J Biol Chem 280(17):17062–17067. doi:10.1074/jbc.M500122200

127. Iannaccone S, Cerami C, Alessio M, Garibotto V, Panzacchi A, Olivieri S, Gelsomino G, Moresco RM, Perani D (2013) In vivo microglia activation in very early dementia with Lewy bodies, comparison with Parkinson's disease. Parkinsonism Relat Disord 19(1):47–52. doi:10.1016/j.parkreldis.2012.07.002

128. Ibáñez P, Bonnet A-M, Débarges B, Lohmann E, Tison F, Agid Y, Dürr A, Brice A, Pollak P (2004) Causal relation between α-synuclein locus duplication as a cause of familial Parkinson's disease. The Lancet 364(9440):1169–1171. doi:10.1016/S0140-6736(04)17104-3

129. Imamura K, Hishikawa N, Sawada M, Nagatsu T, Yoshida M, Hashizume Y (2003) Distribution of major histocompatibility complex class II-positive microglia and cytokine profile of Parkinson's disease brains. Acta Neuropathol 106(6):518–526. doi:10.1007/s00401-003-0766-2

130. Inzelberg R, Schechtman E, Paleacu D (2002) Onset age of Parkinson disease. Am J Med Genet 111(4):459-60; author reply 461. doi:10.1002/ajmg.10586

131. Ip CW, Klaus L-C, Karikari AA, Visanji NP, Brotchie JM, Lang AE, Volkmann J, Koprich JB (2017) AAV1/2-induced overexpression of A53T-alpha-synuclein in the substantia nigra results in degeneration of the nigrostriatal system with Lewy-like pathology and motor impairment. A new mouse model for Parkinson's disease. Acta Neuropathol Commun 5(1):11. doi:10.1186/s40478-017-0416-x

132. Iranzo A, Gelpi E, Tolosa E, Molinuevo JL, Serradell M, Gaig C, Santamaria J (2014) Neuropathology of prodromal Lewy body disease. Mov Disord 29(3):410–415. doi:10.1002/mds.25825

133. Jackson-Lewis V, Przedborski S (2007) Protocol for the MPTP mouse model of Parkinson's disease. Nat Protoc 2:141 EP -. doi:10.1038/nprot.2006.342

134. Jellinger KA (2009) A critical evaluation of current staging of alpha-synuclein pathology in Lewy body disorders. Biochim Biophys Acta 1792(7):730–740. doi:10.1016/j.bbadis.2008.07.006

135. Jeon BS, Jackson-Lewis V, Burke RE (1995) 6-Hydroxydopamine lesion of the rat substantia nigra: time course and morphology of cell death. Neurodegeneration 4(2):131–137

136. Kalia LV, Lang AE (2015) Parkinson's disease. The Lancet 386(9996):896–912. doi:10.1016/S0140-6736(14)61393-3

137. Karachi C, Grabli D, Bernard FA, Tande D, Wattiez N, Belaid H, Bardinet E, Prigent A, Nothacker H-P, Hunot S, Hartmann A, Lehericy S, Hirsch EC, Francois C (2010) Cholinergic mesencephalic neurons are involved in gait and postural disorders in Parkinson disease. J Clin Invest 120(8):2745–2754. doi:10.1172/JCI42642

138. Karampetsou M, Ardah MT, Semitekolou M, Polissidis A, Samiotaki M, Kalomoiri M, Majbour N, Xanthou G, El-Agnaf OMA, Vekrellis K (2017) Phosphorylated exogenous alpha-synuclein fibrils exacerbate pathology and induce neuronal dysfunction in mice. Sci Rep 7(1):16533. doi:10.1038/s41598-017-15813-8

139. Keating GL, Winn P (2002) Examination of the role of the pedunculopontine tegmental nucleus in radial maze tasks with or without a delay. Neuroscience 112(3):687–696. doi:10.1016/S0306-4522(02)00108-2

140. Kim S, Kwon S-H, Kam T-I, Panicker N, Karuppagounder SS, Lee S, Lee JH, Kim WR, Kook M, Foss CA, Shen C, Lee H, Kulkarni S, Pasricha PJ, Lee G, Pomper MG, Dawson VL, Dawson TM, Ko HS (2019) Transneuronal Propagation of Pathologic α-Synuclein from the Gut to the Brain Models Parkinson's Disease. Neuron. doi:10.1016/j.neuron.2019.05.035

141. Kipanyula MJ, Sife AS (2018) Global Trends in Application of Stereology as a Quantitative Tool in Biomedical Research. Biomed Res Int 2018:1825697. doi:10.1155/2018/1825697

142. Kirik D, Rosenblad C, Burger C, Lundberg C, Johansen TE, Muzyczka N, Mandel RJ, Björklund A (2002) Parkinson-like neurodegeneration induced by targeted overexpression of alpha-synuclein in the nigrostriatal system. J Neurosci 22(7):2780–2791

143. Kleiner-Fisman G, Herzog J, Fisman DN, Tamma F, Lyons KE, Pahwa R, Lang AE, Deuschl G (2006) Subthalamic nucleus deep brain stimulation: summary and meta-analysis of outcomes. Mov Disord 21 Suppl 14:S290-304. doi:10.1002/mds.20962

144. Knott C, Wilkin GP, Stern G (1999) Astrocytes and microglia in the substantia nigra and caudate-putamen in Parkinson's disease. Parkinsonism Relat Disord 5(3):115–122. doi:10.1016/S1353-8020(99)00022-X

145. Kojovic M, Sheerin U-M, Rubio-Agusti I, Saha A, Bras J, Gibbons V, Palmer R, Houlden H, Hardy J, Wood NW, Bhatia KP (2012) Young-onset parkinsonism due to homozygous duplication of α-synuclein in a consanguineous family. Mov Disord 27(14):1827–1829. doi:10.1002/mds.25199

146. Komatsu M, Kageyama S, Ichimura Y (2012) p62/SQSTM1/A170: physiology and pathology. Pharmacol Res 66(6):457–462. doi:10.1016/j.phrs.2012.07.004

147. Koprich JB, Johnston TH, Reyes MG, Sun X, Brotchie JM (2010) Expression of human A53T alpha-synuclein in the rat substantia nigra using a novel AAV1/2 vector produces a rapidly evolving pathology with protein aggregation, dystrophic neurite architecture and nigrostriatal degeneration with potential to model the pathology of Parkinson's disease. Mol Neurodegener 5:43. doi:10.1186/1750-1326-5-43

148. Koprich JB, Johnston TH, Huot P, Reyes MG, Espinosa M, Brotchie JM (2011) Progressive neurodegeneration or endogenous compensation in an animal model of Parkinson's disease produced by decreasing doses of alpha-synuclein. PLoS ONE 6(3):e17698. doi:10.1371/journal.pone.0017698

149. Kordower JH, Chu Y, Hauser RA, Freeman TB, Olanow CW (2008) Lewy body–like pathology in long-term embryonic nigral transplants in Parkinson's disease. Nat Med 14:504 EP -. doi:10.1038/nm1747

150. Kordower JH, Dodiya HB, Kordower AM, Terpstra B, Paumier K, Madhavan L, Sortwell C, Steece-Collier K, Collier TJ (2011) Transfer of host-derived α synuclein to grafted dopaminergic neurons in rat. Neurobiol Dis 43(3):552–557. doi:10.1016/j.nbd.2011.05.001

151. Kordower JH, Olanow CW, Dodiya HB, Chu Y, Beach TG, Adler CH, Halliday GM, Bartus RT (2013) Disease duration and the integrity of the nigrostriatal system in Parkinson's disease. Brain 136(Pt 8):2419–2431. doi:10.1093/brain/awt192

152. Kotagal V, Müller MLTM, Kaufer DI, Koeppe RA, Bohnen NI (2012) Thalamic cholinergic innervation is spared in Alzheimer disease compared to parkinsonian disorders. Neurosci Lett 514(2):169–172. doi:10.1016/j.neulet.2012.02.083

153. Kreiner G (2015) Compensatory mechanisms in genetic models of neurodegeneration: are the mice better than humans? Front Cell Neurosci 9:56. doi:10.3389/fncel.2015.00056

154. Kroeger D, Ferrari LL, Petit G, Mahoney CE, Fuller PM, Arrigoni E, Scammell TE (2017) Cholinergic, Glutamatergic, and GABAergic Neurons of the Pedunculopontine Tegmental Nucleus Have Distinct Effects on Sleep/Wake Behavior in Mice. J Neurosci 37(5):1352–1366. doi:10.1523/JNEUROSCI.1405-16.2016

155. Kudo T, Loh DH, Truong D, Wu Y, Colwell CS (2011) Circadian dysfunction in a mouse model of Parkinson's disease. Exp Neurol 232(1):66–75. doi:10.1016/j.expneurol.2011.08.003

156. Kuusisto E, Salminen A, Alafuzoff I (2001) Ubiquitin-binding protein p62 is present in neuronal and glial inclusions in human tauopathies and synucleinopathies. Neuroreport 12(10):2085–2090

157. Kuusisto E, Parkkinen L, Alafuzoff I (2003) Morphogenesis of Lewy bodies: dissimilar incorporation of alpha-synuclein, ubiquitin, and p62. J Neuropathol Exp Neurol 62(12):1241–1253. doi:10.1093/jnen/62.12.1241

158. Kuusisto E, Kauppinen T, Alafuzoff I (2008) Use of p62/SQSTM1 antibodies for neuropathological diagnosis. Neuropathol Appl Neurobiol 34(2):169–180. doi:10.1111/j.1365-2990.2007.00884.x

159. Kuwahara T, Tonegawa R, Ito G, Mitani S, Iwatsubo T (2012) Phosphorylation of α-synuclein protein at Ser-129 reduces neuronal dysfunction by lowering its membrane binding property in Caenorhabditis elegans. J Biol Chem 287(10):7098–7109. doi:10.1074/jbc.M111.237131

160. Kuzkina A, Schulmeyer L, Monoranu C-M, Volkmann J, Sommer C, Doppler K (2019) The aggregation state of α-synuclein deposits in dermal nerve fibers of patients with Parkinson's disease resembles that in the brain. Parkinsonism Relat Disord. doi:10.1016/j.parkreldis.2019.03.003

161. Kwon I, Schaffer DV (2008) Designer gene delivery vectors: molecular engineering and evolution of adeno-associated viral vectors for enhanced gene transfer. Pharm Res 25(3):489–499. doi:10.1007/s11095-007-9431-0

162. La Fuente-Fernández R de, Sellers A, Beyer K, Lao JI (1998) Apolipoprotein E genotypes and age at onset of Parkinson's disease. Ann Neurol 44(2):294–295. doi:10.1002/ana.410440230

163. Lam HA, Wu N, Cely I, Kelly RL, Hean S, Richter F, Magen I, Cepeda C, Ackerson LC, Walwyn W, Masliah E, Chesselet M-F, Levine MS, Maidment NT (2011) Elevated tonic extracellular dopamine concentration and altered dopamine modulation of synaptic activity precede dopamine loss in the striatum of mice overexpressing human α-synuclein. J Neurosci Res 89(7):1091–1102. doi:10.1002/jnr.22611

164. Langston JW, Ballard P, Tetrud JW, Irwin I (1983) Chronic Parkinsonism in humans due to a product of meperidine-analog synthesis. Science 219(4587):979–980

165. Lau LML de, Breteler MMB (2006) Epidemiology of Parkinson's disease. The Lancet Neurology 5(6):525–535. doi:10.1016/S1474-4422(06)70471-9

166. Lauwers E, Debyser Z, Dorpe J, Strooper B, Nuttin B, Baekelandt V (2003) Neuropathology and Neurodegeneration in Rodent Brain Induced by Lentiviral Vectormediated Overexpression of α-Synuclein. Brain Pathology 13(3):364–372. doi:10.1111/j.1750-3639.2003.tb00035.x

167. Lavedan C (1998) The synuclein family. Genome Res 8(9):871–880. doi:10.1101/gr.8.9.871

168. Lawson LJ, Perry VH, Dri P, Gordon S (1990) Heterogeneity in the distribution and morphology of microglia in the normal adult mouse brain. Neuroscience 39(1):151–170. doi:10.1016/0306-4522(90)90229-W

169. Lee H-J, Suk J-E, Bae E-J, Lee J-H, Paik SR, Lee S-J (2008) Assembly-dependent endocytosis and clearance of extracellular alpha-synuclein. Int J Biochem Cell Biol 40(9):1835–1849. doi:10.1016/j.biocel.2008.01.017

170. Lee E-J, Woo M-S, Moon P-G, Baek M-C, Choi I-Y, Kim W-K, Junn E, Kim H-S (2010) Alpha-synuclein activates microglia by inducing the expressions of matrix metalloproteinases and the subsequent activation of protease-activated receptor-1. J Immunol 185(1):615–623. doi:10.4049/jimmunol.0903480

171. Lee MK, Stirling W, Xu Y, Xu X, Qui D, Mandir AS, Dawson TM, Copeland NG, Jenkins NA, Price DL (2002) Human alpha-synuclein-harboring familial Parkinson's disease-linked Ala-53 -- Thr mutation causes neurodegenerative disease with alpha-synuclein aggregation in transgenic mice. Proc Natl Acad Sci U S A 99(13):8968–8973. doi:10.1073/pnas.132197599

172. Lees AJ, Hardy J, Revesz T (2009) Parkinson's disease. The Lancet 373(9680):2055–2066. doi:10.1016/S0140-6736(09)60492-X

173. Levin J, Schmidt F, Boehm C, Prix C, Botzel K, Ryazanov S, Leonov A, Griesinger C, Giese A (2014) The oligomer modulator anle138b inhibits disease progression in a Parkinson mouse model even with treatment started after disease onset. Acta Neuropathol 127(5):779–780. doi:10.1007/s00401-014-1265-3

174. Li SC, Schoenberg BS, Wang CC, Cheng XM, Rui DY, Bolis CL, Schoenberg DG (1985) A prevalence survey of Parkinson's disease and other movement disorders in the People's Republic of China. Arch Neurol 42(7):655–657

175. Lipinski DM, Thake M, MacLaren RE (2013) Clinical applications of retinal gene therapy. Prog Retin Eye Res 32:22–47. doi:10.1016/j.preteyeres.2012.09.001

176. Lo Bianco C, Ridet J-L, Schneider BL, Deglon N, Aebischer P (2002) alpha -Synucleinopathy and selective dopaminergic neuron loss in a rat lentiviral-based model of Parkinson's disease. Proc Natl Acad Sci U S A 99(16):10813–10818. doi:10.1073/pnas.152339799

177. Lue L-F, Walker DG, Adler CH, Shill H, Tran H, Akiyama H, Sue LI, Caviness J, Sabbagh MN, Beach TG (2012) Biochemical increase in phosphorylated alpha-synuclein precedes histopathology of Lewy-type synucleinopathies. Brain Pathol 22(6):745–756. doi:10.1111/j.1750-3639.2012.00585.x

178. Luk KC, Song C, O'Brien P, Stieber A, Branch JR, Brunden KR, Trojanowski JQ, Lee VM-Y (2009) Exogenous alpha-synuclein fibrils seed the formation of Lewy body-like intracellular inclusions in cultured cells. Proc Natl Acad Sci U S A 106(47):20051–20056. doi:10.1073/pnas.0908005106

179. Luk KC, Kehm V, Carroll J, Zhang B, O'Brien P, Trojanowski JQ, Lee VM-Y (2012) Pathological α-synuclein transmission initiates Parkinson-like neurodegeneration in nontransgenic mice. Science 338(6109):949–953. doi:10.1126/science.1227157

180. Luk KC, Covell DJ, Kehm VM, Zhang B, Song IY, Byrne MD, Pitkin RM, Decker SC, Trojanowski JQ, Lee VM-Y (2016) Molecular and Biological Compatibility with Host Alpha-Synuclein Influences Fibril Pathogenicity. Cell Rep 16(12):3373–3387. doi:10.1016/j.celrep.2016.08.053

181. Luquin E, Huerta I, Aymerich MS, Mengual E (2018) Stereological Estimates of Glutamatergic, GABAergic, and Cholinergic Neurons in the Pedunculopontine and Laterodorsal Tegmental Nuclei in the Rat. Front Neuroanat 12:34. doi:10.3389/fnana.2018.00034

182. Mandel RJ, Marmion DJ, Kirik D, Chu Y, Heindel C, McCown T, Gray SJ, Kordower JH (2017) Novel oligodendroglial alpha synuclein viral vector models of multiple system atrophy. Studies in rodents and nonhuman primates. Acta Neuropathol Commun 5(1):47. doi:10.1186/s40478-017-0451-7

183. Mao X, Ou MT, Karuppagounder SS et al (2016) Pathological alpha-synuclein transmission initiated by binding lymphocyte-activation gene 3. Science 353(6307). doi:10.1126/science.aah3374

184. Martin LJ (2007) Transgenic mice with human mutant genes causing Parkinson's disease and amyotrophic lateral sclerosis provide common insight into mechanisms of motor neuron selective vulnerability to degeneration. Rev Neurosci 18(2):115–136

185. Martin LJ, Pan Y, Price AC, Sterling W, Copeland NG, Jenkins NA, Price DL, Lee MK (2006) Parkinson's Disease α-Synuclein Transgenic Mice Develop Neuronal Mitochondrial Degeneration and Cell Death. J. Neurosci. 26(1):41–50. doi:10.1523/JNEUROSCI.4308-05.2006

186. Masliah E (2000) Dopaminergic Loss and Inclusion Body Formation in -Synuclein Mice: Implications for Neurodegenerative Disorders. Science 287(5456):1265–1269. doi:10.1126/science.287.5456.1265

187. Masliah E, Rockenstein E, Mante M, Crews L, Spencer B, Adame A, Patrick C, Trejo M, Ubhi K, Rohn TT, Mueller-Steiner S, Seubert P, Barbour R, McConlogue L, Buttini M, Games D, Schenk D (2011) Passive immunization reduces behavioral and neuropathological deficits in an alpha-synuclein transgenic model of Lewy body disease. PLoS ONE 6(4):e19338. doi:10.1371/journal.pone.0019338

188. Mason DM, Nouraei N, Pant DB, Miner KM, Hutchison DF, Luk KC, Stolz JF, Leak RK (2016) Transmission of α-synucleinopathy from olfactory structures deep into the temporal lobe. Mol Neurodegener 11(1):49. doi:10.1186/s13024-016-0113-4

189. Masuda-Suzukake M, Nonaka T, Hosokawa M, Oikawa T, Arai T, Akiyama H, Mann DMA, Hasegawa M (2013) Prion-like spreading of pathological alpha-synuclein in brain. Brain 136(Pt 4):1128–1138. doi:10.1093/brain/awt037

190. Masuda-Suzukake M, Nonaka T, Hosokawa M, Kubo M, Shimozawa A, Akiyama H, Hasegawa M (2014) Pathological alpha-synuclein propagates through neural networks. Acta Neuropathol Commun 2:88. doi:10.1186/PREACCEPT-1296467154135944

191. Matsuda W, Furuta T, Nakamura KC, Hioki H, Fujiyama F, Arai R, Kaneko T (2009) Single nigrostriatal dopaminergic neurons form widely spread and highly dense axonal arborizations in the neostriatum. J Neurosci 29(2):444–453. doi:10.1523/JNEUROSCI.4029-08.2009

192. Mayeux R, Marder K, Cote LJ, Denaro J, Hemenegildo N, Mejia H, Tang MX, Lantigua R, Wilder D, Gurland B (1995) The frequency of idiopathic Parkinson's disease by age, ethnic group, and sex in northern Manhattan, 1988-1993. Am J Epidemiol 142(8):820–827. doi:10.1093/oxfordjournals.aje.a117721

193. McFarland NR, Fan Z, Xu K, Schwarzschild MA, Feany MB, Hyman BT, McLean PJ (2009) Alpha-synuclein S129 phosphorylation mutants do not alter nigrostriatal toxicity in a rat model of Parkinson disease. J Neuropathol Exp Neurol 68(5):515–524. doi:10.1097/NEN.0b013e3181a24b53

194. McGeer PL, Itagaki S, Boyes BE, McGeer EG (1988) Reactive microglia are positive for HLA-DR in the substantia nigra of Parkinson's and Alzheimer's disease brains. Neurology 38(8):1285–1291

195. Mena-Segovia J, Bolam JP (2017) Rethinking the Pedunculopontine Nucleus: From Cellular Organization to Function. Neuron 94(1):7–18. doi:10.1016/j.neuron.2017.02.027

196. Mena-Segovia J, Sims HM, Magill PJ, Bolam JP (2008) Cholinergic brainstem neurons modulate cortical gamma activity during slow oscillations. J Physiol (Lond) 586(12):2947–2960. doi:10.1113/jphysiol.2008.153874

197. Mendritzki S, Schmidt S, Sczepan T, Zhu X-R, Segelcke D, Lübbert H (2010) Spinal cord pathology in alpha-synuclein transgenic mice. Parkinsons Dis 2010:375462. doi:10.4061/2010/375462

198. Mercuri NB, Bernardi G (2005) The 'magic' of L-dopa: why is it the gold standard Parkinson's disease therapy? Trends Pharmacol Sci 26(7):341–344. doi:10.1016/j.tips.2005.05.002

199. Miyoshi F, Ogawa T, Kitao S-i, Kitayama M, Shinohara Y, Takasugi M, Fujii S, Kaminou T (2013) Evaluation of Parkinson disease and Alzheimer disease with the use of neuromelanin MR imaging and (123)I-metaiodobenzylguanidine scintigraphy. AJNR Am J Neuroradiol 34(11):2113–2118. doi:10.3174/ajnr.A3567

200. Moors TE, Maat CA, Niedieker D, Mona D, Petersen D, Timmermans-Huisman E, Kole J, El-Mashtoly SF, Spycher L, Zago W, Barbour R, Mundigl O, Kaluza K, Huber S, Hug MN, Kremer T, Ritter M, Dziadek S, Geurts JJG, Gerwert K, Britschgi M, van de Berg WDJ (2018) The orchestration of subcellular alpha-synuclein pathology in the Parkinson's disease brain revealed by STED microscopy, Bd 425

201. Müller MLTM, Albin RL, Kotagal V, Koeppe RA, Scott PJH, Frey KA, Bohnen NI (2013) Thalamic cholinergic innervation and postural sensory integration function in Parkinson's disease. Brain 136(Pt 11):3282–3289. doi:10.1093/brain/awt247

202. Musacchio T, Rebenstorff M, Fluri F, Brotchie JM, Volkmann J, Koprich JB, Ip CW (2017) Subthalamic nucleus deep brain stimulation is neuroprotective in the A53T α-synuclein Parkinson's disease rat model. Ann Neurol 81(6):825–836. doi:10.1002/ana.24947

203. Neumann M, Kahle PJ, Giasson BI, Ozmen L, Borroni E, Spooren W, Müller V, Odoy S, Fujiwara H, Hasegawa M, Iwatsubo T, Trojanowski JQ, Kretzschmar HA, Haass C (2002) Misfolded proteinase K-resistant hyperphosphorylated alpha-synuclein in aged transgenic mice with locomotor deterioration and in human alpha-synucleinopathies. J Clin Invest 110(10):1429–1439. doi:10.1172/JCI15777

204. Nicklas WJ, Vyas I, Heikkila RE (1985) Inhibition of NADH-linked oxidation in brain mitochondria by 1-methyl-4-phenyl-pyridine, a metabolite of the neurotoxin, 1-methyl-4-phenyl-1,2,5,6-tetrahydropyridine. Life Sci 36(26):2503–2508

205. Nouraei N, Mason DM, Miner KM, Carcella MA, Bhatia TN, Dumm BK, Soni D, Johnson DA, Luk KC, Leak RK (2018) Critical appraisal of pathology transmission in the α-synuclein fibril model of Lewy body disorders. Exp Neurol 299(Pt A):172–196. doi:10.1016/j.expneurol.2017.10.017

206. Nyholm D (2006) Pharmacokinetic optimisation in the treatment of Parkinson's disease : an update. Clin Pharmacokinet 45(2):109–136. doi:10.2165/00003088-200645020-00001

207. Oertel W, Schulz JB (2016) Current and experimental treatments of Parkinson disease. A guide for neuroscientists. J Neurochem 139 Suppl 1:325–337. doi:10.1111/jnc.13750

208. Oertel WH (2017) Recent advances in treating Parkinson's disease. F1000Res 6:260. doi:10.12688/f1000research.10100.1

209. Ohtsuka C, Sasaki M, Konno K, Koide M, Kato K, Takahashi J, Takahashi S, Kudo K, Yamashita F, Terayama Y (2013) Changes in substantia nigra and locus coeruleus in patients with early-stage Parkinson's disease using neuromelanin-sensitive MR imaging. Neurosci Lett 541:93–98. doi:10.1016/j.neulet.2013.02.012

210. Okuzumi A, Kurosawa M, Hatano T, Takanashi M, Nojiri S, Fukuhara T, Yamanaka T, Miyazaki H, Yoshinaga S, Furukawa Y, Shimogori T, Hattori N, Nukina N (2018) Rapid dissemination of alpha-synuclein seeds through neural circuits in an in-vivo prion-like seeding experiment. Acta Neuropathol Commun 6(1):96. doi:10.1186/s40478-018-0587-0

211. Olanow CW, Obeso JA (2000) Preventing levodopa-induced dyskinesias. Ann Neurol 47(4 Suppl 1):S167-76; discussion S176-8

212. Olszewski J, Baxter D (1954) Cytoarchitecture of the Human Brain Stem.

213. Osterberg VR, Spinelli KJ, Weston LJ, Luk KC, Woltjer RL, Unni VK (2015) Progressive Aggregation of Alpha-Synuclein and Selective Degeneration of Lewy Inclusion-Bearing Neurons in a Mouse Model of Parkinsonism. Cell Rep 10(8):1252–1260. doi:10.1016/j.celrep.2015.01.060

214. O'Sullivan SS, Williams DR, Gallagher DA, Massey LA, Silveira-Moriyama L, Lees AJ (2008) Nonmotor symptoms as presenting complaints in Parkinson's disease: a clinicopathological study. Mov Disord 23(1):101–106. doi:10.1002/mds.21813

215. Ouchi Y, Yoshikawa E, Sekine Y, Futatsubashi M, Kanno T, Ogusu T, Torizuka T (2005) Microglial activation and dopamine terminal loss in early Parkinson's disease. Ann Neurol 57(2):168–175. doi:10.1002/ana.20338

216. Oueslati A, Schneider BL, Aebischer P, Lashuel HA (2013) Polo-like kinase 2 regulates selective autophagic α-synuclein clearance and suppresses its toxicity in vivo. Proc Natl Acad Sci U S A 110(41):E3945-54. doi:10.1073/pnas.1309991110

217. Pacelli C, Giguère N, Bourque M-J, Lévesque M, Slack RS, Trudeau L-É (2015) Elevated Mitochondrial Bioenergetics and Axonal Arborization Size Are Key Contributors to the Vulnerability of Dopamine Neurons. Curr Biol 25(18):2349–2360. doi:10.1016/j.cub.2015.07.050

218. Pallone JA (2007) Introduction to Parkinson's disease. Dis Mon 53(4):195–199. doi:10.1016/j.disamonth.2007.05.001

219. Parkkinen L, Pirttilä T, Alafuzoff I (2008) Applicability of current staging/categorization of alpha-synuclein pathology and their clinical relevance. Acta Neuropathol 115(4):399–407. doi:10.1007/s00401-008-0346-6

220. Paschalis EI, Lei F, Zhou C, Kapoulea V, Thanos A, Dana R, Vavvas DG, Chodosh J, Dohlman CH (2018) The Role of Microglia and Peripheral Monocytes in Retinal Damage after Corneal Chemical Injury. Am J Pathol 188(7):1580–1596. doi:10.1016/j.ajpath.2018.03.005

221. Paulus W, Jellinger K (1991) The Neuropathologic Basis of Different Clinical Subgroups of Parkinson's Disease. J Neuropathol Exp Neurol 50(6):743–755. doi:10.1097/00005072-199111000-00006

222. Paumier KL, Luk KC, Manfredsson FP, Kanaan NM, Lipton JW, Collier TJ, Steece-Collier K, Kemp CJ, Celano S, Schulz E, Sandoval IM, Fleming S, Dirr E, Polinski NK, Trojanowski JQ, Lee VM, Sortwell CE (2015) Intrastriatal injection of pre-formed mouse alpha-synuclein fibrils into rats triggers alpha-synuclein pathology and bilateral nigrostriatal degeneration. Neurobiol Dis 82:185–199. doi:10.1016/j.nbd.2015.06.003

223. Peelaerts W, Bousset L, van der Perren A, Moskalyuk A, Pulizzi R, Giugliano M, van den Haute C, Melki R, Baekelandt V (2015) α-Synuclein strains cause distinct synucleinopathies after local and systemic administration. Nature 522(7556):340–344. doi:10.1038/nature14547

224. Pereira EAC, Green AL, Nandi D, Aziz TZ (2007) Deep brain stimulation: indications and evidence. Expert Rev Med Devices 4(5):591–603. doi:10.1586/17434440.4.5.591

225. Perese DA, Ulman J, Viola J, Ewing SE, Bankiewicz KS (1989) A 6-hydroxydopamine-induced selective parkinsonian rat model. Brain Res 494(2):285–293. doi:10.1016/0006-8993(89)90597-0

226. Pienaar IS, Elson JL, Racca C, Nelson G, Turnbull DM, Morris CM (2013) Mitochondrial Abnormality Associates with Type-Specific Neuronal Loss and Cell Morphology Changes in the Pedunculopontine Nucleus in Parkinson Disease. Am J Pathol 183(6):1826–1840. doi:10.1016/j.ajpath.2013.09.002

227. Pienaar IS, Vernon A, Winn P (2017) The Cellular Diversity of the Pedunculopontine Nucleus: Relevance to Behavior in Health and Aspects of Parkinson's Disease. Neuroscientist 23(4):415–431. doi:10.1177/1073858416682471

228. Polinski NK, Volpicelli-Daley LA, Sortwell CE, Luk KC, Cremades N, Gottler LM, Froula J, Duffy MF, Lee VMY, Martinez TN, Dave KD (2018) Best Practices for Generating and Using Alpha-Synuclein Pre-Formed Fibrils to Model Parkinson's Disease in Rodents. J Parkinsons Dis 8(2):303–322. doi:10.3233/JPD-171248

229. Polymeropoulos MH, Lavedan C, Leroy E, Ide SE, Dehejia A, Dutra A, Pike B, Root H, Rubenstein J, Boyer R, Stenroos ES, Chandrasekharappa S, Athanassiadou A, Papapetropoulos T, Johnson WG, Lazzarini AM, Duvoisin RC, Di Iorio G, Golbe LI, Nussbaum RL (1997) Mutation in the alpha-synuclein gene identified in families with Parkinson's disease. Science 276(5321):2045–2047

230. Popova B, Kleinknecht A, Braus GH (2015) Posttranslational Modifications and Clearing of alpha-Synuclein Aggregates in Yeast. Biomolecules 5(2):617–634. doi:10.3390/biom5020617

231. Postuma RB, Berg D, Stern M, Poewe W, Olanow CW, Oertel W, Obeso J, Marek K, Litvan I, Lang AE, Halliday G, Goetz CG, Gasser T, Dubois B, Chan P, Bloem BR, Adler CH, Deuschl G (2015) MDS clinical diagnostic criteria for Parkinson's disease. Mov Disord 30(12):1591–1601. doi:10.1002/mds.26424

232. Poulopoulos M, Levy OA, Alcalay RN (2012) The neuropathology of genetic Parkinson's disease. Mov Disord 27(7):831–842. doi:10.1002/mds.24962

233. Powers KM, Kay DM, Factor SA, Zabetian CP, Higgins DS, Samii A, Nutt JG, Griffith A, Leis B, Roberts JW, Martinez ED, Montimurro JS, Checkoway H, Payami H (2008) Combined effects of smoking, coffee, and NSAIDs on Parkinson's disease risk. Mov Disord 23(1):88–95. doi:10.1002/mds.21782

234. Prusiner SB (1991) Molecular biology of prion diseases. Science 252(5012):1515–1522. doi:10.1126/science.1675487

235. Przedborski S (2017) The two-century journey of Parkinson disease research. Nature Reviews Neuroscience 18:251 EP -. doi:10.1038/nrn.2017.25

236. Przedborski S, Jackson-Lewis V, Naini AB, Jakowec M, Petzinger G, Miller R, Akram M (2001) The parkinsonian toxin 1-methyl-4-phenyl-1,2,3,6-tetrahydropyridine (MPTP): a technical review of its utility and safety. J Neurochem 76(5):1265–1274. doi:10.1046/j.1471-4159.2001.00183.x

237. Qian L, Wu H-m, Chen S-H, Zhang D, Ali SF, Peterson L, Wilson B, Lu R-B, Hong J-S, Flood PM (2011) beta2-adrenergic receptor activation prevents rodent dopaminergic neurotoxicity by inhibiting microglia via a novel signaling pathway. J Immunol 186(7):4443–4454. doi:10.4049/jimmunol.1002449

238. Rajput AH (1992) Frequency and Cause of Parkinson's Disease. Can. j. neurol. sci. 19(S1):103–107. doi:10.1017/S0317167100041457

239. Recasens A, Dehay B, Bove J, Carballo-Carbajal I, Dovero S, Perez-Villalba A, Fernagut P-O, Blesa J, Parent A, Perier C, Farinas I, Obeso JA, Bezard E, Vila M (2014) Lewy body extracts from Parkinson disease brains trigger alpha-synuclein pathology and neurodegeneration in mice and monkeys. Ann Neurol 75(3):351–362. doi:10.1002/ana.24066

240. Remy P, Doder M, Lees A, Turjanski N, Brooks D (2005) Depression in Parkinson's disease: loss of dopamine and noradrenaline innervation in the limbic system. Brain 128(Pt 6):1314–1322. doi:10.1093/brain/awh445

241. Rey NL, Petit GH, Bousset L, Melki R, Brundin P (2013) Transfer of human alpha-synuclein from the olfactory bulb to interconnected brain regions in mice. Acta Neuropathol 126(4):555–573. doi:10.1007/s00401-013-1160-3

242. Rey NL, Steiner JA, Maroof N, Luk KC, Madaj Z, Trojanowski JQ, Lee VM-Y, Brundin P (2016) Widespread transneuronal propagation of alpha-synucleinopathy triggered in olfactory bulb mimics prodromal Parkinson's disease. J Exp Med 213(9):1759–1778. doi:10.1084/jem.20160368

243. Rey NL, George S, Steiner JA, Madaj Z, Luk KC, Trojanowski JQ, Lee VM-Y, Brundin P (2018) Spread of aggregates after olfactory bulb injection of alpha-synuclein fibrils is associated with early neuronal loss and is reduced long term. Acta Neuropathol 135(1):65–83. doi:10.1007/s00401-017-1792-9

244. Richardson JR, Caudle WM, Guillot TS, Watson JL, Nakamaru-Ogiso E, Seo BB, Sherer TB, Greenamyre JT, Yagi T, Matsuno-Yagi A, Miller GW (2007) Obligatory role for complex I inhibition in the dopaminergic neurotoxicity of 1-methyl-4-phenyl-1,2,3,6-tetrahydropyridine (MPTP). Toxicol Sci 95(1):196–204. doi:10.1093/toxsci/kfl133

245. Richter-Landsberg C, Leyk J (2013) Inclusion body formation, macroautophagy, and the role of HDAC6 in neurodegeneration. Acta Neuropathol 126(6):793–807. doi:10.1007/s00401-013-1158-x

246. Rieker C, Dev KK, Lehnhoff K, Barbieri S, Ksiazek I, Kauffmann S, Danner S, Schell H, Boden C, Ruegg MA, Kahle PJ, van der Putten H, Shimshek DR (2011) Neuropathology in mice expressing mouse alpha-synuclein. PLoS ONE 6(9):e24834. doi:10.1371/journal.pone.0024834

247. Rijk MC de, Breteler MMB, Graveland GA, Ott A, Grobbee DE, van der Meche FGA, Hofman A (1995) Prevalence of Parkinson's disease in the elderly: The Rotterdam Study. Neurology 45(12):2143–2146. doi:10.1212/WNL.45.12.2143

248. Rijk MC de, Tzourio C, Breteler MM, Dartigues JF, Amaducci L, Lopez-Pousa S, Manubens-Bertran JM, Alpérovitch A, Rocca WA (1997) Prevalence of parkinsonism and Parkinson's disease in Europe: the EUROPARKINSON Collaborative Study. European Community Concerted Action on the Epidemiology of Parkinson's disease. Journal of Neurology, Neurosurgery & Psychiatry 62(1):10–15. doi:10.1136/jnnp.62.1.10

249. Rinne JO, Ma SY, Lee MS, Collan Y, Roytta M (2008) Loss of cholinergic neurons in the pedunculopontine nucleus in Parkinson's disease is related to disability of the patients. Parkinsonism Relat Disord 14(7):553–557. doi:10.1016/j.parkreldis.2008.01.006

250. Rodríguez-Martín T, Cuchillo-Ibáñez I, Noble W, Nyenya F, Anderton BH, Hanger DP (2013) Tau phosphorylation affects its axonal transport and degradation. Neurobiol Aging 34(9):2146–2157. doi:10.1016/j.neurobiolaging.2013.03.015

251. Rodriguez-Oroz MC, Jahanshahi M, Krack P, Litvan I, Macias R, Bezard E, Obeso JA (2009) Initial clinical manifestations of Parkinson's disease: features and pathophysiological mechanisms. The Lancet Neurology 8(12):1128–1139. doi:10.1016/S1474-4422(09)70293-5

252. Romero-Sandoval A, Nutile-McMenemy N, DeLeo JA (2008) Spinal microglial and perivascular cell cannabinoid receptor type 2 activation reduces behavioral hypersensitivity without tolerance after peripheral nerve injury. Anesthesiology 108(4):722–734. doi:10.1097/ALN.0b013e318167af74

253. Roodveldt C, Labrador-Garrido A, Gonzalez-Rey E, Fernandez-Montesinos R, Caro M, Lachaud CC, Waudby CA, Delgado M, Dobson CM, Pozo D (2010) Glial innate immunity generated by non-aggregated alpha-synuclein in mouse: differences between wild-type and Parkinson's disease-linked mutants. PLoS ONE 5(10):e13481. doi:10.1371/journal.pone.0013481

254. Roseberry TK, Lee AM, Lalive AL, Wilbrecht L, Bonci A, Kreitzer AC (2016) Cell-Type-Specific Control of Brainstem Locomotor Circuits by Basal Ganglia. Cell 164(3):526–537. doi:10.1016/j.cell.2015.12.037

255. Rusconi R, Ulusoy A, Aboutalebi H, Di Monte DA (2018) Long-lasting pathological consequences of overexpression-induced alpha-synuclein spreading in the rat brain. Aging Cell. doi:10.1111/acel.12727

256. Sachs C, Jonsson G (1975) Mechanisms of action of 6-hydroxydopamine. Biochem Pharmacol 24(1):1–8. doi:10.1016/0006-2952(75)90304-4

257. Sacino AN, Brooks M, Thomas MA, McKinney AB, Lee S, Regenhardt RW, McGarvey NH, Ayers JI, Notterpek L, Borchelt DR, Golde TE, Giasson BI (2014) Intramuscular injection of α-synuclein induces CNS α-synuclein pathology and a rapid-onset motor phenotype in transgenic mice. Proc Natl Acad Sci U S A 111(29):10732–10737. doi:10.1073/pnas.1321785111

258. Saha AR, Hill J, Utton MA, Asuni AA, Ackerley S, Grierson AJ, Miller CC, Davies AM, Buchman VL, Anderton BH, Hanger DP (2004) Parkinson's disease alpha-synuclein mutations exhibit defective axonal transport in cultured neurons. J Cell Sci 117(Pt 7):1017–1024. doi:10.1242/jcs.00967

259. Saito Y, Kawashima A, Ruberu NN, Fujiwara H, Koyama S, Sawabe M, Arai T, Nagura H, Yamanouchi H, Hasegawa M, Iwatsubo T, Murayama S (2003) Accumulation of phosphorylated alpha-synuclein in aging human brain. J Neuropathol Exp Neurol 62(6):644–654. doi:10.1093/jnen/62.6.644

260. Samii A, Nutt JG, Ransom BR (2004) Parkinson's disease. The Lancet 363(9423):1783–1793. doi:10.1016/S0140-6736(04)16305-8

261. Sampson TR, Debelius JW, Thron T, Janssen S, Shastri GG, Ilhan ZE, Challis C, Schretter CE, Rocha S, Gradinaru V, Chesselet M-F, Keshavarzian A, Shannon KM, Krajmalnik-Brown R, Wittung-Stafshede P, Knight R, Mazmanian SK (2016) Gut Microbiota Regulate Motor Deficits and Neuroinflammation in a Model of Parkinson's Disease. Cell 167(6):1469-1480.e12. doi:10.1016/j.cell.2016.11.018

262. Samuel F, Flavin WP, Iqbal S, Pacelli C, Sri Renganathan SD, Trudeau L-E, Campbell EM, Fraser PE, Tandon A (2016) Effects of Serine 129 Phosphorylation on α-Synuclein Aggregation, Membrane Association, and Internalization. J Biol Chem 291(9):4374–4385. doi:10.1074/jbc.M115.705095

263. Sanchez-Guajardo V, Febbraro F, Kirik D, Romero-Ramos M (2010) Microglia acquire distinct activation profiles depending on the degree of alpha-synuclein neuropathology in a rAAV based model of Parkinson's disease. PLoS ONE 5(1):e8784. doi:10.1371/journal.pone.0008784

264. Sanchez-Guajardo V, Tentillier N, Romero-Ramos M (2015) The relation between α-synuclein and microglia in Parkinson's disease: Recent developments. Neuroscience 302:47–58. doi:10.1016/j.neuroscience.2015.02.008

265. Sara SJ (2009) The locus coeruleus and noradrenergic modulation of cognition. Nat Rev Neurosci 10(3):211–223. doi:10.1038/nrn2573

266. Sara SJ, Bouret S (2012) Orienting and reorienting: the locus coeruleus mediates cognition through arousal. Neuron 76(1):130–141. doi:10.1016/j.neuron.2012.09.011

267. Sasaki M, Shibata E, Tohyama K, Takahashi J, Otsuka K, Tsuchiya K, Takahashi S, Ehara S, Terayama Y, Sakai A (2006) Neuromelanin magnetic resonance imaging of locus ceruleus and substantia nigra in Parkinson's disease. Neuroreport 17(11):1215–1218. doi:10.1097/01.wnr.0000227984.84927.a7

268. Sauer H, Oertel WH (1994) Progressive degeneration of nigrostriatal dopamine neurons following intrastriatal terminal lesions with 6-hydroxydopamine: A combined retrograde tracing and immunocytochemical study in the rat. Neuroscience 59(2):401–415. doi:10.1016/0306-4522(94)90605-X

269. Sauerbier A, Cova I, Rosa-Grilo M, Taddei RN, Mischley LK, Chaudhuri KR (2017) Treatment of Nonmotor Symptoms in Parkinson's Disease. Int Rev Neurobiol 132:361–379. doi:10.1016/bs.irn.2017.03.002

270. Scheckel C, Aguzzi A (2018) Prions, prionoids and protein misfolding disorders. Nature Reviews Genetics 19(7):405–418. doi:10.1038/s41576-018-0011-4

271. Schindelin J, Arganda-Carreras I, Frise E, Kaynig V, Longair M, Pietzsch T, Preibisch S, Rueden C, Saalfeld S, Schmid B, Tinevez J-Y, White DJ, Hartenstein V, Eliceiri K, Tomancak P, Cardona A (2012) Fiji. An open-source platform for biological-image analysis. Nat Methods 9(7):676–682. doi:10.1038/nmeth.2019

272. Schmitz C, Hof PR (2005) Design-based stereology in neuroscience. Neuroscience 130(4):813–831. doi:10.1016/j.neuroscience.2004.08.050

273. Schrag A, Horsfall L, Walters K, Noyce A, Petersen I (2015) Prediagnostic presentations of Parkinson's disease in primary care: a case-control study. The Lancet Neurology 14(1):57–64. doi:10.1016/S1474-4422(14)70287-X

274. Schrag A, Anastasiou Z, Ambler G, Noyce A, Walters K (2019) Predicting diagnosis of Parkinson's disease: A risk algorithm based on primary care presentations. Mov Disord 34(4):480–486. doi:10.1002/mds.27616

275. Schulz-Schaeffer WJ (2010) The synaptic pathology of α-synuclein aggregation in dementia with Lewy bodies, Parkinson's disease and Parkinson's disease dementia. Acta Neuropathol 120(2):131–143. doi:10.1007/s00401-010-0711-0

276. Schwarz LA, Luo L (2015) Organization of the Locus Coeruleus-Norepinephrine System. Current Biology 25(21):R1051-R1056. doi:10.1016/j.cub.2015.09.039

277. Schwarz LA, Miyamichi K, Gao XJ, Beier KT, Weissbourd B, DeLoach KE, Ren J, Ibanes S, Malenka RC, Kremer EJ, Luo L (2015) Viral-genetic tracing of the input–output organization of a central noradrenaline circuit. Nature 524(7563):88–92. doi:10.1038/nature14600

278. Schwarz ST, Xing Y, Tomar P, Bajaj N, Auer DP (2017) In Vivo Assessment of Brainstem Depigmentation in Parkinson Disease: Potential as a Severity Marker for Multicenter Studies. Radiology 283(3):789–798. doi:10.1148/radiol.2016160662

279. Séguéla P, Watkins KC, Geffard M, Descarries L (1990) Noradrenaline axon terminals in adult rat neocortex: An immunocytochemical analysis in serial thin sections. Neuroscience 35(2):249–264. doi:10.1016/0306-4522(90)90079-J

280. Serpell LC, Berriman J, Jakes R, Goedert M, Crowther RA (2000) Fiber diffraction of synthetic alpha-synuclein filaments shows amyloid-like cross-beta conformation. Proc Natl Acad Sci U S A 97(9):4897–4902. doi:10.1073/pnas.97.9.4897

281. Shahmoradian SH, Lewis AJ, Genoud C et al (2019) Lewy pathology in Parkinson's disease consists of crowded organelles and lipid membranes. Nat Neurosci 22(7):1099–1109. doi:10.1038/s41593-019-0423-2

282. Shelkovnikova TA, Ustyugov AA, Millership S, Peters O, Anichtchik O, Spillantini MG, Buchman VL, Bachurin SO, Ninkina NN (2011) Dimebon does not ameliorate pathological changes caused by expression of truncated (1-120) human alpha-synuclein in dopaminergic neurons of transgenic mice. Neurodegener Dis 8(6):430–437. doi:10.1159/000324989

283. Sherer TB, Betarbet R, Testa CM, Seo BB, Richardson JR, Kim JH, Miller GW, Yagi T, Matsuno-Yagi A, Greenamyre JT (2003) Mechanism of toxicity in rotenone models of Parkinson's disease. J Neurosci 23(34):10756–10764

284. Shulman LM, Taback RL, Rabinstein AA, Weiner WJ (2002) Non-recognition of depression and other non-motor symptoms in Parkinson's disease. Parkinsonism Relat Disord 8(3):193–197. doi:10.1016/S1353-8020(01)00015-3

285. Singleton AB, Farrer M, Johnson J, Singleton A, Hague S, Kachergus J, Hulihan M, Peuralinna T, Dutra A, Nussbaum R, Lincoln S, Crawley A, Hanson M, Maraganore D, Adler C, Cookson MR, Muenter M, Baptista M, Miller D, Blancato J, Hardy J, Gwinn-Hardy K (2003) alpha-Synuclein locus triplication causes Parkinson's disease. Science 302(5646):841. doi:10.1126/science.1090278

286. Smith Y, Wichmann T, Factor SA, DeLong MR (2012) Parkinson's disease therapeutics: new developments and challenges since the introduction of levodopa. Neuropsychopharmacology 37(1):213–246. doi:10.1038/npp.2011.212

287. Smith WW, Margolis RL, Li X, Troncoso JC, Lee MK, Dawson VL, Dawson TM, Iwatsubo T, Ross CA (2005) Alpha-synuclein phosphorylation enhances eosinophilic cytoplasmic inclusion formation in SH-SY5Y cells. J Neurosci 25(23):5544–5552. doi:10.1523/JNEUROSCI.0482-05.2005

288. Sokoloff P, Giros B, Martres M-P, Bouthenet M-L, Schwartz J-C (1990) Molecular cloning and characterization of a novel dopamine receptor (D3) as a target for neuroleptics. Nature 347:146 EP -. doi:10.1038/347146a0

289. Soulet D, Rivest S (2008) Microglia. Curr Biol 18(12):R506-8. doi:10.1016/j.cub.2008.04.047

290. Spillantini MG, Schmidt ML, Lee VM, Trojanowski JQ, Jakes R, Goedert M (1997) Alpha-synuclein in Lewy bodies. Nature 388(6645):839–840. doi:10.1038/42166

291. Stanic D, Parish CL, Zhu WM, Krstew EV, Lawrence AJ, Drago J, Finkelstein DI, Horne MK (2003) Changes in function and ultrastructure of striatal dopaminergic terminals that regenerate following partial lesions of the SNpc. J Neurochem 86(2):329–343. doi:10.1046/j.1471-4159.2003.01843.x

292. Stocchi F, Vacca L, Ruggieri S, Olanow CW (2005) Intermittent vs continuous levodopa administration in patients with advanced Parkinson disease: a clinical and pharmacokinetic study. Arch Neurol 62(6):905–910. doi:10.1001/archneur.62.6.905

293. Streit WJ, Kincaid-Colton CA (1995) The brain's immune system. Sci Am 273(5):54-5, 58-61

294. Sturkenboom, Ingrid H W M, Graff MJL, Hendriks JCM, Veenhuizen Y, Munneke M, Bloem BR, der Sanden, Maria W Nijhuis-van (2014) Efficacy of occupational therapy for patients with Parkinson's disease: a randomised controlled trial. The Lancet Neurology 13(6):557–566. doi:10.1016/S1474-4422(14)70055-9

295. Su X, Maguire-Zeiss KA, Giuliano R, Prifti L, Venkatesh K, Federoff HJ (2008) Synuclein activates microglia in a model of Parkinson's disease. Neurobiol Aging 29(11):1690–1701. doi:10.1016/j.neurobiolaging.2007.04.006

296. Surmeier DJ, Obeso JA, Halliday GM (2017) Parkinson's Disease Is Not Simply a Prion Disorder. J Neurosci 37(41):9799–9807. doi:10.1523/JNEUROSCI.1787-16.2017

297. Surmeier DJ, Obeso JA, Halliday GM (2017) Selective neuronal vulnerability in Parkinson disease. Nat Rev Neurosci 18(2):101–113. doi:10.1038/nrn.2016.178

298. Szabadi E (2013) Functional neuroanatomy of the central noradrenergic system. J Psychopharmacol (Oxford) 27(8):659–693. doi:10.1177/0269881113490326

299. Taguchi K, Watanabe Y, Tsujimura A, Tatebe H, Miyata S, Tokuda T, Mizuno T, Tanaka M (2014) Differential expression of alpha-synuclein in hippocampal neurons. PLoS ONE 9(2):e89327. doi:10.1371/journal.pone.0089327

300. Taguchi K, Watanabe Y, Tsujimura A, Tanaka M (2016) Brain region-dependent differential expression of alpha-synuclein. J Comp Neurol 524(6):1236–1258. doi:10.1002/cne.23901

301. Takahashi K, Kayama Y, Lin JS, Sakai K (2010) Locus coeruleus neuronal activity during the sleep-waking cycle in mice. Neuroscience 169(3):1115–1126. doi:10.1016/j.neuroscience.2010.06.009

302. Tanner CM, Kamel F, Ross GW, Hoppin JA, Goldman SM, Korell M, Marras C, Bhudhikanok GS, Kasten M, Chade AR, Comyns K, Richards MB, Meng C, Priestley B, Fernandez HH, Cambi F, Umbach DM, Blair A, Sandler DP, Langston JW (2011) Rotenone, paraquat, and Parkinson's disease. Environ Health Perspect 119(6):866–872. doi:10.1289/ehp.1002839

303. Tenreiro S, Reimão-Pinto MM, Antas P, Rino J, Wawrzycka D, Macedo D, Rosado-Ramos R, Amen T, Waiss M, Magalhães F, Gomes A, Santos CN, Kaganovich D, Outeiro TF (2014) Phosphorylation modulates clearance of alpha-synuclein inclusions in a yeast model of Parkinson's disease. PLoS Genet 10(5):e1004302. doi:10.1371/journal.pgen.1004302

304. Thakur P, Breger LS, Lundblad M, Wan OW, Mattsson B, Luk KC, Lee VMY, Trojanowski JQ, Bjorklund A (2017) Modeling Parkinson's disease pathology by combination of fibril seeds and alpha-synuclein overexpression in the rat brain. Proc Natl Acad Sci U S A 114(39):E8284-E8293. doi:10.1073/pnas.1710442114

305. Theodore S, Cao S, McLean PJ, Standaert DG (2008) Targeted overexpression of human alpha-synuclein triggers microglial activation and an adaptive immune response in a mouse model of Parkinson disease. J Neuropathol Exp Neurol 67(12):1149–1158. doi:10.1097/NEN.0b013e31818e5e99

306. Tison F, Dartigues JF, Dubes L, Zuber M, Alperovitch A, Henry P (1994) Prevalence of Parkinson's disease in the elderly: a population study in Gironde, France. Acta Neurol Scand 90(2):111–115

307. Tofaris GK, Garcia Reitbock P, Humby T, Lambourne SL, O'Connell M, Ghetti B, Gossage H, Emson PC, Wilkinson LS, Goedert M, Spillantini MG (2006) Pathological changes in dopaminergic nerve cells of the substantia nigra and olfactory bulb in mice transgenic for truncated human alpha-synuclein(1-120). Implications for Lewy body disorders. J Neurosci 26(15):3942–3950. doi:10.1523/JNEUROSCI.4965-05.2006

308. Tran HT, Chung CH-Y, Iba M, Zhang B, Trojanowski JQ, Luk KC, Lee VMY (2014) A-synuclein immunotherapy blocks uptake and templated propagation of misfolded α-synuclein and neurodegeneration. Cell Rep 7(6):2054–2065. doi:10.1016/j.celrep.2014.05.033

309. Uchihara T, Giasson BI (2016) Propagation of alpha-synuclein pathology. Hypotheses, discoveries, and yet unresolved questions from experimental and human brain studies. Acta Neuropathol 131(1):49–73. doi:10.1007/s00401-015-1485-1

310. Uchiyama M, Isse K, Tanaka K, Yokota N, Hamamoto M, Aida S, Ito Y, Yoshimura M, Okawa M (1995) Incidental Lewy body disease in a patient with REM sleep behavior disorder. Neurology 45(4):709–712. doi:10.1212/wnl.45.4.709

311. Ulusoy A, Rusconi R, Pérez-Revuelta BI, Musgrove RE, Helwig M, Winzen-Reichert B, Di Monte DA (2013) Caudo-rostral brain spreading of α-synuclein through vagal connections. EMBO Mol Med 5(7):1051–1059. doi:10.1002/emmm.201302475

312. Ulusoy A, Musgrove RE, Rusconi R, Klinkenberg M, Helwig M, Schneider A, Di Monte DA (2015) Neuron-to-neuron α-synuclein propagation in vivo is independent of neuronal injury. Acta Neuropathol Commun 3:13. doi:10.1186/s40478-015-0198-y

313. Ulusoy A, Phillips RJ, Helwig M, Klinkenberg M, Powley TL, Di Monte DA (2017) Brain-to-stomach transfer of alpha-synuclein via vagal preganglionic projections. Acta Neuropathol 133(3):381–393. doi:10.1007/s00401-016-1661-y

314. Ungerstedt U (1968) 6-hydroxy-dopamine induced degeneration of central monoamine neurons. European Journal of Pharmacology 5(1):107–110. doi:10.1016/0014-2999(68)90164-7

315. Uversky VN, Li J, Fink AL (2001) Evidence for a partially folded intermediate in alpha-synuclein fibril formation. J Biol Chem 276(14):10737–10744. doi:10.1074/jbc.M010907200

316. van de Warrenburg BP, Lammens M, Lücking CB, Denèfle P, Wesseling P, Booij J, Praamstra P, Quinn N, Brice A, Horstink MW (2001) Clinical and pathologic abnormalities in a family with parkinsonism and parkin gene mutations. Neurology 56(4):555–557. doi:10.1212/wnl.56.4.555

317. van der Perren A, van den Haute C, Baekelandt V (2015) Viral vector-based models of Parkinson's disease. Curr Top Behav Neurosci 22:271–301. doi:10.1007/7854_2014_310

318. Vekrellis K, Xilouri M, Emmanouilidou E, Rideout HJ, Stefanis L (2011) Pathological roles of α-synuclein in neurological disorders. The Lancet Neurology 10(11):1015–1025. doi:10.1016/S1474-4422(11)70213-7

319. Verma A (2016) Prions, prion-like prionoids, and neurodegenerative disorders. Ann Indian Acad Neurol 19(2):169–174. doi:10.4103/0972-2327.179979

320. Volpicelli-Daley LA, Luk KC, Patel TP, Tanik SA, Riddle DM, Stieber A, Meaney DF, Trojanowski JQ, Lee VM-Y (2011) Exogenous alpha-synuclein fibrils induce Lewy body pathology leading to synaptic dysfunction and neuron death. Neuron 72(1):57–71. doi:10.1016/j.neuron.2011.08.033

321. Volpicelli-Daley LA, Luk KC, Lee VM-Y (2014) Addition of exogenous α-synuclein preformed fibrils to primary neuronal cultures to seed recruitment of endogenous α-synuclein to Lewy body and Lewy neurite–like aggregates. Nat Protoc 9:2135 EP -. doi:10.1038/nprot.2014.143

322. Volpicelli-Daley LA, Kirik D, Stoyka LE, Standaert DG, Harms AS (2016) How can rAAV-alpha-synuclein and the fibril alpha-synuclein models advance our understanding of Parkinson's disease? J Neurochem 139 Suppl 1:131–155. doi:10.1111/jnc.13627

323. Wagner J, Ryazanov S, Leonov A et al (2013) Anle138b: a novel oligomer modulator for disease-modifying therapy of neurodegenerative diseases such as prion and Parkinson's disease. Acta Neuropathol 125(6):795–813. doi:10.1007/s00401-013-1114-9

324. Wakabayashi K, Tanji K, Mori F, Takahashi H (2007) The Lewy body in Parkinson's disease: Molecules implicated in the formation and degradation of α-synuclein aggregates. Neuropathology 27(5):494–506. doi:10.1111/j.1440-1789.2007.00803.x

325. Wakabayashi K, Tanji K, Odagiri S, Miki Y, Mori F, Takahashi H (2013) The Lewy body in Parkinson's disease and related neurodegenerative disorders. Mol Neurobiol 47(2):495–508. doi:10.1007/s12035-012-8280-y

326. Walsh DM, Selkoe DJ (2016) A critical appraisal of the pathogenic protein spread hypothesis of neurodegeneration. Nat Rev Neurosci 17(4):251–260. doi:10.1038/nrn.2016.13

327. Wang H-L, Morales M (2009) Pedunculopontine and laterodorsal tegmental nuclei contain distinct populations of cholinergic, glutamatergic and GABAergic neurons in the rat. European Journal of Neuroscience 29(2):340–358. doi:10.1111/j.1460-9568.2008.06576.x

328. Wang S, Chu C-H, Stewart T, Ginghina C, Wang Y, Nie H, Guo M, Wilson B, Hong J-S, Zhang J (2015) α-Synuclein, a chemoattractant, directs microglial migration via H2O2-dependent Lyn phosphorylation. Proc Natl Acad Sci U S A 112(15):E1926-35. doi:10.1073/pnas.1417883112

329. Ward DG, Gunn CG (1976) Locus coeruleus complex: elicitation of a pressor response and a brain stem region necessary for its occurence. Brain Res 107(2):401–406. doi:10.1016/0006-8993(76)90236-5

330. Watson MB, Richter F, Lee SK, Gabby L, Wu J, Masliah E, Effros RB, Chesselet M-F (2012) Regionally-specific microglial activation in young mice over-expressing human wildtype alpha-synuclein. Exp Neurol 237(2):318–334. doi:10.1016/j.expneurol.2012.06.025

331. Wegrzynowicz M, Bar-On D, Calo' L, Anichtchik O, Iovino M, Xia J, Ryazanov S, Leonov A, Giese A, Dalley JW, Griesinger C, Ashery U, Spillantini MG (2019) Depopulation of dense α-synuclein aggregates is associated with rescue of dopamine neuron dysfunction and death in a new Parkinson's disease model. Acta Neuropathol. doi:10.1007/s00401-019-02023-x

332. Weihofen A, Liu Y, Arndt JW, Huy C, Quan C, Smith BA, Baeriswyl J-L, Cavegn N, Senn L, Su L, Marsh G, Auluck PK, Montrasio F, Nitsch RM, Hirst WD, Cedarbaum JM, Pepinsky RB, Grimm J, Weinreb PH (2019) Development of an aggregate-selective, human-derived α-synuclein antibody BIIB054 that ameliorates disease phenotypes in Parkinson's disease models. Neurobiol Dis 124:276–288. doi:10.1016/j.nbd.2018.10.016

333. Weinshenker D (2018) Long Road to Ruin. Noradrenergic Dysfunction in Neurodegenerative Disease. Trends Neurosci. doi:10.1016/j.tins.2018.01.010

334. Weintraub D (2008) Dopamine and impulse control disorders in Parkinson's disease. Ann Neurol 64 Suppl 2:S93-100. doi:10.1002/ana.21454

335. Weintraub D, Comella CL, Horn S (2008) Parkinson's disease--Part 1: Pathophysiology, symptoms, burden, diagnosis, and assessment. Am J Manag Care 14(2 Suppl):S40-8

336. Weintraub D, Koester J, Potenza MN, Siderowf AD, Stacy M, Voon V, Whetteckey J, Wunderlich GR, Lang AE (2010) Impulse control disorders in Parkinson disease: a cross-sectional study of 3090 patients. Arch Neurol 67(5):589–595. doi:10.1001/archneurol.2010.65

337. Wessler S (1976) Animal Models of Thrombosis and Hemorrhagic Diseases. National Academies Press, Washington, D.C.

338. Willner P (1984) The validity of animal models of depression. Psychopharmacology (Berl) 83(1):1–16

339. Witt K, Kalbe E, Erasmi R, Ebersbach G (2017) Nichtmedikamentöse Therapieverfahren beim Morbus Parkinson. Nervenarzt 88(4):383–390. doi:10.1007/s00115-017-0298-y

340. Wood SJ, Wypych J, Steavenson S, Louis JC, Citron M, Biere AL (1999) alpha-synuclein fibrillogenesis is nucleation-dependent. Implications for the pathogenesis of Parkinson's disease. J Biol Chem 274(28):19509–19512. doi:10.1074/jbc.274.28.19509

341. Worth PF (2013) How to treat Parkinson's disease in 2013. Clin Med (Lond) 13(1):93–96. doi:10.7861/clinmedicine.13-1-93

342. Wu Z, Asokan A, Samulski RJ (2006) Adeno-associated virus serotypes: vector toolkit for human gene therapy. Mol Ther 14(3):316–327. doi:10.1016/j.ymthe.2006.05.009

343. Wu N, Joshi PR, Cepeda C, Masliah E, Levine MS (2010) Alpha-synuclein overexpression in mice alters synaptic communication in the corticostriatal pathway. J Neurosci Res 88(8):1764–1776. doi:10.1002/jnr.22327

344. Yamada M, Iwatsubo T, Mizuno Y, Mochizuki H (2004) Overexpression of alpha-synuclein in rat substantia nigra results in loss of dopaminergic neurons, phosphorylation of alpha-synuclein and activation of caspase-9. Resemblance to pathogenetic changes in Parkinson's disease. J Neurochem 91(2):451–461. doi:10.1111/j.1471-4159.2004.02728.x

345. Yamada K, Iwatsubo T (2018) Extracellular α-synuclein levels are regulated by neuronal activity. Mol Neurodegener 13(1):9. doi:10.1186/s13024-018-0241-0

346. Zweig RM, Jankel WR, Hedreen JC, Mayeux R, Price DL (1989) The pedunculopontine nucleus in Parkinson's disease. Ann Neurol 26(1):41–46. doi:10.1002/ana.410260106

347. Zweig RM, Cardillo JE, Cohen M, Giere S, Hedreen JC (1993) The locus ceruleus and dementia in Parkinson's disease. Neurology 43(5):986. doi:10.1212/WNL.43.5.986